AD-A275 311

REPORT DOCUMENTATION PAGE

Form Approved
OMB No 0704-0188

1. AGENCY USE ONLY (Leave blank)	2. REPORT DATE	3. REPORT TYPE AND DATES COVERED
	Dec 93	THESIS/DISSERTATION

4. TITLE AND SUBTITLE
Aberrated Point-Spread Functions and Beam Quality for Optical Systems with Annular Pupils

5. FUNDING NUMBERS

6. AUTHOR(S)
Carl F. Maes

7. PERFORMING ORGANIZATION NAME(S) AND ADDRESS(ES)
AFIT Student Attending: Univ of Southern California

8. PERFORMING ORGANIZATION REPORT NUMBER
AFIT/CI/CIA- 93-150

9. SPONSORING/MONITORING AGENCY NAME(S) AND ADDRESS(ES)
DEPARTMENT OF THE AIR FORCE
AFIT/CI
2950 P STREET
WRIGHT-PATTERSON AFB OH 45433-7765

10. SPONSORING/MONITORING AGENCY REPORT NUMBER

11. SUPPLEMENTARY NOTES

12a. DISTRIBUTION/AVAILABILITY STATEMENT
Approved for Public Release IAW 190-1
Distribution Unlimited
MICHAEL M. BRICKER, SMSgt, USAF
Chief Administration

12b. DISTRIBUTION CODE

13. ABSTRACT (Maximum 200 words)

14. SUBJECT TERMS	15. NUMBER OF PAGES 110
	16. PRICE CODE

17. SECURITY CLASSIFICATION OF REPORT	18. SECURITY CLASSIFICATION OF THIS PAGE	19. SECURITY CLASSIFICATION OF ABSTRACT	20. LIMITATION OF ABSTRACT

ABERRATED POINT-SPREAD FUNCTIONS AND BEAM QUALITY FOR OPTICAL SYSTEMS WITH ANNULAR PUPILS

by

Carl F. Maes

A Thesis Presented to the

FACULTY OF THE GRADUATE SCHOOL

UNIVERSITY OF SOUTHERN CALIFORNIA

In Partial Fulfillment of the

Requirements for the Degree

MASTER OF SCIENCE

(Physics)

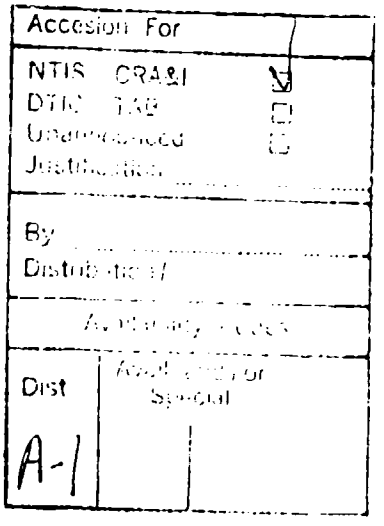

December 1993

UNIVERSITY OF SOUTHERN CALIFORNIA
THE GRADUATE SCHOOL
UNIVERSITY PARK
LOS ANGELES, CALIFORNIA 90007

This thesis, written by

Carl F. Maes

under the direction of h.is Thesis Committee, and approved by all its members, has been presented to and accepted by the Dean of The Graduate School, in partial fulfillment of the requirements for the degree of

MASTER OF SCIENCE

Barbara Lamson

Dean

Date August 13, 1993

THESIS COMMITTEE

Chairman

Mel D. Daybell

V. M. Mahajan

A Tatita Dios

Acknowledgments

This thesis has been made possible by many. In particular I wish to acknowledge and thank: Dr. Rich Boucher of the Aerospace Corporation who provided many a tutorial on the intricacies of Phocas, a computer code which he developed for use in electro-optical systems analysis. Dr. Boucher also provided much theoretical guidance. Dr. Vini Mahajan has graciously made time to be my advisor and introduce me to optical imaging and aberration theory . And finally, many thanks to my wife Patricia who inspired me to climb this mountain.

TABLE OF CONTENTS

LIST OF TABLES

LIST OF FIGURES

ABSTRACT

The effect of the central obscuration of an annular pupil of an incoherent optical imaging system on its aberrated point-spread function (PSF) is discussed. A simple model is presented which approximates the aberrated PSF by an aberration-free PSF scaled by its Strehl ratio. The approximation of a PSF with rotationally symmetric aberrations by an aberration-free PSF scaled by the Strehl ratio improves as the obscuration of the pupil increases. Specifically, as the obscuration approaches the outer radius, the PSF of optical systems with rotationally symmetric aberrations becomes increasingly similar to the aberration-free PSF scaled by the Strehl ratio in regions within the central Airy disk. A PSF with balanced coma aberration can also be approximated with similar accuracy and over the same region as for rotationally symmetric aberrations. For the rotationally nonsymmetric aberrations of astigmatism, balanced astigmatism, and coma the aberrated PSF in its central region can also be approximated by the scaled aberration-free PSF but for large Strehl ratios. For rotationally nonsymmetric aberrations, the region or spot sizes are given for which the aberration-free encircled energy without scaling by the Strehl ratio provides better agreement with the actual aberrated encircled energy than the aberration-free encircled energy scaled by the Strehl ratio.

CHAPTER 1

INTRODUCTION

This thesis describes a simple model that can be used to approximately calculate the point-spread function (PSF), Strehl ratio, and encircled energy for an aberrated imaging or a laser transmitter system. This work is an extension of the work done by Mahajan,[1] who developed a simple model for estimating the effects of rotationally symmetric aberrations on the PSF of a system with a circular pupil. It has been shown[1,2] for circular pupils that the irradiance distribution within the central region of the Airy disk of a rotationally symmetric aberrated PSF is largely unchanged from the aberration-free case except for a scaling factor equal to the Strehl ratio. The current work focuses on the applicability of such a model to systems with annular pupils, for both rotationally symmetric and nonsymmetric aberrations, with uniform and Gaussian illuminations. Gaussian illumination is of interest for example, to determine the focal-plane distribution of a $TEM_{0,0}$ mode laser beam.

The irradiance distribution, or PSF, and the encircled energy for an aberrated system with an annular pupil can also be estimated from a knowledge of the Strehl ratio and the aberration-free PSF. This holds true for defocus, spherical, balanced spherical, and balanced coma aberration. They can also be estimated for astigmatism, balanced astigmatism, and coma but for smaller spot radii and larger Strehl ratios. In particular, the PSF and encircled energy for an aberrated system can be estimated by scaling the aberration-free PSF and encircled energy by a factor equal to the Strehl

ratio as was shown for circular pupils by Mahajan. The difference between the actual aberrated PSF (and encircled energy) and the aberration-free PSF (and encircled energy) scaled by the Strehl ratio decreases as the obscuration ratio increases for rotationally symmetric aberrations. The percentage difference between estimated and actual encircled energy is less than 20% within the Airy disk for Strehl ratios $S \geq 0.4$ for rotationally symmetric aberrations, balanced coma, and astigmatism for all obscurations. The percentage difference drops to less than 5% for rotationally symmetric aberrations for Strehl ratios as low as 0.1 for an obscuration ratio of 0.9.

The difference between the actual and estimated encircled energies, in general, increases (up to an asymptotic level) as the spot radius (used to calculate encircled energy) increases. This is a result of encircled energies of aberrated PSFs converging to the unaberrated values as the radius increases. The region or spot sizes for which the aberration-free encircled energy without scaling by the Strehl ratio provides better agreement with the actual aberrated encircled energy than the aberration-free encircled energy scaled by the Strehl ratio depends on the type and amount of aberration. The smallest region is for the case of coma and is approximately half the Airy disk. Other types of aberrations : spot sizes ranging from the Airy disk (for rotationally nonsymmetric aberrations and rotationally symmetric aberrations with unobscured pupils) up to several times the Airy disk (for rotationally symmetric aberrations with large obscurations).

CHAPTER 2

THEORY AND BACKGROUND

The irradiance distribution of the image of an incoherent point object of wavelength λ formed by a system with an aperture or pupil is called its diffraction point-spread function (PSF). It is given by[3]

$$I(x,y) = \frac{1}{(\lambda R)^2}\left|\int_{-\infty}^{\infty}\int_{-\infty}^{\infty} G(\xi,\eta)\exp[-\frac{2\pi i}{\lambda R}(x\xi + y\eta)]d\xi d\eta\right|^2. \qquad (1)$$

$G(\xi,\eta)$ is the pupil function of the system given by

$$G(\xi,\eta) = A(\xi,\eta)\exp[(2\pi i/\lambda)W(\xi,\eta)] \quad \text{at points inside the pupil} \qquad (2)$$

$$= 0 \quad \text{at points outside the pupil,}$$

where $A(\xi,\eta)$ is the amplitude and $W(\xi,\eta)$ is the wave aberration at a point (ξ,η) on the pupil. $W(\xi,\eta)$ is the optical path length difference between the aberrated wavefront and the Gaussian reference sphere. The reference sphere passes through the center of the exit pupil and has a radius of curvature R. It is centered at the Gaussian image point, the origin of the (x,y) image plane.

The diffraction PSF written in terms of polar coordinates and located in a plane normal to the z axis at a distance z from the exit pupil (such that z does not necessarily equal R) is,[4,5]

$$I(r,\theta_i;z;\varepsilon) = \frac{PS_p}{(\pi\lambda z)^2}\left|\int_{\varepsilon}^{1}\int_{0}^{2\pi} A(\rho)\exp[i\Phi(\rho,\theta)]\exp[-\pi i\frac{R}{z}r\rho\cos(\theta-\theta_i)]\rho d\rho d\theta\right|^2. \qquad (3)$$

Here, $\xi = \rho\cos\theta$, $\eta = \rho\sin\theta$, $x = r\cos\theta_i$, $y = r\sin\theta_i$, $\varepsilon \le \rho \le 1$ and $0 \le \theta < 2\pi$. $\Phi(\rho,\theta)$ is the phase aberration and is related to the wave aberration according to $\Phi =$

$(2\pi/\lambda)W$. The explicit dependence on z is of interest in the case of a defocused system where $z \neq R$; otherwise, $z = R$, and Eq. (3) reduces to Eq. (1) with a change of coordinates. The integral is taken over the clear region of the pupil with coordinates (ρ, θ), where ρ is in units of the outer radius a of the pupil. The obscuration ratio, ε, is defined such that $a\varepsilon$ is the inner radius of the pupil. The coordinates of the observation point of the PSF are (r, θ_i, z) where r is in units of $\lambda R/2a = \lambda F$ (F being the f-number or the focal ratio of the Gaussian image forming light cone). The amplitude $A(\rho)$ is assumed to be rotationally symmetric in view of Gaussian beams discussed later. The total power transmitted through the exit pupil is P, and $S_p = \pi a^2(1-\varepsilon^2)$ is the area of the exit pupil.

If the wave aberration is expanded into a power series, the resulting aberration terms of lowest order are of degree 4 and are called the primary (or Seidel) aberrations.[6] The primary aberration function may be written in polar coordinates as[6, 7]

$$W(\rho, \theta) = A_S \rho^4 + A_C \rho^3 \cos\theta + A_a \rho^2 \cos^2\theta + A_d \rho^2 + A_t \rho \cos\theta, \qquad (4)$$

where A_i is the peak value of the corresponding aberration term. Thus A_S is the peak value for spherical, A_C is for coma, A_a is for astigmatism, A_d is for defocus, and A_t is for tilt.

The aberration function may also be expanded in terms of a complete set of Zernike circle polynomials in the case of a circular pupil[8] and Zernike annular polynomials in the case of an annular pupil.[9] The Zernike polynomials are useful in that the aberration terms are of the form[10,11]

$$\Phi_{nm}(\rho;\varepsilon) = \varepsilon_m \, c_{nm} \sqrt{2(n+1)} \, R_n^m(\rho;\varepsilon) \cos m\theta, \qquad (5)$$

where n and m are positive integers (including zero), $n - m \geq 0$ and even,

$$\varepsilon_m = 1/\sqrt{2},\ m = 0$$
$$\varepsilon_m = 1, \qquad m \neq 0, \tag{6}$$

and c_{nm} represents the standard deviation of the aberration across the pupil (unless $n = m = 0$). Each Zernike polynomial is composed of terms of the form $A_{pq}\ \rho^p \cos^q\theta$, where p and q are positive integers, such that the variance of the aberration is minimized.[10] That is, an aberration of a certain order in the power series expansion is mixed or balanced with aberrations of lower order such that its variance is minimized thereby maximizing the central irradiance for small aberrations.[9, 10, 11] The standard deviation, $\sigma_\phi(A_i; \varepsilon)$, is given by[12]

$$\sigma_\phi^2 = \langle \Phi^2 \rangle - \langle \Phi \rangle^2 \tag{7}$$

such that $\sigma_\phi = c_{nm}$ if Φ is expressed as an orthonormal Zernike polynomial.

The average values of the nth power of Φ are defined according to

$$\langle \Phi^n \rangle = \int_\varepsilon^1 \int_0^{2\pi} A(\rho)\Phi^n(\rho,\theta)\rho d\rho d\theta \Big/ \int_\varepsilon^1 \int_0^{2\pi} A(\rho)\rho d\rho d\theta. \tag{8}$$

The primary aberrations and their standard deviations, $\sigma_\phi(A_i; \varepsilon)$, have been summarized by Mahajan[13] and are shown in Table 1 for the case of uniform illumination. Note that Szapiel has studied aberration balancing by extending the approach used by Maréchal to non-uniform, radially symmetric amplitude distributions.[14] He finds that for the case of a Gaussian amplitude (or apodization) function, Zernike polynomials result in optimal aberration balancing when the Gaussian beam waist is three or more times the pupil radius. For weakly truncated pupils where the pupil is about three or more times the Gaussian beam waist, however, the optimum aberration balancing is obtained using Laguerre polynomials.[14] Mahajan has followed the same Gram-Schmidt orthogonalization process used to derive Zernike annular polynomials to generate orthogonal aberration polynomials for Gaussian illumination of annular pupils.[9] Standard deviations of aberration functions and representations of

Table 1
Primary Aberrations and Their Standard Deviations for Optical Systems with Uniformly Illuminated Annular Pupils[13]

Aberration	$\Phi(\rho, \theta; \varepsilon)$	$\sigma_\phi(A_i; \varepsilon)$
Spherical	$A_s \rho^4$	$\frac{1}{3\sqrt{5}}(4-\varepsilon^2-6\varepsilon^4-\varepsilon^6+4\varepsilon^8)^{1/2} A_s$
Balanced Spherical	$A_s[\rho^4 - (1+\varepsilon^2)\rho^2]$	$\frac{1}{6\sqrt{5}}(1-\varepsilon^2)^2 A_s$
Coma	$A_c \rho^3 \cos\theta$	$\frac{1}{\sqrt{8}}(1+\varepsilon^2+\varepsilon^4+\varepsilon^6)^{1/2} A_c$
Balanced Coma	$A_c(\rho^3 - \frac{2}{3}\frac{1+\varepsilon^2+\varepsilon^4}{1+\varepsilon^2}\rho)\cos\theta$	$\frac{(1-\varepsilon^2)(1+4\varepsilon^2+\varepsilon^4)^{1/2}}{6\sqrt{2}(1+\varepsilon^2)^{1/2}} A_c$
Astigmatism	$A_a \rho^2 \cos^2\theta$	$\frac{1}{4}(1+\varepsilon^4)^{1/2} A_a$
Balanced Astigmatism	$A_a \rho^2(\cos^2\theta - 1/2)$	$\frac{1}{2\sqrt{6}}(1+\varepsilon^2+\varepsilon^4)^{1/2} A_a$
Defocus	$A_d \rho^2$	$\frac{1}{2\sqrt{3}}(1-\varepsilon^2) A_d$
Tilt	$A_t \rho\cos\theta$	$\frac{1}{2}(1+\varepsilon^2)^{1/2} A_t$

balanced aberrations for the case of Gaussian illuminated annular pupils have also been reported by Mahajan.[11]

The ratio of central irradiances (i. e., at the origin) of aberrated and unaberrated PSFs is called the Strehl ratio and is given by[13,15]

$$S = I(0)_{\phi} / I(0)_{\phi=0} \tag{9}$$

$$= \left| \frac{\int_{\varepsilon}^{1} \int_{0}^{2\pi} A(\rho) \exp[i\Phi(\rho,\theta)] \rho d\rho d\theta}{\int_{\varepsilon}^{1} \int_{0}^{2\pi} A(\rho) \rho d\rho d\theta} \right|^2 . \tag{10}$$

Maréchal,[16] Born and Wolf,[17] Mahajan,[13] and Szapiel,[14] among others, have discussed approximate expressions for the Strehl ratio based on the aberration variance:

$$S_m = (1 - \sigma_{\phi}^2/2)^2 \tag{11}$$

and

$$S_g = \exp[-(\sigma_{\phi})^2], \tag{12}$$

where the subscripts *m* and *g* refer to the Maréchal and Gaussian approximations respectively. Mahajan has shown that the Gaussian approximation gives a better approximation than the Maréchal approximation for classical as well as balanced (Zernike) aberrations in systems with uniformly illuminated pupils.[13,18] Szapiel presents a method for modifying the Maréchal approximation to account for non uniform, radially symmetric apodization functions. The method described by Szapiel does not require an explicit analytical expression for optimum balanced wavefronts, aberration variance, or minimization derivatives.[14] Instead, the approach requires the calculation of moments of the apodizing function and resulting determinants of a set of linear equations of aberration functions which minimize the aberration variance.

Conversely, the maximum aberration for a given Strehl ratio can be estimated and is referred to as the optical tolerance. The Maréchal tolerance condition for a

Strehl ratio of greater than or equal to 0.8 at the diffraction focus is that *the root-mean square departure of the wave-front from the reference sphere that is centered on the diffraction focus shall not exceed the value* $\lambda/14$; i. e., $\sigma_w \leq \lambda/14$ which follows from $S = 0.8 \geq 1-(2\pi/\lambda)^2(\sigma_w^2)$.[19] Although not explicit in the Strehl approximations above, the Maréchal tolerance condition is relatively insensitive to variation of obscuration ratio and the type of aberration. The Rayleigh criterion on the other hand specifies that for a Strehl ratio of $S = 0.8$, $W_{max} = \lambda/4$, which is applicable only to primary spherical aberration[20] for $\varepsilon \cong 0$.

The PSF for rotationally symmetric aberrations may further be simplified using the identity[21]

$$J_0(x) = \frac{1}{2\pi}\int_0^{2\pi} \exp[ix\cos(\theta-\alpha)]d\theta, \tag{13}$$

and so the PSF in Eq. (3) becomes proportional to the modulus square of the Hankle transform of the pupil function,

$$I(r;z;\varepsilon) = \frac{4PS_p}{(\lambda z)^2}\left|\int_\varepsilon^1 A(\rho)\exp[i\Phi(\rho)]J_0(\pi r\rho\frac{R}{z})\rho d\rho\right|^2. \tag{14}$$

The corresponding fraction of the total energy contained within a circle of radius r_c (the encircled energy) is

$$E(r_c) = 2\pi\int_0^{r_c} I(r)r\,dr. \tag{15}$$

For the aberration-free case, $\Phi(\rho) = 0$, with uniform illumination, $A(\rho) = 1$, the PSF in the plane of the geometric focus, $z = R$, becomes[22]

$$I(r;R;\varepsilon) = \frac{1}{(\lambda R)^2}\frac{PS_p}{(1-\varepsilon^2)^2}\left[\frac{2J_1(\pi r)}{\pi r} - \varepsilon^2\frac{2J_1(\pi\varepsilon r)}{\pi\varepsilon r}\right]^2. \tag{16}$$

In the case of a circular pupil, $\varepsilon = 0$, and Eq. (16) reduces to

$$I(r;R) = \frac{PS_p}{(\lambda R)^2}\left[\frac{2J_1(\pi r)}{\pi r}\right]^2. \tag{17}$$

The corresponding encircled energy of an aberration-free PSF for a circular pupil is given by[23]

$$E(r_c) = 1 - J_0^2(\pi r_c) - J_1^2(\pi r_c) \tag{18}$$

Mahajan[1] and Szapiel[2] have shown for the case of circular pupils with rotationally symmetric aberrations that the irradiance distribution of an aberrated PSF may be approximated. In particular, the irradiance distribution of an aberrated PSF within the Airy disk is very nearly described by an aberration-free PSF scaled by the Strehl ratio. That is, within the Airy disk, the diffraction PSF,

$$I(r) = 4\left|\int_0^1 \exp[i\Phi(\rho)] J_0(\pi r \rho)\rho d\rho\right|^2 \tag{19}$$

can be approximated by

$$I(r) \cong S\left[\frac{2J_1(\pi r)}{\pi r}\right]^2, \tag{20}$$

where S is the Strehl ratio (given in Eq. (9) or approximated in Eqs. (11) and (12)) and the aberration-free PSF has been normalized to unity at the center $r = 0$ by the central irradiance $PS_p/(\lambda R)^2$. The corresponding encircled energy may similarly be approximated. Mahajan has shown for the orthonormal Zernike polynomials of fourth, sixth, and eighth order spherical aberrations (which are balanced) that the encircled energy within small radii ($r_c \leq 1\ \lambda F$) can be estimated with a percentage error of $< 10\%$ for Strehl ratios $S \geq 0.1$. Szapiel provides an analytical basis for Eq. (20) using a Dini-sampling method which involves expressing the Hankle transform in Eq. (19) in terms of samples taken at successive points given by the first few zeros of $J_1(x)$.[2] The advantage of the Szapiel approach is that rotationally symmetric aberrations which are not balanced tend to spread the PSF over a larger radius and may be accounted for by

$$I(r) \cong S\left[\frac{2J_1(\pi r)}{\pi r}\right]^2 \sigma(\pi r), \tag{21}$$

where $\sigma(\pi r)$ is the spreading factor (which is not related to the standard deviation of the aberration). Szapiel proves that for the special case of Zernike polynomial aberrations, the spreading factor $\sigma(\pi r) = 1$. The disadvantage of the Szapiel approach is that the calculation of the spreading factor is somewhat tedious (although it can be done with a desk-top calculator) and overestimates the central irradiance, $I(0)$, for $S \leq 0.4$.[2]

The focus of this thesis is to report on the extension of Mahajan's model, Eq. (20), to annular pupils with rotationally symmetric and nonsymmetric aberrations, with uniform and Gaussian illumination. Thus, the general expression of the aberrated diffraction PSF given in Eq. (3) is approximated for spot radii within the Airy disk by

$$I(r,\theta_i;\varepsilon) \cong S \cdot I(r,\theta_i;\varepsilon)_{\Phi=0}, \tag{22}$$

and for the uniformly illuminated case by

$$I(r,\theta_i;\varepsilon) \cong S \cdot \frac{1}{(\lambda R)^2} \frac{PS_F}{(1-\varepsilon^2)^2} \left[\frac{2J_1(\pi r)}{\pi r} - \varepsilon^2 \frac{2J_1(\pi\varepsilon r)}{\pi\varepsilon r} \right]^2 \tag{23}$$

Similarly the corresponding encircled energies of aberrated PSFs are also approximated by scaling the aberration-free encircled energy by the Strehl ratio. This thesis reports on the accuracy of such a model for approximating aberrated PSFs over a range of obscuration ratios for primary and balanced primary aberrations.

CHAPTER 3

NUMERICAL RESULTS

General Remarks and Methodology

Defocus, spherical, astigmatism, coma, and the corresponding balanced aberrations with uniform and Gaussian amplitudes are considered in this thesis. The Gaussian amplitude is given by $A(\rho) = A_o \exp(-\gamma\rho^2)$ where A_o is a constant and the truncation is defined such that $\gamma = (a/w)^2$. As in Eq. (3), a is the radius of the exit pupil, and w is the radial distance at which the amplitude falls off to 1/e of the value at the center (known as the beam waist of Gaussian laser beams). A Gaussian amplitude with a truncation factor of $\gamma = 1$ is considered.

The methodology consisted of varying the obscuration ratio, ε, from 0, 0.1, 0.2,..., to 0.9. The value for $\sigma_\phi(A_i,\varepsilon)$ was estimated using the Gaussian approximation of the Strehl ratio, $S_G = \exp[-(\sigma_\phi)^2]$, to obtain Strehl ratios of 0.8, 0.6, 0.4, 0.2, and 0.1. The magnitude of σ_ϕ was then iteratively refined over the Gaussian approximation, such that the desired Strehl ratios were obtained. The aberration coefficient, A_i, was determined through the standard deviation, $\sigma_\phi(A_i,\varepsilon)$, and used to calculate the PSF and encircled energy (which were normalized by the central irradiance $PS_p/(\lambda R)^2$ of the aberration-free PSF) for each case of A_i and ε. Each aberrated PSF was then normalized to unity at the center by a scale factor equal to S; i. e., the PSF was divided by its respective Strehl ratio, which by definition is the ratio

of the central irradiances of the PSF, as shown in Eq. (9). Encircled energies were again calculated for the PSFs normalized by the Strehl ratio.

The numerical results presented in this thesis describe the difference between actual aberrated encircled energies E_a and unaberrated encircled energy E_u scaled by the Strehl ratio S. The difference is quantified in terms of a percentage error defined as

$$\%Error_{NENC} = 100\left[1 - \frac{(S)(E_u)}{E_a}\right], \tag{24}$$

where the subscript *NENC* specifies *normalized encircled energy* (by the Strehl ratio).

Instead of using the actual Strehl ratio of an aberrated PSF for normalization of the aberration-free encircled energy, the Gaussian approximation of the Strehl ratio, S_g may also be used (in practice, the aberration variance may be more readily measured, and thus Strehl ratio estimated with S_g, than a measurement of the actual Strehl ratio). The $\%Error_{NENC}$ in Eq. (24) above should then be adjusted for the percentage error of the Strehl approximation,

$$\%Error_{S_g} = 100(1-S_g S), \tag{25}$$

such that

$$\%Error_{Gaussian} = (\%Error_{NENC}) + (\%Error_{S_g}) - (\%Error_{NENC})(\%Error_{S_g}) \tag{26}$$

Note that if $S_g > S$ then $\%Error_{S_g} < 0$, and if $|\%Error_{S_g}| > \%Error_{NENC} > 0$ then the overall error of the model is improved. This factor may be significant for $S < 0.5$ where the Gaussian approximation does overestimate the actual Strehl ratio (coma being the only exception, for $\varepsilon < 0.5$) by more than a few percent.[18]

In contrast to the scaling of aberration-free encircled energies by the Strehl ratio, an alternate method for estimating encircled energies for rotationally non-

symmetric aberrations that provides relatively good accuracy at larger spot radii and over a broader range of Strehl ratios is the comparison of encircled energies of an aberrated PSF to aberration-free PSF without any normalization by the Strehl ratio. Although encircled energies vary considerably within the first Airy disk, the encircled energies converge rapidly at larger radii. As Mahajan has reported, to a first order, the encircled energy for large radii is independent of the aberration and exhibit an asymptotic behavior.[24] The difference between the actual encircled energies of aberrated and aberration-free PSFs is also quantified in terms of a percentage error defined as

$$\%Error_{ENC'} = 100\left[1 - \frac{E_a}{E_d}\right]. \qquad (27)$$

The subscript *ENC'* refers to *encircled energy without normalization* by the Strehl ratio.

Just as encircled energy increases with radius (up to the total energy), percentage error of estimated encircled energy relative to actual encircled energy for an aberrated system with a given obscuration and Strehl ratio changes with radius. For small radii, a better estimate of aberrated encircled energy is given by the aberration-free encircled energy scaled by the Strehl ratio. At larger radii, a better estimate of aberrated encircled energy is obtained by using the aberration-free encircled energy without any scaling by the Strehl ratio.

The results obtained for the cases studied indicate that rotationally symmetric aberrations and balanced coma have lower $\%\ Error_{NENC'}$ than $\%\ Error_{ENC'}$ over a larger range of radii than rotationally nonsymmetric aberrations. The radius for optimal estimation of encircled energies without scaling by the Strehl ratio ranges from $r_c \cong 0.8\lambda F$ (and larger) for coma, to $r_c \cong 1.1\lambda F$ (and larger) for astigmatism, and $r_c \cong$

$1.3\lambda F$ (and larger) for rotationally symmetric aberrations with no obscuration ($\varepsilon = 0$). For rotationally symmetric aberrations at large obscuration ratios, $\varepsilon \geq 0.7$, the radius increases to greater than $r_c \cong 2.5\lambda F$ (hereafter radius will be specified without the units of λF).

In terms of percentage errors, $\%\ Error_{NENC}$ is less than $\%\ Error_{ENC}$ for $\%Error_{NENC} < 11\%$, $< 25\%$, $< 43\%$, $< 67\%$, and $< 81\%$ for Strehl ratios of $S = 0.8$, 0.6, 0. ., 0.2, and 0.1 respectively (see Appendix for discussion on these percentage error values). Practically, percentage errors greater than 20% to 30% may not be of interest. Similarly, encircled energy may be of interest only within the central Airy disk except where off-axis energy rejection is a concern.

In addition to reduction of the total encircled energy in a beam by a factor equal to the fraction of obscured area of the pupil, $1-\varepsilon^2$, the increase of obscuration ratio affects the PSF and encircled energy. The radius of the central bright spot of the aberration-free PSF is slightly reduced; for example, from $r = 1.22$ at $\varepsilon = 0$ to $r = 0.81$ at $\varepsilon = 0.9$, as shown in Figure 1. The other effect is seen in the limit as the obscuration ratio approaches unity where the PSF and encircled energies of the rotationally symmetric aberrated beam become nearly identical to the aberration-free case when scaled by the Strehl ratio within the second and even the third dark ring. The normalized PSF plots for the cases of $\varepsilon = 0$ and 0.9 are shown in Figures 2 and 3 for defocus and spherical aberrations respectively. This is consistent with the effect of obscuration ratio on the Strehl ratio. Mahajan has shown that Strehl ratio increases with obscuration for rotationally symmetric aberrations and balanced coma, but decreases for astigmatism, balanced astigmatism, and coma.[13]

The results given here are a subset of all the data obtained as part of this thesis. Results for each aberration considered are given below in tabular form for $\varepsilon = 0$, 0.3

Plots for ε = 0, 0.3, 0.5, 0.7, and 0.9 are shown.

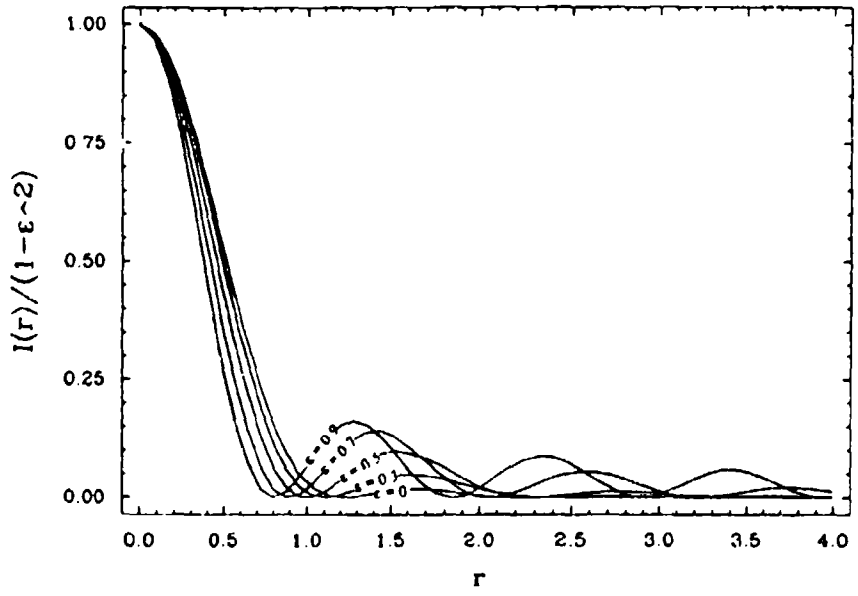

Aberration-free PSFs normalized to unity.

Figure 1.

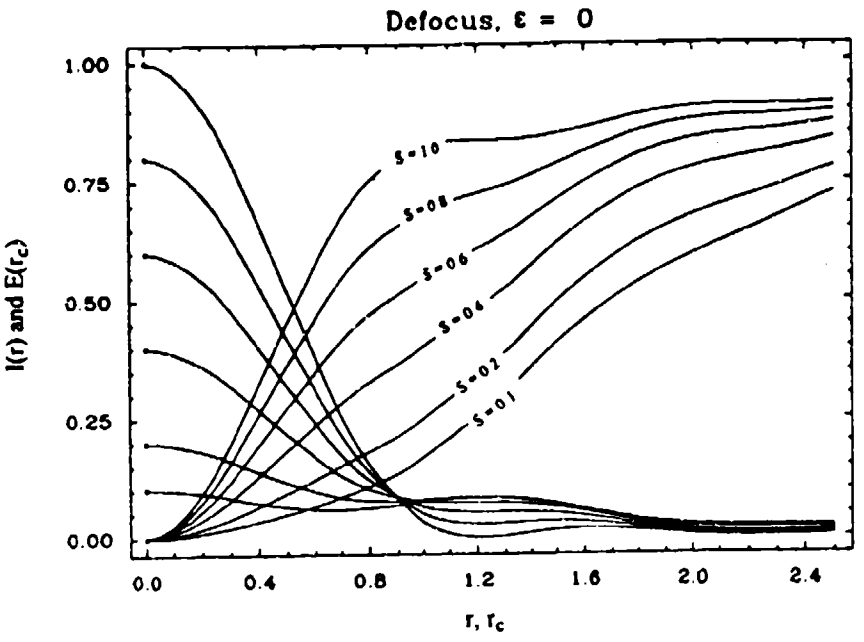

PSFs and encircled energies
Figure 2a.

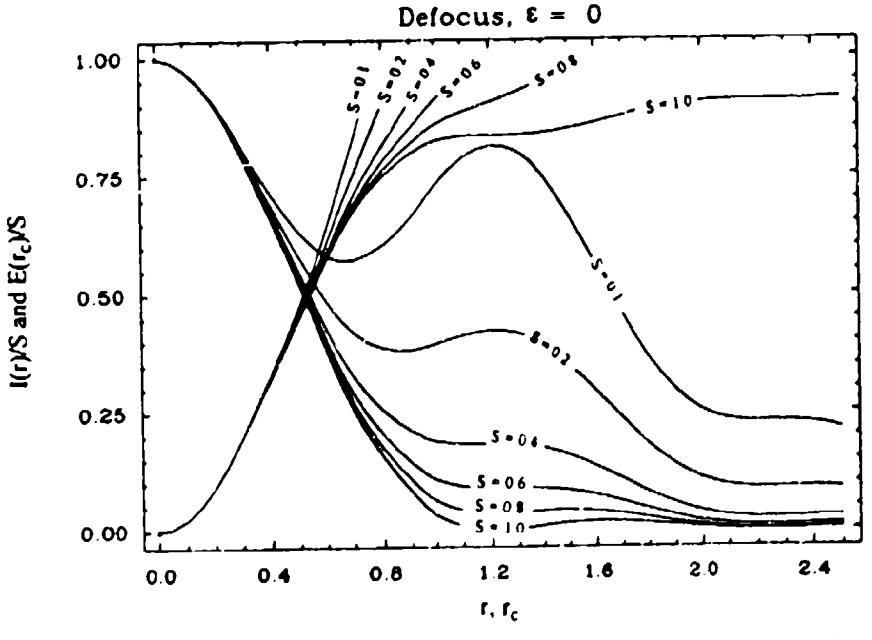

Normalized PSFs and encircled energies
Figure 2b.

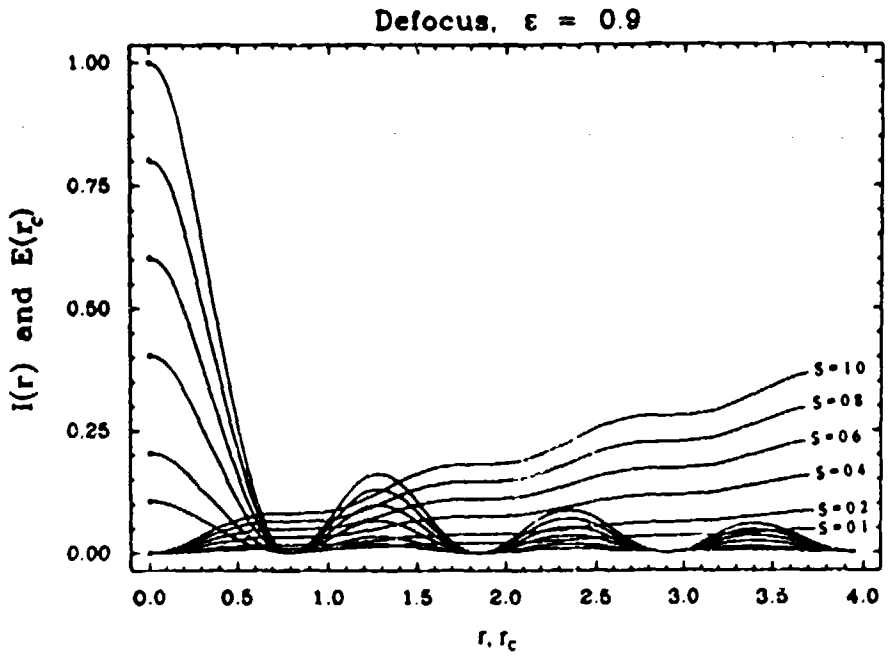

PSFs and encircled energies
Figure 2c.

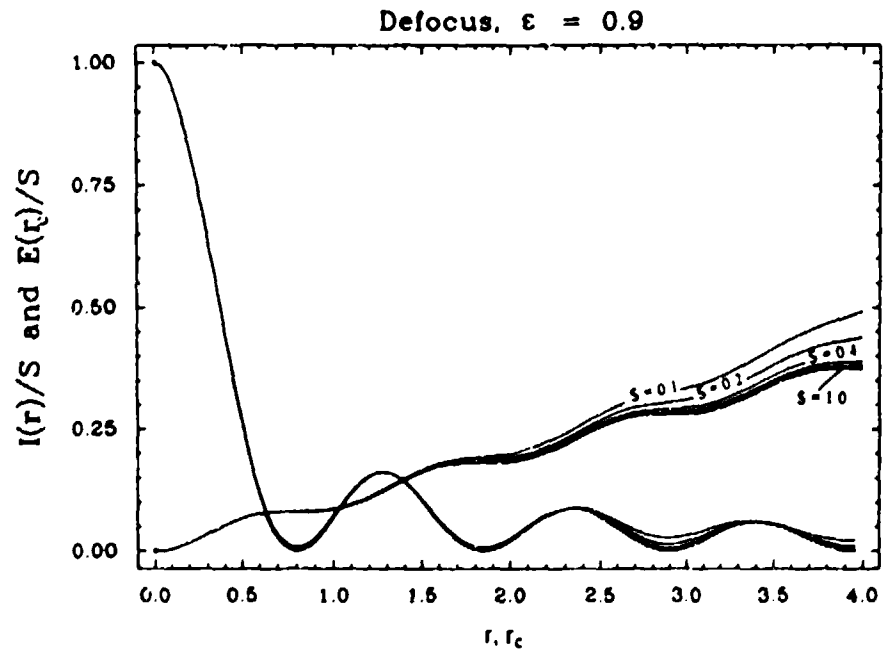

Normalized PSFs and encircled energies
Figure 2d.

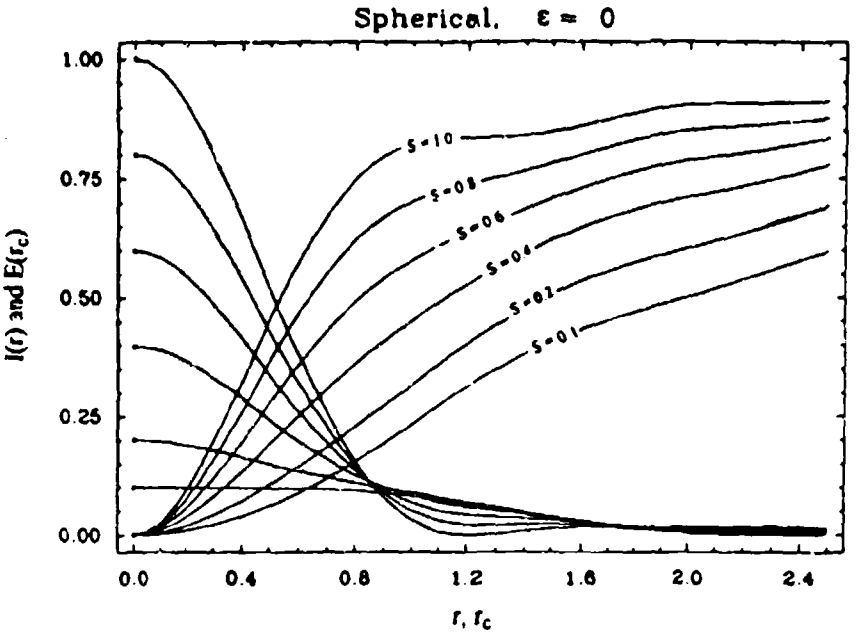

PSFs and encircled energies
Figure 3a.

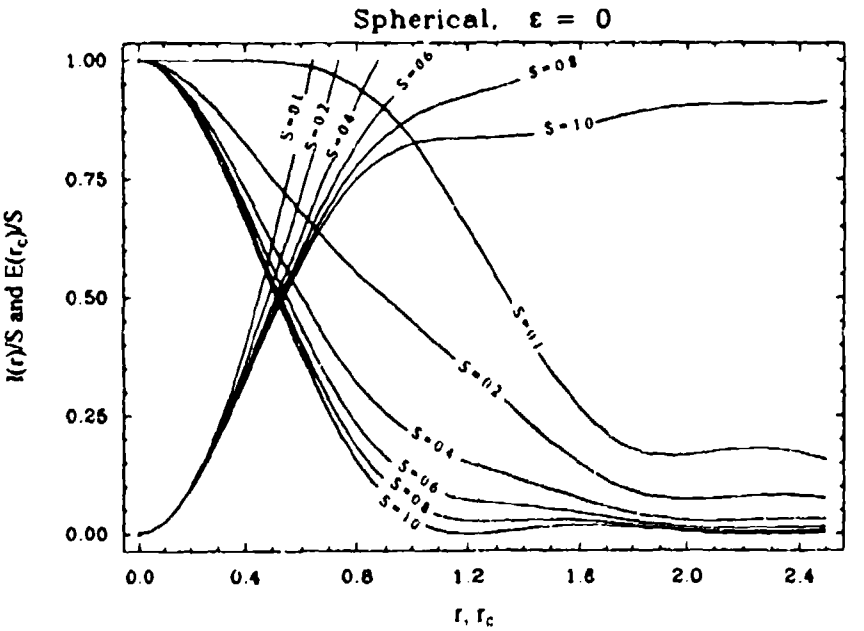

Normalized PSFs and encircled energies
Figure 3b.

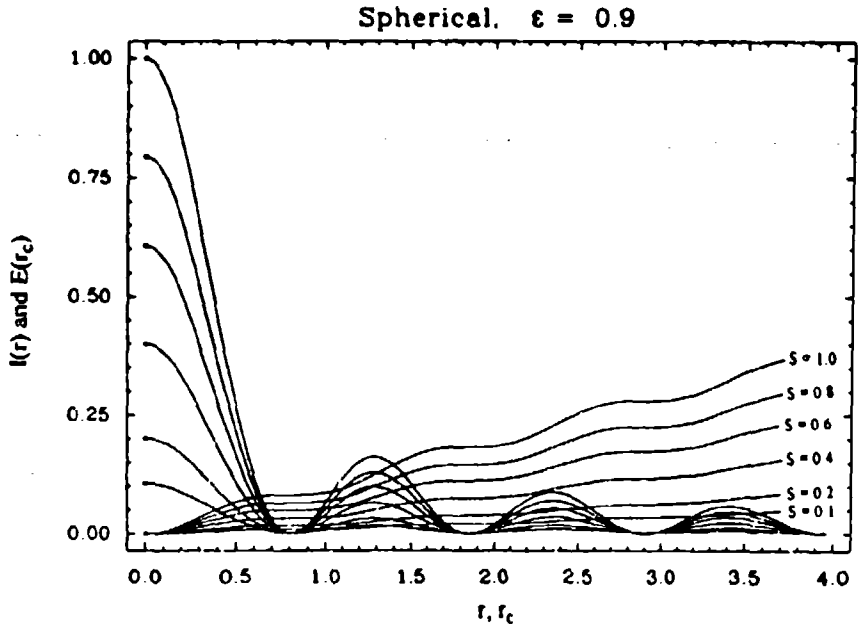

PSFs and encircled energies
Figure 3c.

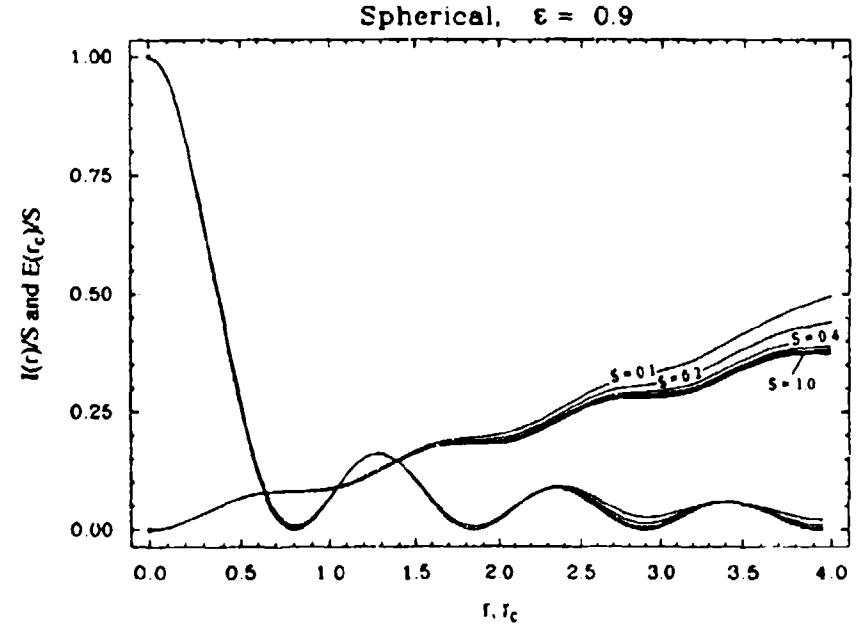

Normalized PSFs and encircled energies
Figure 3d.

0.5, and 0.7. Plots of PSFs, normalized PSFs, encircled energies, and percentage error for $\varepsilon = 0$ and 0.5 are also included in the appendix for aberrations other than defocus.

Defocus

The amount of defocus A_d was determined by using the corresponding standard deviation for defocus given in Table 1. Strehl ratios of 0.8, 0.6, 0.4, 0.2, and 0.1 were obtained for standard deviations of $\sigma_w = 0.0744\lambda$, 0.111λ, 0.145λ, 0.186λ, and 0.213λ respectively. The Strehl ratios varied by less than 1% as the obscuration was changed from $\varepsilon = 0$ to 0.9 for each corresponding value of standard deviation. That is, the Strehl ratio was held relatively constant about the desired values such that it was not necessary to change the corresponding values of σ_w. This is consistent with the Gaussian approximation, Eq. (12), where Strehl ratio is a function of only the aberration variance. This implies that A_d decreases as ε increases for $\varepsilon = 0$ to 0.9. Effectively, increasing the obscuration increases the optical tolerance. The increase in depth of focus by increasing the obscuration ratio is well known.[25]

The percentage difference between actual encircled energy for an aberrated PSF and the scaled encircled energy of an aberration-free PSF for circular pupils is as low as < 5% for $S \geq 0.1$ and $r_c \leq 0.5$.[1] For annular pupils, as the obscuration ratio increases, the model provides even better agreement as shown in Figures 4 and 5. For $\varepsilon = 0.5$, $S \geq 0.1$ and $r_c \leq 0.5$ the difference is < 4%. For $\varepsilon = 0.7$, $S \geq 0.1$ and $r_c \leq 0.5$ the difference is < 2%. The percentage error for $S \geq 0.4$ and $r_c \leq 0.8$ ranges from < 8% for $\varepsilon = 0$, < 5% for $\varepsilon = 0.5$ to < 3 % for $\varepsilon = 0.7$. The limiting case of $\varepsilon = 0.9$ has a difference of < 4% for $S \geq 0.4$ and < 14% for $S \geq 0.1$ at $r_c = 2.9$, the 3rd dark ring. The aberrated PSF thus becomes increasingly similar to the aberration-free PSF when

scaled by the Strehl ratio for $\varepsilon = 0.9$ such that even for $S = 0.1$, the percentage error is < 2% for $r_c \leq 0.81$. Plots of PSFs, encircled energies, and percentage errors are shown in Figures 2, 4, and 5 for uniformly illuminated pupils and in Figures 6 and 7 for the Gaussian illumination case. Percentage errors ($\%\ Error_{NENC}$) for a given Strehl ratio may be directly read off the plots for a specified radius (Figures 4, 5c, 6c, and 7c). Table 2 summarizes the percentage errors for $\varepsilon = 0$, 0.3, 0.5, and 0.7.

The Gaussian approximation for the Strehl ratio behaves well throughout all values of ε for the case of defocus. Percentage error is relatively unaffected by variation of ε with errors ranging from < 9% for $S \geq 0.4$ to < 29% for $S \geq 0.2$. Percentage error here is defined in Eq. (25). The percentage error varied by less than 2% for a given Strehl ratio as the obscuration changed from $\varepsilon = 0$ to $\varepsilon = 0.9$.

Spherical Aberration

As in the case of defocus, although the phase aberration and standard deviation are functions of A_i and ε, as can be seen in Table 1, the Strehl ratio is largely dependent on σ_w and not explicitly on A_i or ε. For example, in the case of spherical aberration for $\varepsilon = 0$ and $A_s = 0.25\lambda$, $\sigma_w = 0.07454\lambda$ and S = 0.8; but for $\varepsilon = 0.9$ and $A_s = 0.25\lambda$, $\sigma_w = 0.05885\lambda$ and S = 0.976. Conversely, for $\varepsilon = 0.9$ and $\sigma_w = 0.0754\lambda$, $A_s = 0.7505\lambda$ and S = 0.8. Thus the aberration tolerance increases by a factor of three for $\varepsilon = 0.9$ compared to that for $\varepsilon = 0$.

Plots of PSFs, encircled energies, normalized PSFs, normalized encircled energies, and percentage errors (as defined in Eqs. (24) and (27) above) are shown in Figures 8 and 9 (pages 55-58) for spherical aberration with a uniformly illuminated pupil. The percentage errors for the encircled energy approximation with scaling by

Table 2. Percentage Errors, $\%\ Error_{NENC}$, of Estimated Encircled Energies Relative to Actual Encircled Energies for *Defocus* With Uniform and Gaussian Illumination

	Uniform Illumination			Gaussian Illumination		
$S \geq$	$r_c \leq 0.8$	$r_c \leq 1.0$	$r_c \leq 1.2$	$r_c \leq 0.8$	$r_c \leq 1.0$	$r_c \leq 1.2$
			$\varepsilon = 0$			
0.8	2	4	8	4	5	9
0.6	4	9	16	6	12	19
0.4	8	18	30	13	22	32
0.2	16	34	50	25	39	51
			$\varepsilon = 0.3$			
0.8	1	3	6	2	4	7
0.6	4	8	14	6	10	16
0.4	6	15	26	12	19	28
0.2	15	30	45	22	35	47
			$\varepsilon = 0.5$			
0.8	1	2	4	2	3	5
0.6	2	5	10	4	7	11
0.4	5	11	18	8	14	20
0.2	10	23	34	17	28	36
			$\varepsilon = 0.7$			
0.8	1	1	1	1	2	2
0.6	1	2	3	2	3	4
0.4	2	5	7	4	7	8
0.2	5	11	15	9	14	17
0.1	9	19	25	16	24	27

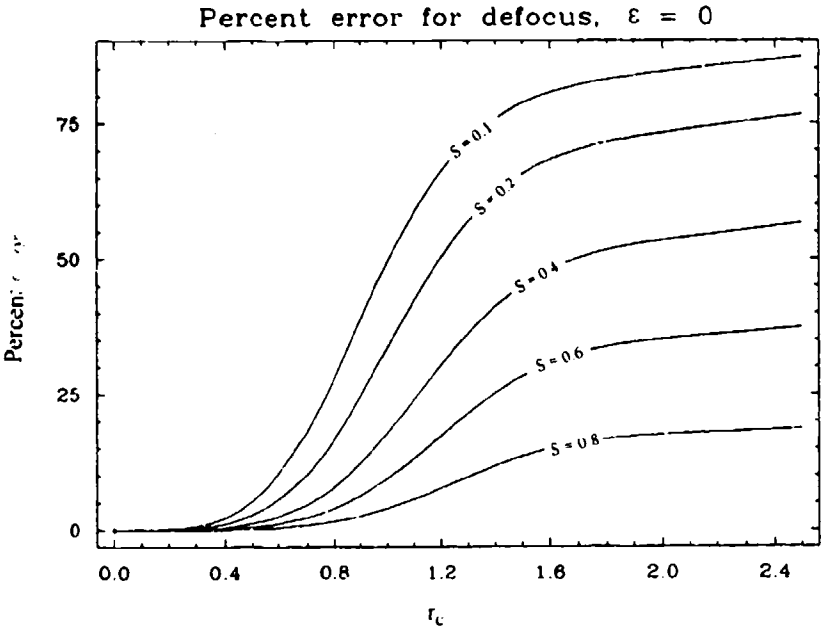

$\%Error_{NENC}$

Figure 4a.

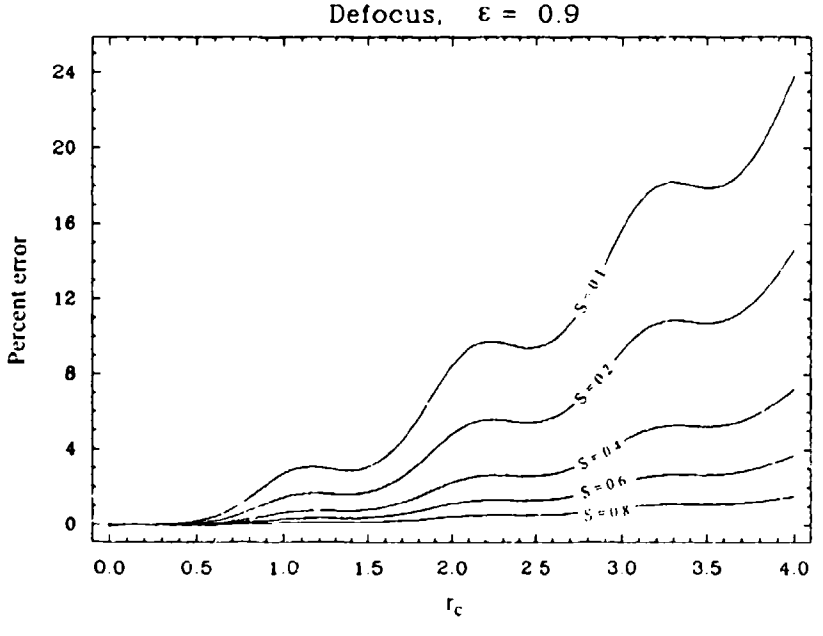

%Error

Figure 4b.

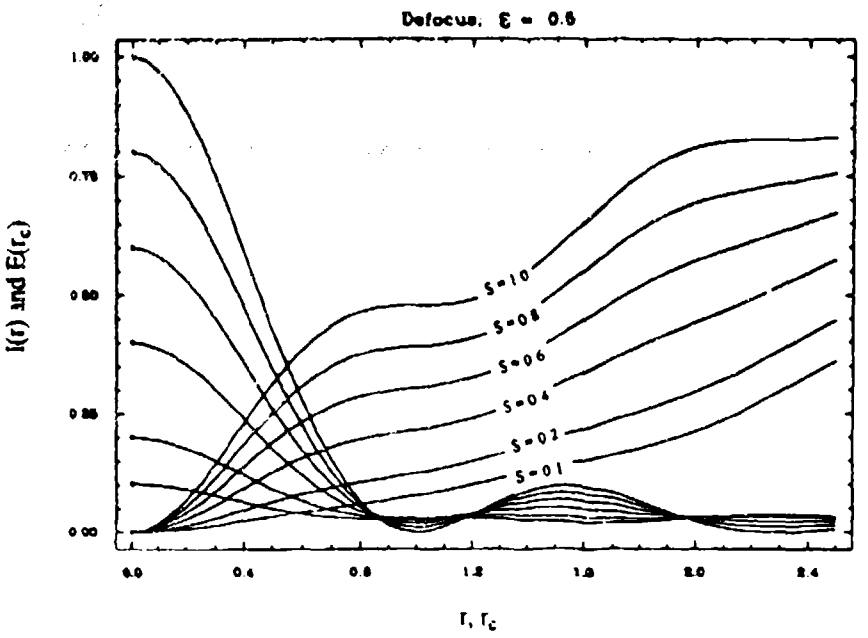

PSFs encircled energies

Figure 5a.

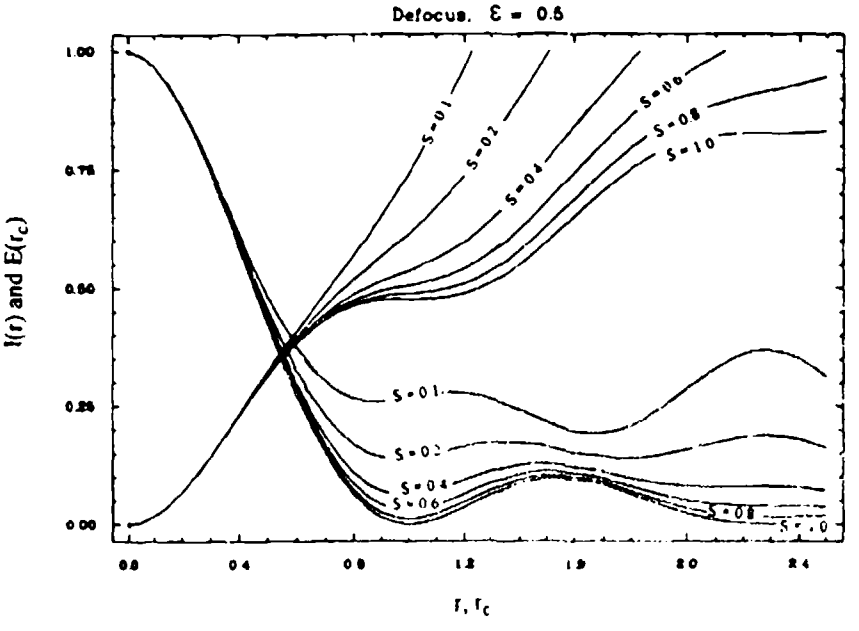

Normalized PSFs and encircled energies

Figure 5b.

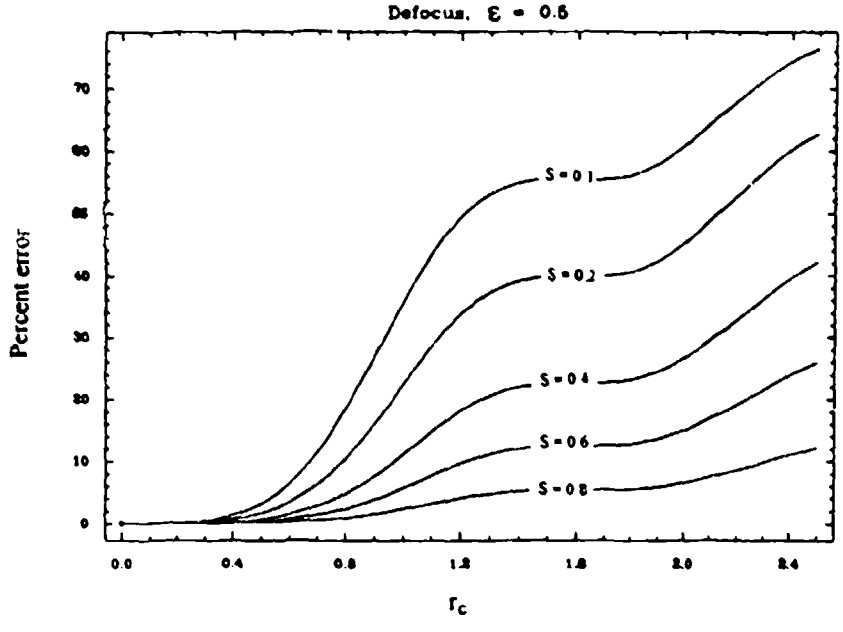

$\%Error_{NENC}$

Figure 5c.

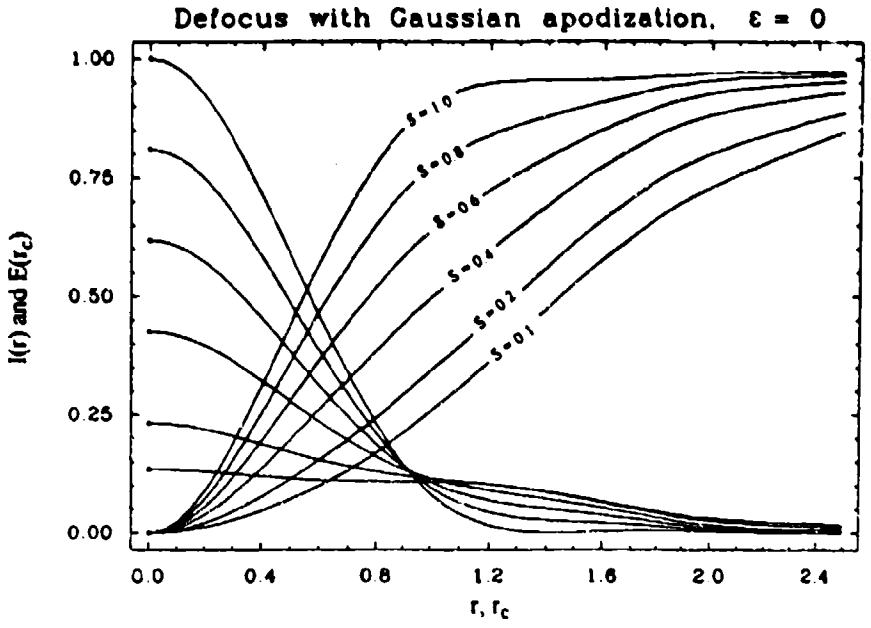

PSFs and encircled energies
Figure 6a.

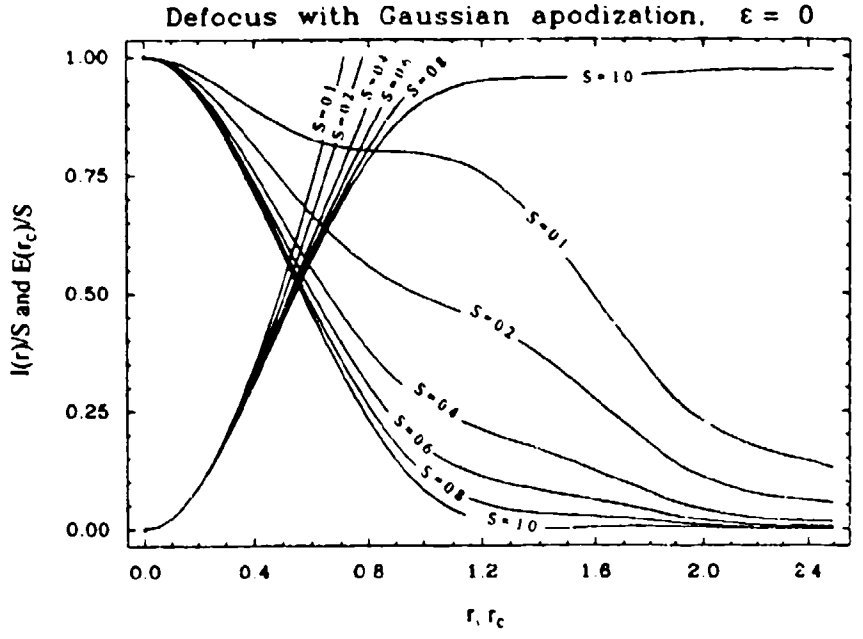

Normalized PSFs and encircled energies
Figure 6b.

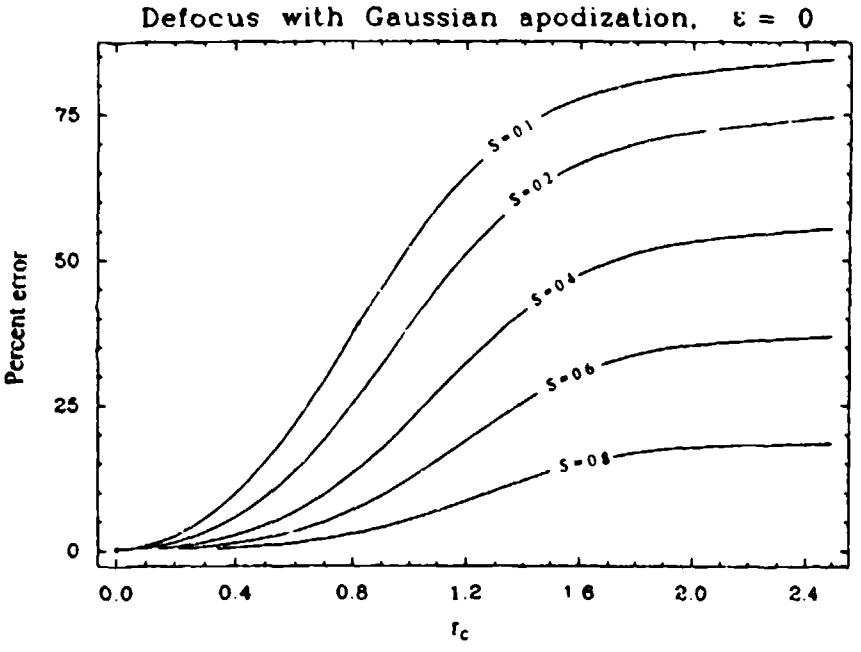

$\%Error_{NENC}$

Figure 6c.

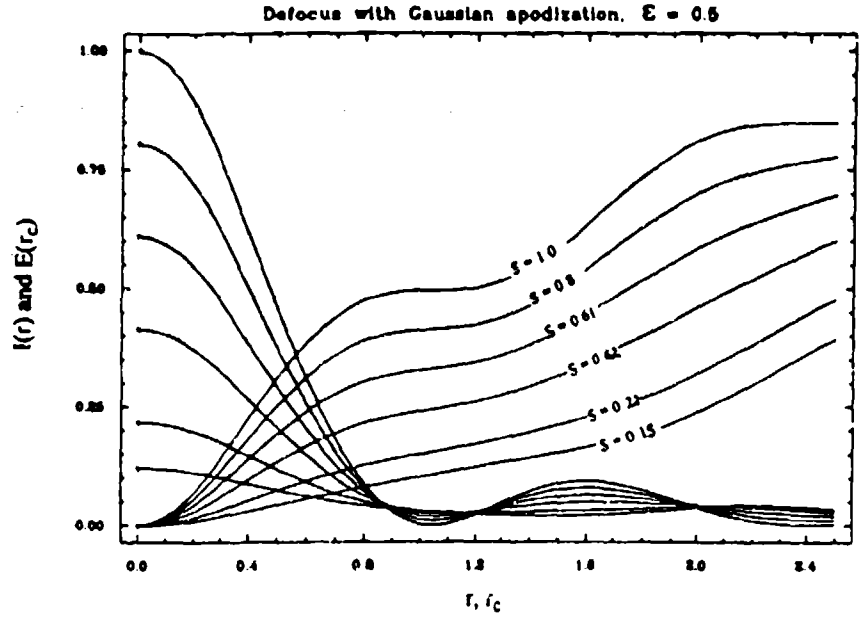

PSFs and encircled energies
Figure 7a.

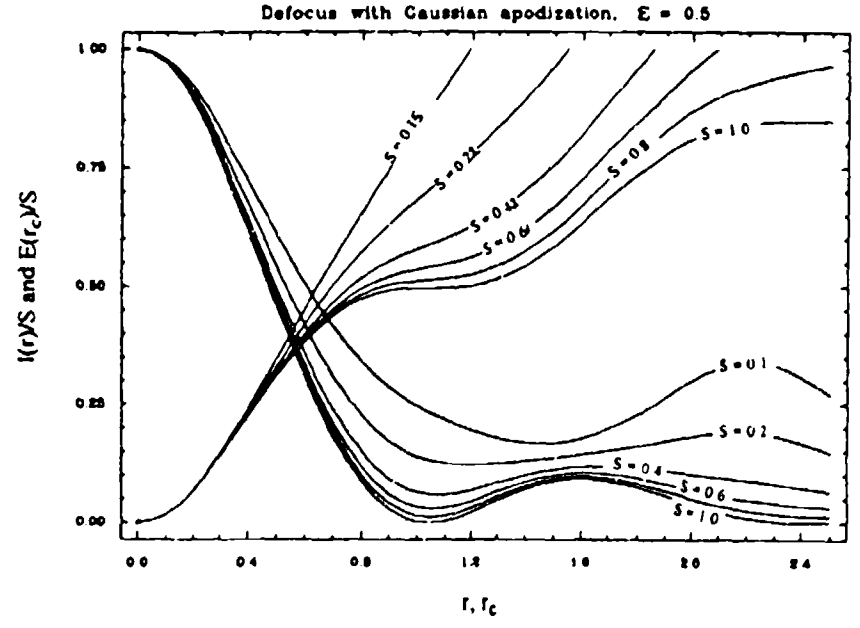

Normalized PSFs and encircled energies
Figure 7b.

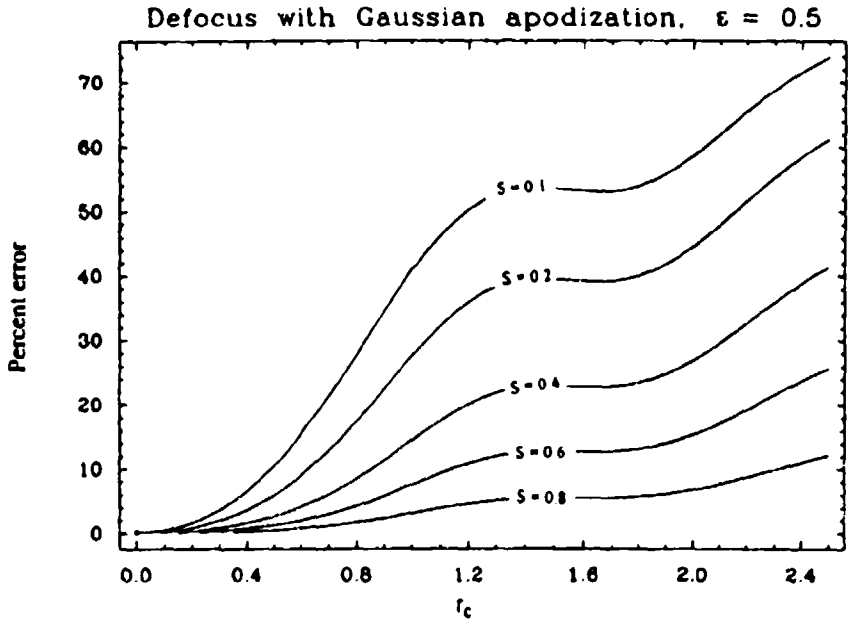

$\%Error_{NENC}$

Figure 7c.

the Strehl ratio for spherical aberration, at a radius $r_c \leq 0.8$, and with no obscuration, $\varepsilon = 0$, are < 13% for $S \geq 0.4$ and < 25% for $S \geq 0.2$. Within this same radius, but for $\varepsilon = 0.5$, the errors are < 9% for $S \geq 0.4$ and < 21% for $S \geq 0.2$. The percentage errors continue to decrease as the obscuration increases and are < 4% for $S \geq 0.4$ and < 9% for $S \geq 0.2$ at $\varepsilon = 0.7$.

The error within a radius defined by the Airy disk ($r = 1.22$) is < 38% for $S \geq 0.4$ and is <10% for $S \geq 0.8$ at $\varepsilon = 0$. The difference is < 21% for $S \geq 0.4$ and is < 5% for $S \geq 0.8$ at $\varepsilon = 0.5$ (for $r_c \leq 1.22$). Perhaps a more useful radius to compare the results for the obscured, $\varepsilon = 0.5$ case is the slightly reduced radius of the first dark ring, $r = 1.00$. The percentage errors for $r_c \leq 1.00$ are < 16% for $S \geq 0.4$ and < 3% for $S \geq 0.8$ for $\varepsilon = 0.5$.

Gaussian apodization does not have a significantly large effect on the percentage error results and tends to be within a few percent of the results for uniform illumination. The results are shown in Table 3 and in Figures 10 and 11 (pages 59-62).

Balanced Spherical Aberration

Similar results are obtained for the case of balanced spherical aberration. It can be seen from Table 1, that the balancing defocus for spherical aberration is given by $A_d = -(1+\varepsilon^2)A_s$. This amount of defocus minimizes the aberration variance and hence results in the maximum Strehl ratio for small aberrations.[26]

The σ_ϕ values for $\varepsilon = 0$ for a given Strehl ratio are the same σ_ϕ values as used for $\varepsilon = 0.9$. Furthermore, the Strehl ratios are essentially constant as ε is changed for each given σ_ϕ value. This implies that $S_g = \exp[-(2\pi\sigma_\phi)^2]$ approximates the Strehl ratio with similar results for both circular and annular pupils. The percentage error for S_g

Table 3. Percentage Errors, $\%\ Error_{NENC}$, of Estimated Encircled Energies Relative to Actual Encircled Energies for *Spherical Aberration* With Uniform and Gaussian Illumination

	Uniform Illumination			Gaussian Illumination		
$S \geq$	$r_c \leq 0.8$	$r_c \leq 1.0$	$r_c \leq 1.2$	$r_c \leq 0.8$	$r_c \leq 1.0$	$r_c \leq 1.2$
			$\varepsilon = 0$			
0.8	4	6	9	4	6	9
0.6	9	15	21	10	14	20
0.4	17	27	37	17	25	35
0.2	39	49	59	28	39	48
			$\varepsilon = 0.3$			
0.8	3	5	7	4	6	9
0.6	6	12	16	10	15	20
0.4	14	23	30	19	28	36
0.2	29	42	53	35	46	55
			$\varepsilon = 0.5$			
0.8	2	3	4	2	4	5
0.6	5	8	11	6	10	13
0.4	9	16	21	13	19	23
0.2	35	47	59	41	51	56
			$\varepsilon = 0.7$			
0.8	1	2	2	1	2	2
0.6	2	4	5	3	4	5
0.4	4	7	8	6	8	9
0.2	10	15	17	14	18	19

relative the actual Strehl ranges from 4% to 5.2% for $S = 0.4$, for an obscuration $0 \leq \varepsilon \leq 0.9$. The maximum agreement between the aberrated PSF and the aberration-free PSF scaled by the Strehl ratio is obtained for the case of balanced spherical aberration. As reported by Mahajan, for $\varepsilon = 0$, the percentage error is < 10% for $S \geq 0.1$ and $r_c \leq 1.0$.[1] The difference increases only to < 12% at $r_c \leq 1.4$. The percentage error fluctuates; it is negative for $r_c \leq 1.3$ then increases rapidly as radius increases. The difference is < 6% for $S \geq 0.2$ and < 3% for $S \geq 0.4$ at $r_c \leq 1.3$.

As in the case of spherical aberration and defocus, the model gives more and more accurate results as the obscuration increases. For $\varepsilon = 0.3$, the difference is < 8% for $S \geq 0.1$ and < 4% for $S \geq 0.2$ at $r_c \leq 1.3$. For $\varepsilon = 0.5$ and $\varepsilon = 0.7$ the difference is < 5% and < 3% respectively for $S \geq 0.1$ at $r_c \leq 1.2$. At larger radii, for $\varepsilon = 0.3$ at $r_c \leq 2.4$ the difference is < 31% for $S \geq 0.4$, and for $\varepsilon = 0.5$ the difference is < 13% for $S \geq 0.4$ at $r_c \leq 2.0$, which are the respective radii of the second dark ring. For $\varepsilon = 0.3$ the percentage difference within the third dark ring at $r = 3.22$ is < 20% for $S \geq 0.2$ and < 10% for $S \geq 0.4$. The percentage errors are summarized in Table 4. Note the error shown is the maximum within the specified radius. The plots of normalized encircled energy share a common value at $r_c \cong 1.2$ such that the percentage error at this radius is zero as is shown in Figures 12 and 13 (pages 63-70). Optimum balancing of spherical aberration with Gaussian apodization is not in general given by the same amount of defocus as for uniformly illuminated pupils. Rather, the minimum of the aberration variance is modified to include the Gaussian weighting.[9] The results with Gaussian apodization with $\gamma = 1$ are very similar to uniform illumination and are shown in Figures 12e-g and 13e-g (pages 65-66 and 69-70).

Table 4. Percentage Errors, $\%\ Error_{NENC}$, of Estimated Encircled Energies Relative to Actual Encircled Energies for *Balanced Spherical Aberration* With Uniform and Gaussian Illumination

	Uniform Illumination			Gaussian Illumination		
S ≥	$r_c \le 0.8$	$r_c \le 1.0$	$r_c \le 1.2$	$r_c \le 0.8$	$r_c \le 1.0$	$r_c \le 1.2$
			ε = 0			
0.8	0	-1	-1	1	2	2
0.6	-1	-1	-1	2	3	4
0.4	-2	-2	-3	3	3	7
0.2	-3	-5	-6	3	5	7
0.1	-6	-10	-12	-10	-12	-13
			ε = 0.3			
0.8	-1	-1	-1	1	1	2
0.6	-1	-1	-1	1	2	2
0.4	-2	-2	-2	1	2	3
0.2	-3	-4	-4	-1	-1	4
0.1	-5	-8	-8	-11	-14	-8
			ε = 0.5			
0.8	0	-1	-5	1	1	0
0.6	-1	-1	-3	1	1	1
0.4	-1	-2	-2	1	2	1
0.2	-2	-3	-3	2	2	-2
0.1	-3	-5	-5	-7	-8	-8
			ε = 0.7			
0.8	0	0	1	0	0	0
0.6	0	0	1	0	0	1
0.4	-1	-1	1	-1	-1	1
0.2	-1	-1	2	-2	-2	-2
0.1	-2	-2	3	-5	-5	-5

Rotationally Nonsymmetric Aberrations

In general, an aberrated PSF for astigmatism, balanced astigmatism, and coma when scaled by S^{-1} was substantially less in agreement with the aberration-free PSF than the rotationally symmetric aberrations. Furthermore, the agreement of the model is largely unimproved as the obscuration increases. This is consistent with the effect of a change in obscuration ratio on the Strehl ratio for astigmatism, balanced astigmatism, and coma which has been reported.[13] The Strehl ratio for a given amount of aberration decreases as obscuration increases for these three aberrations. Note that the PSFs and normalized PSFs considered here are plotted along the $\theta_i = 0$ axis for which the effects of small astigmatism and coma aberrations are most apparent (assuming cosθ terms in the aberration and no sinθ terms).

Astigmatism

The percentage difference at $r_c \leq 0.8$ and $\varepsilon = 0$ is < 5% for $S \geq 0.8$, < 11% for $S \geq 0.6$, and < 20% for $S \geq 0.4$. The error does not change by more than 2% for larger obscurations up to $\varepsilon = 0.7$ within the radius of $r_c \leq 0.8$. The error more than doubles at $r_c \leq 1.2$ and is < 11% for $S \geq 0.8$, < 25% for $S \geq 0.6$, and < 52% for $S \geq 0.4$ at $\varepsilon = 0$ and fluctuates by 5% as the obscuration increases ($S = 0.8$) and up to 12% ($S = 0.4$) for obscurations $\varepsilon \leq 0.7$. Thus, although the percentage error does not change considerably with a change in obscuration ratio, the model has a limited applicability to large Strehl ratios of about $S \geq 0.4$ for errors in the order of 20% or less at a radius $r_c \leq 0.8$. Plots of PSFs, normalized PSFs, encircled energies, and percentage error are shown in Figures 14 and 15 (pages 71-74) for uniform illumination and Figures 16 and 17 (pages 75-78) for Gaussian illumination.

Alternatively, the percentage differences between the actual encircled energies of aberrated and aberration-free PSFs without normalization by the Strehl ratio provide a better estimate for radii $r_c \geq 1.2$. For $\varepsilon = 0$ at $r_c = 1.2$, the percentage differences (now defined in Eq. (27) and are negative) between actual aberrated and aberration-free encircled energies are 10%, 25%, 50%, and 450% for $S = 0.8$, 0.6, 0.4, and 0.2, respectively. The error drops to 3%, 5%, 14%, and 37% for the same respective Strehl ratios at $r_c = 2.0$. At $r_c \geq 3.0$, the percentage difference for $S \geq 0.2$ is < 9%. Table 5 summarizes the results.

Since one of the effects of an annular pupil is to increase the energy in the outer regions relative to the energy within the Airy disk, it is to be expected that for larger obscurations, the encircled energies do not converge as rapidly. For $\varepsilon = 0.3$ at $r_c = 2.0$ the percentage differences are 4%, 12%, 22%, and 42% for $S = 0.8$, 0.6, 0.4, and 0.2 respectively. The encircled energies at $r_c \geq 3.0$ converge to the same percentage differences as for $\varepsilon = 0$, < 5%. The results for $\varepsilon = 0.5$ are within 2% of the values for $\varepsilon = 0.3$ at $r_c \geq 2.0$. The most significant difference for $\varepsilon = 0.5$ is that the $S = 0.1$ case is within 27% of the aberration-free encircled energy for radius of $r_c = 3.0$. The percentage differences for $\varepsilon \geq 0.7$ at $r_c = 2.0$ are 3%, 8%, 16%, and 28% for $S = 0.8$, 0.6, 0.4, and 0.2 respectively. For the highly obscured case of $\varepsilon = 0.9$, the percentage difference is < 10% for $S \geq 0.1$ at a radius of $r_c \geq 2.1$.

Although encircled energies at regions greater than the Airy disk may not be of interest in some applications, some useful generalizations can be made in the case of astigmatism. The region where a better estimate of encircled energy is obtained by using actual aberration-free encircled energy rather than that scaled by the Strehl ratio is a radius of $r_c \geq 1.2$ for $S \geq 0.6$. The same is true for a radius of $r_c \geq 1.3$ for $S \geq 0.4$

Table 5. Percentage Errors, $\%\ Error_{NENC}$, of Estimated Encircled Energies Relative to Actual Encircled Energies for *Astigmatism* With Uniform and Gaussian Illumination

	Astigmatism Uniform Illumination			Astigmatism Gaussian Illumination		
$S \geq$	$r_c \leq 0.8$	$r_c \leq 1.0$	$r_c \leq 1.2$	$r_c \leq 0.8$	$r_c \leq 1.0$	$r_c \leq 1.2$
			$\varepsilon = 0$			
0.8	5	9	11	5	8	11
0.6	11	17	25	12	18	25
0.4	20	30	52	20	30	39
0.2	33	46	57	22	35	40
			$\varepsilon = 0.3$			
0.8	4	8	12	5	8	11
0.6	10	17	25	11	17	24
0.4	18	29	40	19	28	38
0.2	32	46	58	24	37	49
			$\varepsilon = 0.5$			
0.8	4	9	13	5	9	14
0.6	10	19	27	10	19	28
0.4	18	31	42	17	29	41
0.2	32	49	62	36	54	63
			$\varepsilon = 0.7$			
0.8	5	10	16	5	11	16
0.6	11	24	34	11	23	33
0.4	21	39	50	20	38	50
0.2	39	60	70	36	58	72

and $r_c \geq 1.5$ for $S \geq 0.2$. These regions are valid for all cases of obscuration ratios ε = 0 to $\varepsilon = 0.9$ as shown in Figures 14d and 15d (pages 72 and 74).

Balanced Astigmatism

The results obtained for balanced astigmatism are similar to astigmatism. Here, balanced astigmatism is defined as astigmatism with a balancing defocus, where $A_d = -\frac{1}{2} A_a$ is introduced into the aberration. The percentage errors given in Table 6 refer to the percentage difference between actual encircled energies of aberrated PSF and aberration-free encircled energy scaled by the Strehl ratio. For $\varepsilon = 0$, the errors within $r_c \leq 0.8$ are < 6%, <13%, and < 23% for $S \geq 0.8$, 0.6, and 0.4, respectively. At $r_c \leq 1.2$ the errors are < 14% for $S \geq 0.8$ and < 28% for $S \geq 0.6$. The percentage errors for $\varepsilon = 0.3$ are the same as at $\varepsilon = 0$ with the exception that for $S \geq 0.6$ and $S \geq 0.4$ the error is < 12% and < 22% respectively at $r_c \leq 0.8$. Similarly, the percentage errors are within 2% of values at $\varepsilon = 0$ for $\varepsilon = 0.5$. For $\varepsilon = 0.7$ the percentage errors are different than $\varepsilon = 0$ only for $r_c \leq 1.2$ and are < 16% and < 34% for $S \geq 0.8$ and $S \geq 0.6$ respectively. The results are summarized in Figures 18 through 21 (pages 79-86) and Table 6 for uniform illumination and Gaussian illumination with a truncation factor of $\gamma = 1$.

Following the same approach as astigmatism above, the percentage difference of encircled energy for an aberrated PSF relative to an aberration-free PSF without scaling by the Strehl ratio is significantly less than that scaled by the Strehl ratio at larger radii. The percentage differences of actual encircled energies relative to aberration-free encircled energy for $\varepsilon = 0$, are < 2%, < 4%, < 7%, and < 13% for $S \geq$ 0 8, 0.6, 0.4, and 0.2 respectively at a radius $r_c \geq 2.0$. For $\varepsilon = 0.3$ and $\varepsilon = 0.5$ at $r_c \geq$ 2.0 the differences are < 3%, < 7%, < 13%, and < 24% for the same values of Strehl

Table 6. Percentage Errors, $\%\ Error_{NENC}$, of Estimated Encircled Energies Relative to Actual Encircled Energies for *Balanced Astigmatism* With Uniform and Gaussian Illumination

	Balanced Astigmatism Uniform Illumination			Balanced Astigmatism Gaussian Illumination		
S ≥	$r_c \leq 0.8$	$r_c \leq 1.0$	$r_c \leq 1.2$	$r_c \leq 0.8$	$r_c \leq 1.0$	$r_c \leq 1.2$
			ε = 0			
0.8	6	10	14	6	9	12
0.6	13	20	28	14	20	26
0.4	23	34	44	23	33	41
0.2	38	52	64	36	50	60
			ε = 0.3			
0.8	5	9	14	5	9	14
0.6	12	20	27	12	19	26
0.4	22	33	44	21	31	41
0.2	36	51	64	35	49	60
			ε = 0.5			
0.8	5	9	14	5	9	14
0.6	10	20	30	10	19	28
0.4	20	34	46	19	32	44
0.2	35	54	66	33	51	65
			ε = 0.7			
0.8	5	11	16	5	10	16
0.6	11	24	34	11	29	34
0.4	22	40	52	21	39	51
0.2	40	61	73	39	60	71

ratio. For $\varepsilon = 0.7$ the percentage differences are slightly improved: < 3%, < 6%, < 11%, and < 19%. At a smaller radius of $r_c \geq 1.2$ the percentage differences are < 8% and < 20 % for $S \geq 0.8$ and $S \geq 0.6$ respectively, for all obscurations $0 \leq \varepsilon \leq 0.9$, which is a smaller error than that obtained with the scaled encircled energies considered above.

Coma

A coma aberration is known to cause a line of sight error which is essentially a shift of the centroid of the PSF away from the central axis.[26] Although Mahajan has shown that the peak and centroid of the PSF are not coincident for an aberrated system, the peak also shifts with a coma aberration, $\rho^n \cos\theta$, as well as any Zernike aberration with $R_n^1(\rho)\cos\theta$ terms were n is an odd integer.[26] Given that the peak of the PSF is displaced from the origin, the Strehl ratio does not describe the maximum value of the PSF, but rather the irradiance at the center. For example, for an aberration of $A_c = 0.81\lambda$ and an obscuration ratio of $\varepsilon = 0$, the Strehl ratio is $S = 0.10$ whereas the maximum value of the PSF is 0.7 (normalized to the $\varepsilon = 0$, aberration-free PSF) and is located a distance $r = 1.05$ away from the central axis. For an obscuration of $\varepsilon = 0.9$ and an aberration of $A_c = 0.34\lambda$, the Strehl ratio is still $S = 0.10$ although the PSF maximum is 0.99 (normalized to the $\varepsilon = 0.9$, aberration-free PSF) and is located at a distance $r = 0.60$ away from the center. It has been reported that the distance of the peak from the origin increases monotonically with A_c up to $A_c \cong 1.6\lambda$ for $\varepsilon = 0$ and up to $A_c \cong 2.5\lambda$ for $\varepsilon^2 = 0.5$, but fluctuates for larger aberrations.[26]

For a given value of aberration variance, as the obscuration ratio increases, the Strehl ratio decreases. Conversely, the peak of an aberrated PSF increases, relative to

Table 7. Percentage Errors for *Coma*, With and Without Strehl Ratio Scaling, for Uniform Illumination. Note That Results With Gaussian Apodization Are Within 2% of the Values Given Below

	$\%Error_{NENC}$			$\%Error_{ENC}$	
S ≥	$r_c \leq 0.8$	$r_c \leq 1.2$	$r_c \geq 1.2$	$r_c \geq 2.0$	$r_c \geq 2.5$
		ε = 0			
0.8	11	18	4	3	1
0.6	24	36	8	5	2
0.4	37	53	17	10	3
		ε = 0.3			
0.8	12	18	5	5	1
0.6	25	37	12	10	2
0.4	38	54	20	18	4
		ε = 0.5			
0.8	13	21	6	4	2
0.6	27	40	13	9	3
0.4	43	58	23	22	5
		ε = 0.7			
0.8	16	23	5	3	3
0.6	33	43	12	7	7
0.4	50	62	8	10	10

an aberration-free PSF, with the obscuration ratio for a given value of aberration variance. Additionally, the width of the PSF, or the "spot size," was relatively unchanged for a given obscuration ratio for the aberration considered ($S \geq 0.1$) as shown in Figures 22a and 23a (pages 87 and 89). This suggests that with an optimal amount of tilt introduced, the model presented in this thesis provides high accuracy for balanced coma aberration. Just as in the case of astigmatism and balanced astigmatism above, the percentage error of the encircled energy of the aberration-free beam scaled by the Strehl ratio relative to the actual encircled energies of a beam aberrated with coma are considerably larger than the results obtained for rotationally symmetric aberrations. For $S \geq 0.8$ at $r_c \leq 0.8$ the error is < 11% for $\varepsilon = 0$ and increases steadily to < 16% for $\varepsilon = 0.7$. Similarly, for $S \geq 0.6$ at $r_c \leq 0.8$ the error is < 24% for $\varepsilon = 0$ and increases to < 33% at $\varepsilon = 0.7$. The plots for PSFs, normalized PSFs, encircled energies, and percentage error are shown in Figures 22 through 25 (pages 87-94). The percentage errors are summarized in Table 7.

Balanced Coma

For balanced coma, the amount of balancing tilt for uniform illumination is given by

$$A_t = -\frac{2}{3}\frac{(1+\varepsilon^2+\varepsilon^4)}{1+\varepsilon^2}A_c \qquad (28)$$

as can be seen from the phase aberration in Table 1. As with balanced spherical aberration, A_t is determined such that aberration variance is a minimum (which is affected by Gaussian apodization as before). This amount of tilt maximizes the Strehl ratio for small aberrations, $A_c \leq 0.7\lambda$.[26] The tilt, given by $\beta = A_t \quad a$ where a is the

outer radius of the pupil in units of waves, is the amount of angular or pointing compensation for the line of sight error due to coma.

In general, for the cases studied, the effect of introducing a tilt given by Eq. (28) was consistent in over-correcting the effect of coma and shifting the peak beyond the origin (in the opposite direction as the original coma) for larger aberrations. This can be seen in Figures 26b and 27b (pages 95 and 97). The maximum value of the PSF is centered at the origin (within the sampling resolution where the sample size is $0.05\lambda F$) for Strehl ratios $S \geq 0.8$ which corresponds to $A_c = 0.64\lambda$. It is evident that at Strehl ratios less than $S = 0.8$ the amount of tilt given by Eq. (28) does not maximize the Strehl ratio for $\varepsilon = 0$. At larger obscuration ratios, the tilt given in Eq. (28) more effectively balances the coma by moving the peak of the PSF closer to the center for larger amounts of coma aberration. At $\varepsilon = 0.7$, A_t given in Eq. (28) centers the peak of the PSF for $S \geq 0.4$ which is for a coma of $A_c = 1.71\lambda$.

Unlike the rotationally symmetric aberrations discussed above, the percentage errors for balanced coma do not change considerably (< 4% for $S \geq 0.2$) as the obscuration ratio increases for radii $r_c \leq 1.2$. For larger radii, however, the errors decrease as obscuration increases such that at $\varepsilon = 0.7$, the error is approximately one-half that at $\varepsilon = 0$ at radii $r_c \geq 1.65$ (error for $S = 0.4$ is 21% at $\varepsilon = 0.7$). The percentage errors obtained are comparable to rotationally symmetric aberrations as shown in Figures 26 through 29 (pages 95-102). The percent errors are given in Table 8. At $r_c \leq 0.8$ and $\varepsilon = 0$ the errors are < 9% for $S \geq 0.2$ and < 18% for $S \geq 0.1$. At $r_c \leq 0.8$ and $\varepsilon = 0.3$ and $\varepsilon = 0.5$ the errors are < 7% for $S \geq 0.2$ and < 17% at $S \geq 0.1$. The errors increase somewhat for $\varepsilon = 0.7$, being < 10% and < 24% for $S \geq 0.2$ and $S \geq 0.1$ respectively. Results for the Gaussian illumination case are approximately double the percentage errors as for the uniform illumination case at radius $r_c \leq 0.8$ but are

Table 8. Percentage Errors, $\%\ Error_{NENC}$, of Estimated Encircled Energies Relative to Actual Encircled Energies for *Balanced Coma Aberration* With Uniform and Gaussian Illumination

	Uniform Illumination			Gaussian Illumination	
$S \geq$	$r_c \leq 0.8$	$r_c \leq 1.2$		$r_c \leq 0.8$	$r_c \leq 1.2$
			$\varepsilon = 0$		
0.8	1	4		2	5
0.6	2	9		5	12
0.4	4	18		9	23
0.2	9	37		18	42
0.1	18	55		28	58
			$\varepsilon = 0.3$		
0.8	1	3		2	4
0.6	1	8		4	11
0.4	2	18		7	22
0.2	7	38		15	43
0.1	16	59		28	63
			$\varepsilon = 0.5$		
0.8	1	3		2	4
0.6	1	8		3	9
0.4	2	18		7	20
0.2	7	40		15	43
0.1	17	60		28	64
			$\varepsilon = 0.7$		
0.8	1	2		3	3
0.6	1	7		5	7
0.4	3	16		9	16
0.2	10	40		17	38
0.1	24	61		31	60

only slightly larger than uniform illumination at a radii of $r_c \approx 1.2$.

Mixed Aberrations

So far we have discussed the PSFs aberrated by a single primary aberration. Now we briefly consider examples of mixed aberrations. A mixture of spherical, astigmatism, and coma was studied, as well as a mixture of spherical, astigmatism, coma, and defocus. The balancing defocus that was introduced is the same as used for optimally balanced spherical aberration, namely, $A_d = -(1+\varepsilon^2)A_s$, which minimizes the aberration variance of spherical aberration only. The same standard deviation of aberration was used to calculate the respective aberrations; thus, the magnitudes of each type of aberration was not equal. For example, for a Strehl ratio of $S = 0.1$, a peak aberration of $A_s = 1.5\lambda$, $A_d = -1.5\lambda$, $A_c = 1.3\lambda$, and $A_a = 1.8\lambda$ was used. The PSFs, encircled energies, and percentage error plots are shown in Figures 30 and 31 (pages 103-106) for the aberration mixture without defocus and in Figures 32 and 33 (pages 107-110) for the mixture with defocus. The percentage errors of the encircled energy of the aberration-free PSF scaled by the Strehl ratio relative to the actual encircled energy of the aberrated PSF are shown in Table 9. Note the percentage errors are very comparable to errors for cases of the other rotationally nonsymmetric aberrations, with the exception of balanced coma which behaved similar to the rotationally symmetric aberrations.

Table 9. Percentage Errors, $\%\ Error_{NENC}$, of Estimated Encircled Energies Relative to Actual Encircled Energies for Mixed Aberrations With Uniform Illumination

Spherical, Coma, Astigmatism				Spherical, Coma, Astigmatism, & Defocus			
S ≥	$r_c \leq 0.8$	$r_c \leq 1.0$	$r_c \leq 1.2$	S ≥	$r_c \leq 0.8$	$r_c \leq 1.0$	$r_c \leq 1.2$
ε = 0				**ε = 0**			
0.87	4	5	8	0.8	9	12	15
0.64	11	17	23	0.6	17	24	28
0.43	20	29	36	0.4	20	28	35
0.20	29	41	50	0.2	28	40	50
0.09	44	58	67	0.1	35	50	62
ε = 0.3				**ε = 0.3**			
0.87	4	5	7	0.8	8	12	15
0.64	11	16	20	0.6	18	25	30
0.42	20	28	35	0.4	24	32	39
0.19	27	37	45	0.2	30	43	54
0.08	40	54	64	0.1	39	55	66
ε = 0.5				**ε = 0.5**			
0.87	4	5	6	0.8	9	14	16
0.65	10	16	20	0.6	20	28	34
0.42	20	28	34	0.4	31	42	49
0.17	24	34	41	0.2	35	49	60
0.07	31	45	55	0.1	44	59	70
ε = 0.7				**ε = 0.7**			
0.88	5	8	9	0.8	11	16	19
0.66	12	18	22	0.6	24	34	37
0.42	23	33	37	0.4	39	50	55
0.13	32	43	49	0.2	46	62	71
0.05	34	46	51	0.1	55	67	72

CHAPTER 4

DISCUSSION AND CONCLUSIONS

The aberrated point-spread function and encircled energy, may be approximated within the central Airy disk for both circular and annular pupils for each of the primary and balanced primary aberrations using the aberration-free PSF normalized by the Strehl ratio. The range of spot radii that may be used in this approximation depends on the amount and type of the aberration. The effect of a central obscuration on the accuracy of the model also depends on the type of aberration. For defocus, spherical, balanced spherical, and balanced coma aberrations, an increase in obscuration ratio improves the accuracy of the model (i. e., the percentage error decreases). An increase in obscuration ratio has little effect on accuracy for astigmatism and balanced astigmatism for $S \geq 0.4$ and tends to increase the percentage error for smaller Strehl ratios. Coma without a balancing tilt is the only aberration for which the accuracy of the model degrades significantly with an increase in obscuration ratio. With the exception of coma and balanced astigmatism, the percentage error of the estimated encircled energy relative to the actual value is no greater than 20% for Strehl ratios $S \geq 0.4$ at spot radii $r_c \leq 0.8\ \lambda F$.

The model accuracy is maintained for the mixed aberrations of spherical, astigmatism, and coma at $r_c \leq 0.8\ \lambda F$, with slightly better accuracy than for other rotationally nonsymmetric, single aberrations (except balanced coma). Mixed aberrations with a balancing defocus have larger percentage error than mixed

aberrations without defocus, by nearly double the amount. Even with defocus, however, the percentage errors are lower than coma aberration without balancing tilt.

The effect of a Gaussian apodization (with $1/e^2$ irradiance at the edge of the pupil compared to its central value in the absence of obscuration) was to degrade the accuracy of the model for balanced coma to approximately twice the error obtained for the case of uniform illumination for radii $r_c \leq 0.8\ \lambda F$ but was within 5% of uniform illumination results at $r_c \approx 1.2\ \lambda F$. Gaussian apodization results for astigmatism, balanced astigmatism, coma, and the rotationally symmetric aberrations were within 5% of the results obtained for uniform illumination for Strehl ratios $S \geq 0.4$ and for radii $r_c \leq 1.0\ \lambda F$.

The applicability of the model over a given radii is directly affected by how the actual encircled energies of aberrated optical systems converge to the aberration-free encircled energy as the radius of the spot increases. The asymptotic behavior depends on the type of the aberration and obscuration ratio. The radii for which a better estimate of encircled energy is obtained (i. e., less percentage error) by using the actual aberration-free encircled energy rather than the aberration-free encircled energy scaled by the Strehl ratio ranges from $r_c > 0.8\ \lambda F$ for coma without tilt to $r_c > 1.2\ \lambda F$ for astigmatism, balanced astigmatism, balanced coma, defocus ($\varepsilon < 0.5$), and spherical ($\varepsilon < 0.5$) aberrations. For balanced spherical and other rotationally symmetric aberrations (at large obscuration ratios, $\varepsilon > 0.5$), actual encircled energies converge much more slowly, and the encircled energy is better estimated with the aberration-free encircled energy scaled by the Strehl ratio out to radii of at least the second and even third dark ring.

The behavior of balanced coma and rotationally symmetric aberrations at large obscuration ratios results in a high degree of model accuracy when the encircled

energy is estimated using the aberration-free encircled energy scaled by the Strehl ratio of the aberrated PSF. This effect can be understood intuitively by analyzing the behavior of the aberration variance of these aberrations in the limit of $\varepsilon \rightarrow 1$ (see Table 1). Note that unlike the other aberrations (astigmatism, balanced astigmatism, and coma) the aberration variance equals zero when the obscuration approaches unity. The effect of the aberration then tends to scale the central region of the PSF by the Strehl ratio but otherwise does not disturb the PSF in this central region. This approach to predicting the behavior cannot, however, hold true as the radius increases to large values because of the asymptotic behavior of all aberrations wherein the encircled energy of even a highly obscured, aberrated beam must eventually converge to the aberration-free encircled energy (i. e., the total energy).

Areas where future work may be worthwhile include revisiting the Szapiel approach of modifying the basic equation for the model, Eq. 21, to account for aberrations that tend to spread the spot radii. An attempt to simplify the determination of such a factor could permit application of the model described in this thesis with a simple adjustment that would be used for certain aberrations (such as defocus and spherical aberration at low obscuration ratios and rotationally nonsymmetric aberrations).

REFERENCES

REFERENCES

1. V. N. Mahajan, "Aberrated point-spread functions for rotationally symmetric aberrations," Appl. Opt. **22**, 3035-3041 (1983).

2. S. Szapiel, "Aberration-variance-based formula for calculating point-spread functions: rotationally symmetric aberrations," Appl. Opt. **25**, 244-251(1986).

3. M. Born and E. Wolf, *Principles of Optics* (Pergamon, New York, 1980), p. 460.

4. See Ref. 3, p. 461.

5. V. N. Mahajan, *Aberration Theory Made Simple* (SPIE Optical Engineering Press, Bellingham, Washington, 1991), p. 70.

6. See Ref. 3, p. 211.

7. See Ref. 3, p. 11.

8. See Ref. 3, p. 464.

9. V. N. Mahajan, "Zernike annular polynomials for imaging systems with annular pupils," J. Opt. Soc. Am. **71**, 75-85 (1981) and **71**, 1408 (1981).

10. See Ref. 3, p. 467.

11. V. N. Mahajan, "Uniform versus Gaussian beams: a comparison of the effects of diffraction, obscuration, and aberrations," J. Opt. Soc. Am. A**3**, 470-485 (1986).

12. See Ref. 5, p. 76.

13. V. N. Mahajan, "Strehl ratio for primary aberrations: some analytical results for circular and annular pupils," J. Opt. Soc. Am. **72**, 1258-1266 (1982).

14. S. Szapiel, "Aberration-balancing technique for radially symmetric amplitude distributions: a generalization of the Maréchal approach," J. Opt. Soc. Am. **72**, 947-956 (1982).

15. See Ref. 3, p. 462.

16. A. Maréchal, "Etude des effets combines de la diffraction et des aberrations geometriques sur l'image d'un point lumineux," Rev. d' Opt **26**, 257-277 (1947).

17. See Ref. 3, p. 463.

18. V. N. Mahajan, "Strehl ratio for primary aberrations in terms of their aberration variance," J. Opt. Soc. Am. **73**, 860-861 (1983).

19. See Ref. 3, p. 469.

20. See Ref. 5, p. 80.

21. A. Papoulis, *Systems and Transforms with Applications in Optics* (McGraw-Hill, New York, 1968), p. 140.

22. See Ref. 5, p. 111.

23. See Ref. 3, p. 398.

24. V. N. Mahajan, "Asymptotic behavior of diffraction images," Can. J. Phys. **57**, 1426-1431 (1979).

25. W. T. Welford, "Use of annular apertures to increase focal depth," J. Opt. Soc. Am. **50**, 749-753 (1960).

26. V. N. Mahajan, "Line of sight of an aberrated optical system," J. Opt. Soc. Am. A**2**, 833-846 (1985).

APPENDIX

The range of radii for optimum estimation approach (that scaled by Strehl versus not scaled by Strehl) can be determined by setting the percentage errors defined in Eqs. (24) and (27) equal to each other. Thus for a given Strehl ratio, S, the region where a better estimate using the aberration-free encircled energy scaled by the Strehl ratio is obtained is for:

$$\frac{E_u}{E_a} > \frac{2}{1+S} \tag{29}$$

Thus the percentage errors where $\%\ Error_{NENC}$ is less than $\%\ Error_{ENC}$ are $\%Error_{NENC} < 11\%, < 25\%, < 43\%, < 67\%$ and $< 81\%$ for Strehl ratios of $S = 0.8$, 0.6, 0.4, 0.2, and 0.1 respectively.

In light of the asymptotic behavior of encircled energy which results in the encircled energies of an aberrated system converging to the aberration-free value and eventually to the total energy as radius increases, the asymptotic behavior of the percentage errors may similarly be understood. The following conditions hold true:

$$\text{as } E_a \longrightarrow E_u \tag{30}$$
$$\%\ Error_{NENC} \longrightarrow 100\ (1\text{-}S)$$
$$\text{and } \%\ Error_{ENC} \longrightarrow 0$$

Conversely,

$$\text{as } E_a \longrightarrow (S)(E_u) \tag{31}$$
$$\%\ Error_{NENC} \longrightarrow 0$$
$$\text{and } \%\ Error_{ENC} \longrightarrow 100\ (1\text{-}1/S).$$

Figures 8 through 35.

Plots of PSFs, normalized PSFs, encircled energies, and percentage errors for spherical, balanced spherical, astigmatism, balanced astigmatism, coma, balanced coma, and mixed aberrations.

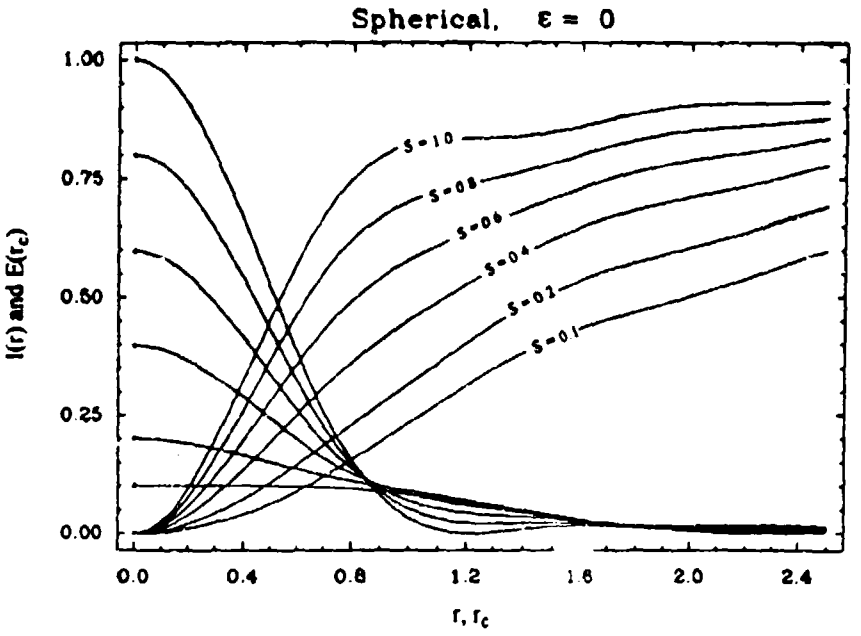

PSFs and encircled energies
Figure 8a.

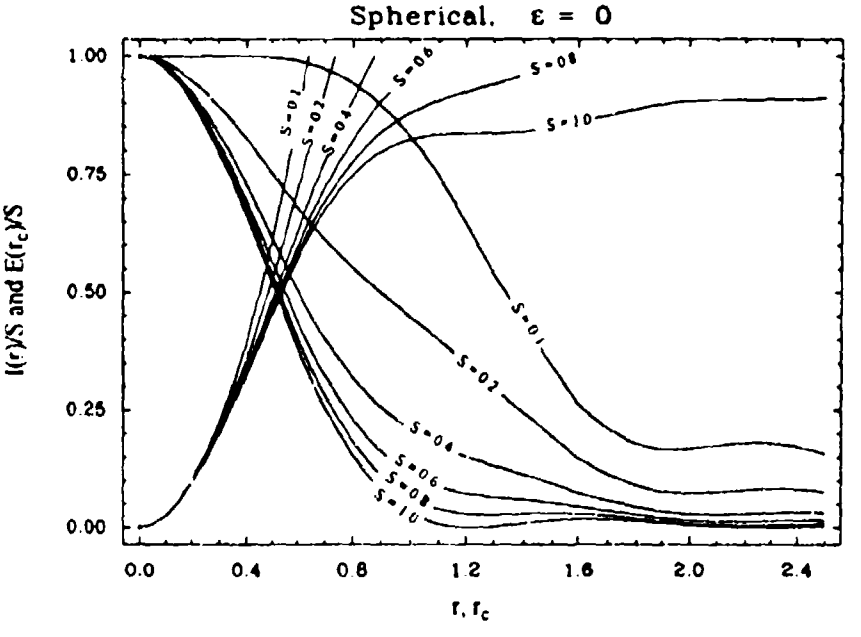

Normalized PSFs and encircled energies
Figure 8b.

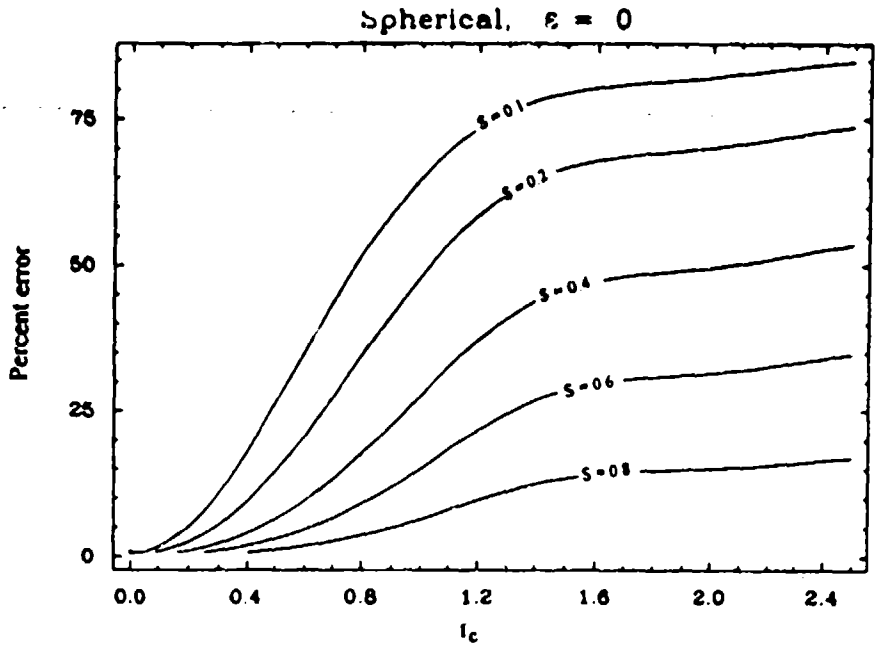

$\%Error_{NENC}$
Figure 8c.

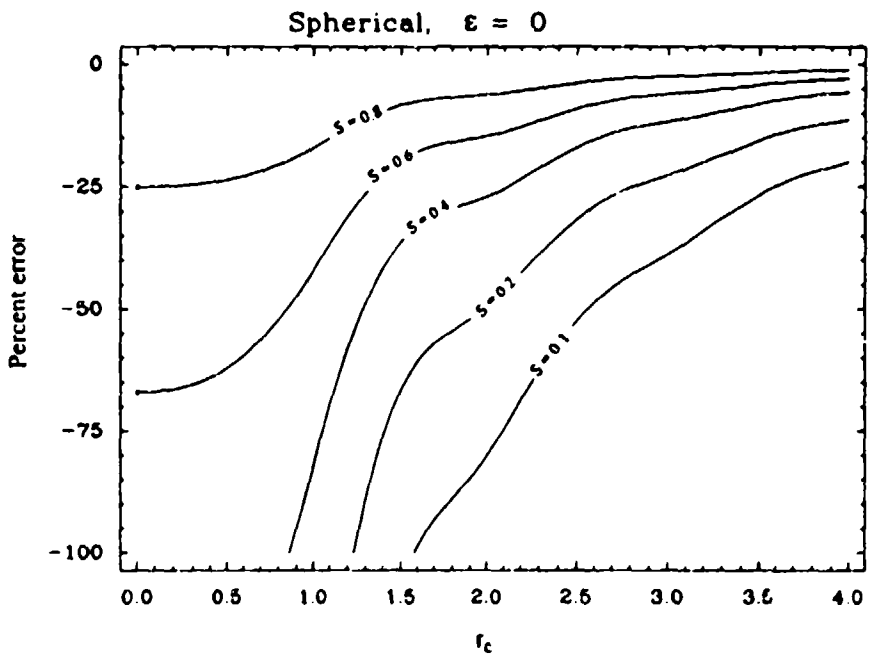

$\%Error_{ENC}$
Figure 8d.

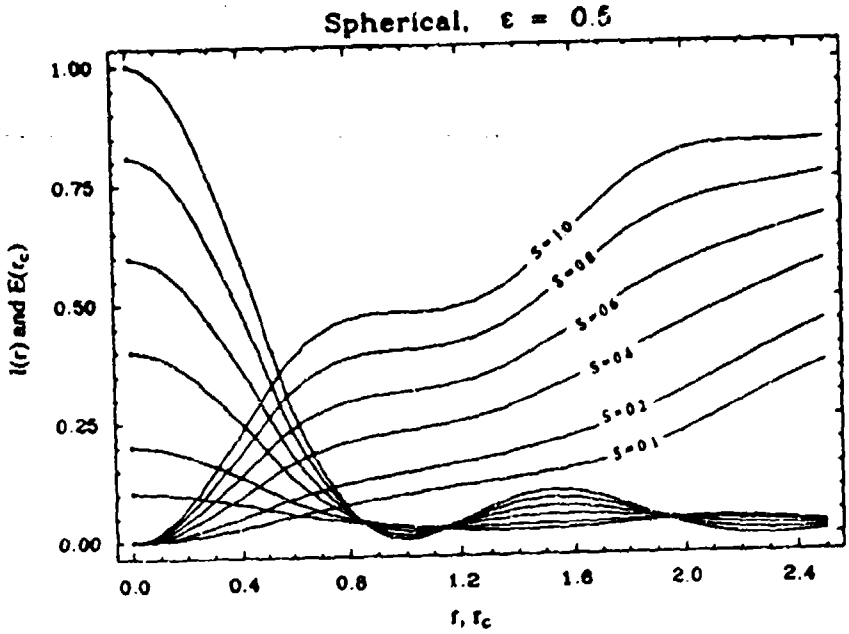

PSFs and encircled energies
Figure 9a.

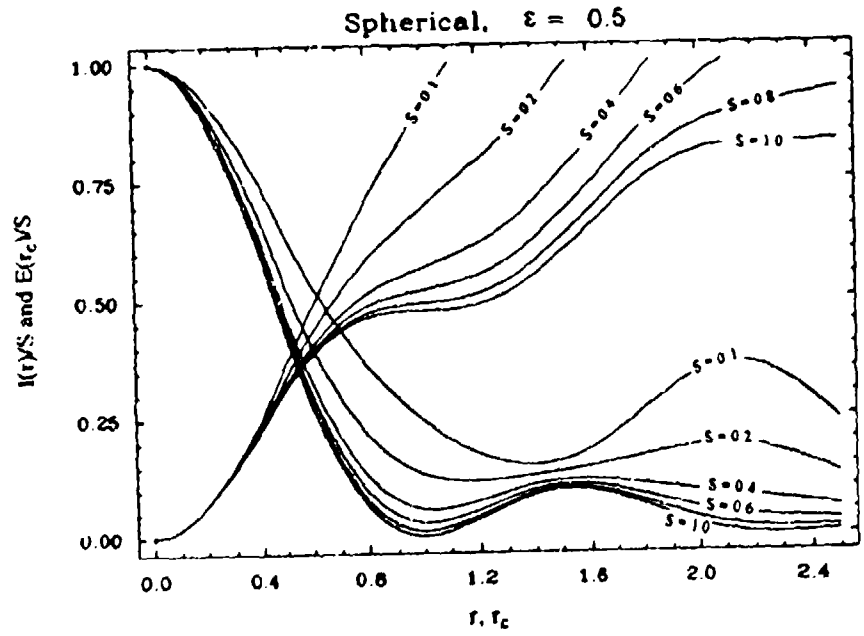

Normalized PSFs and encircled energies
Figure 9b.

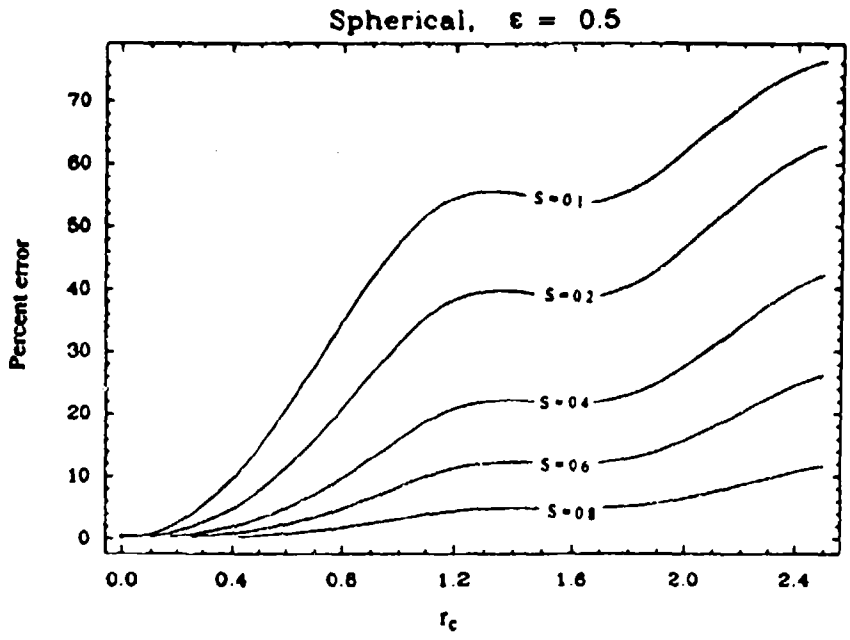

$\%Error_{NENC}$

Figure 9c.

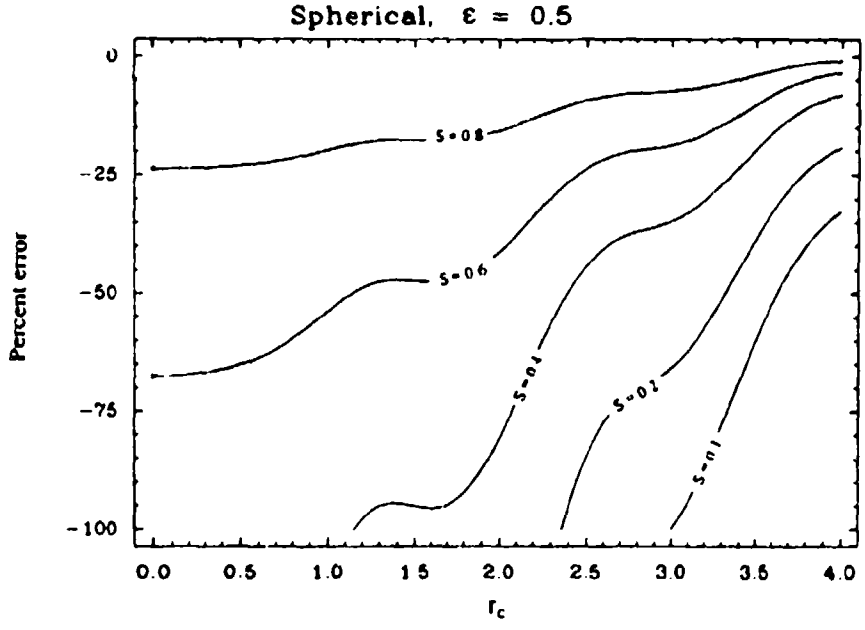

$\%Error_{ENC}$

Figure 9d.

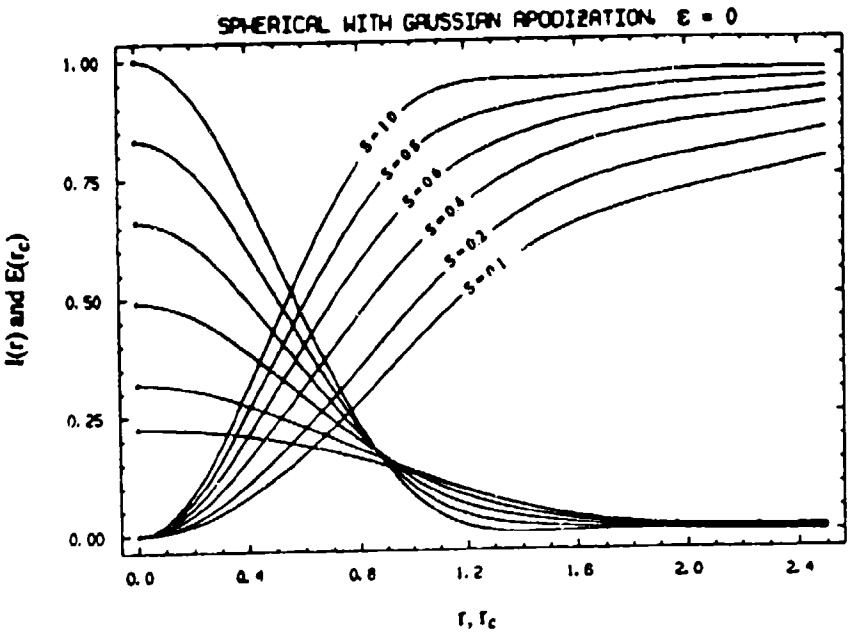

PSFS AND ENCIRCLED ENERGIES
Figure 10a.

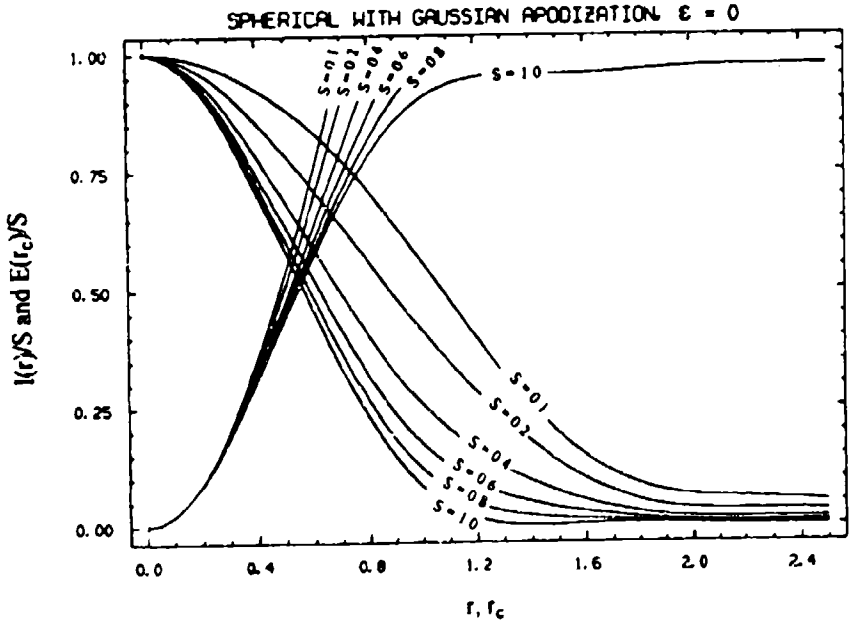

NORMALIZED PSFS AND ENCIRCLED ENERGIES
Figure 10b.

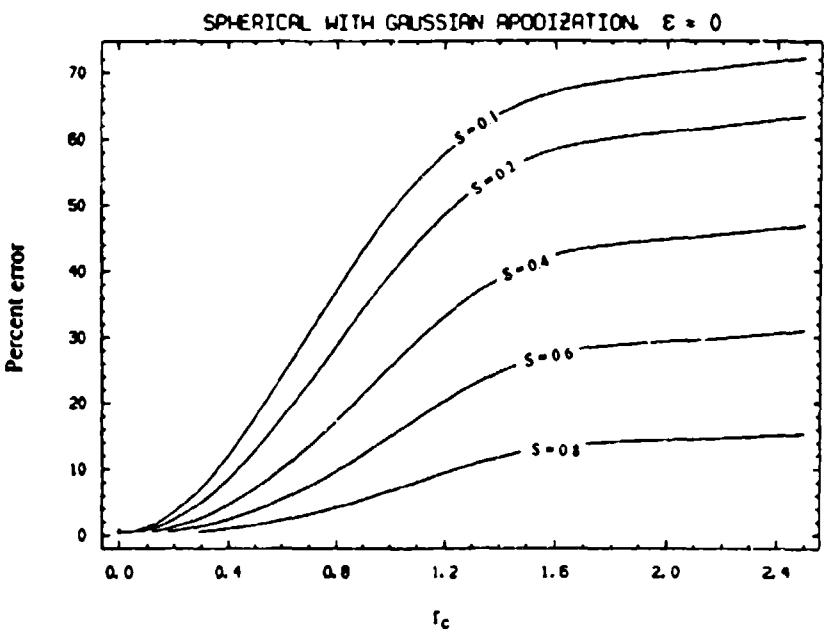
SPHERICAL WITH GAUSSIAN APODIZATION ε = 0
Percent error
70
60
50
40
30
20
10
0
0.0
0.4
0.8
1.2
1.6
2.0
2.4
S=0.1
S=0.2
S=0.4
S=0.6
S=0.8
r_c
%ERROR $_{NENC}$

Figure 10c.

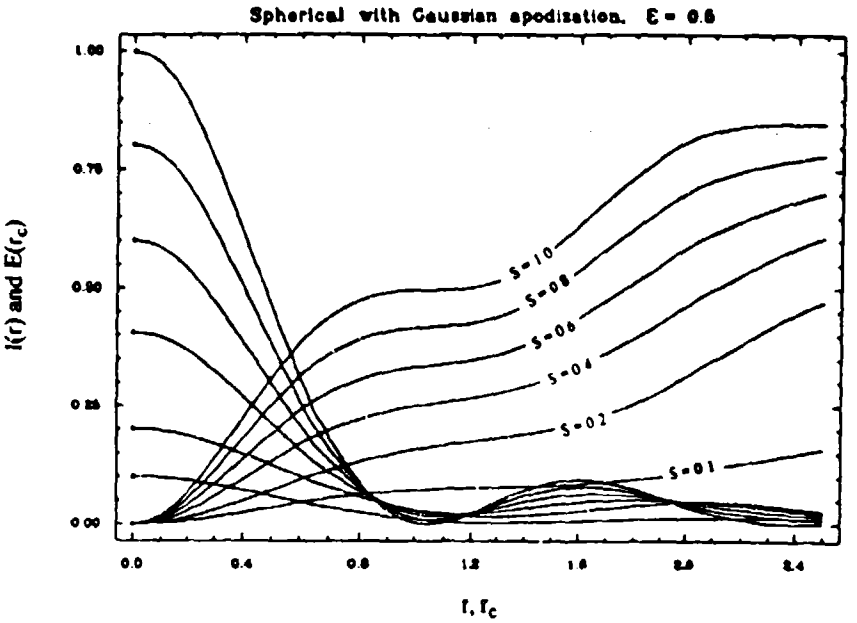

PSFs and encircled energies

Figure 11a.

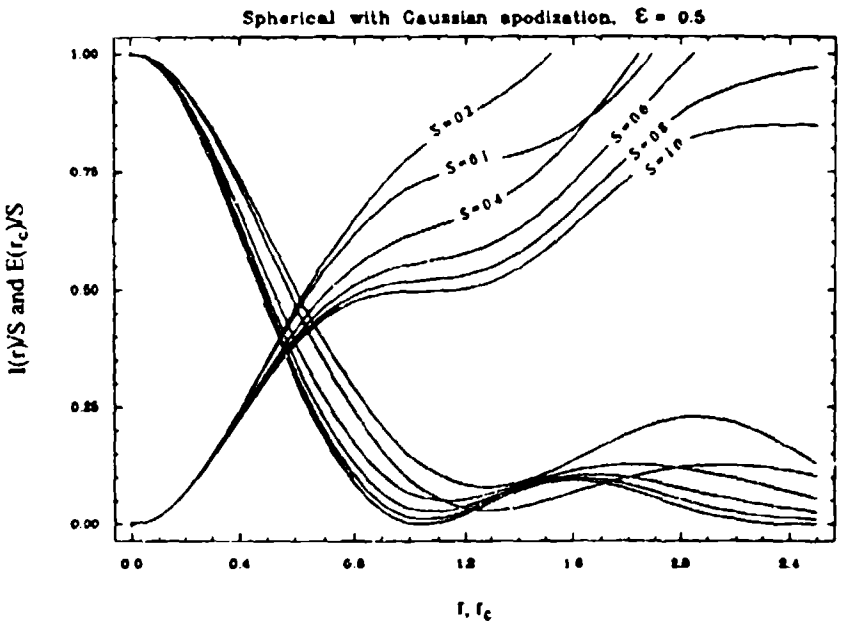

Normalized PSFs and encircled energies

Figure 11b.

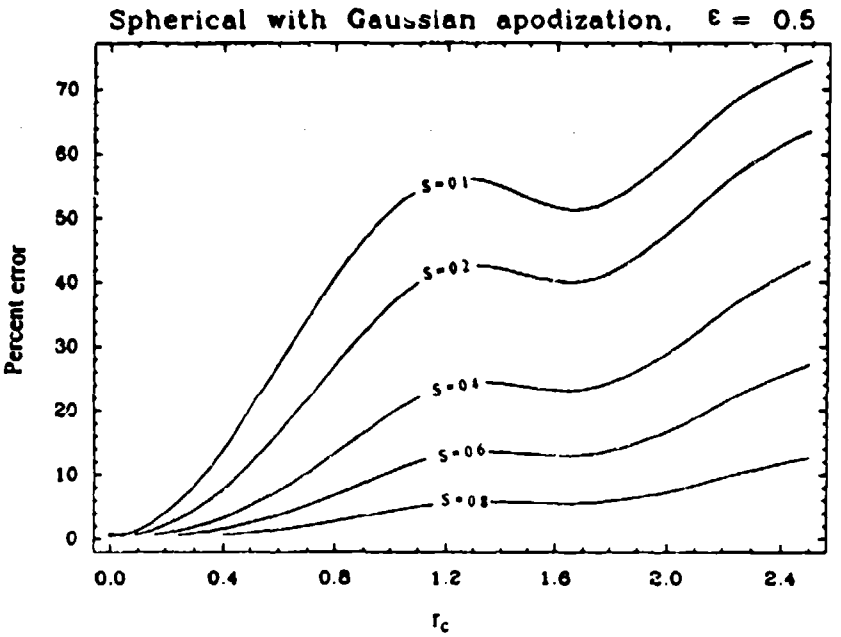

$\%Error_{NENC}$

Figure 11c.

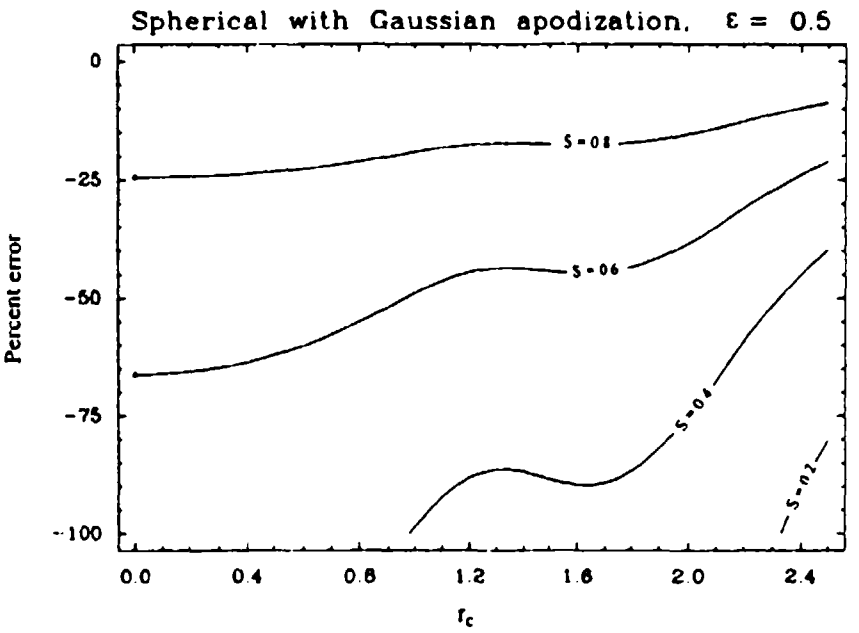

$\%Error_{ENC}$

Figure 11d.

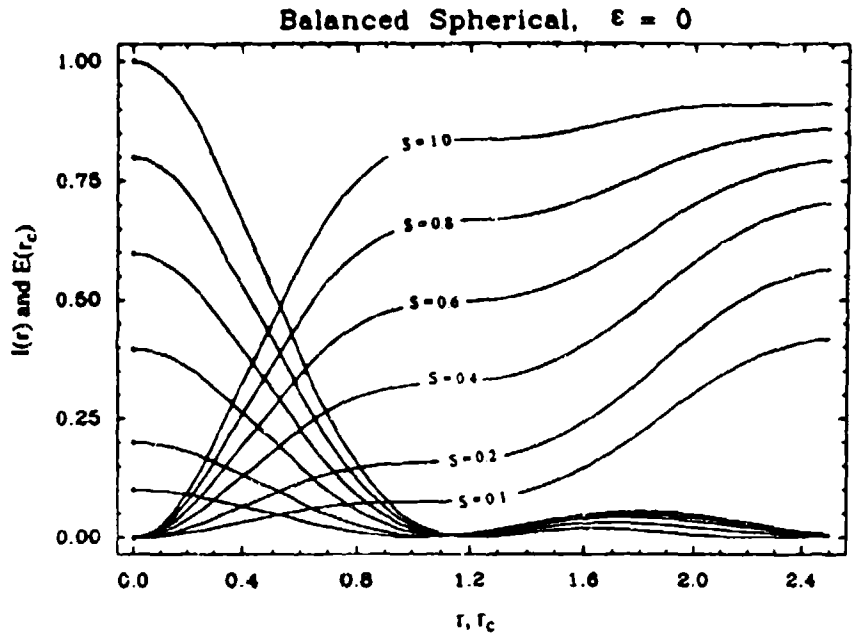

PSFs and encircled energies
Figure 12a.

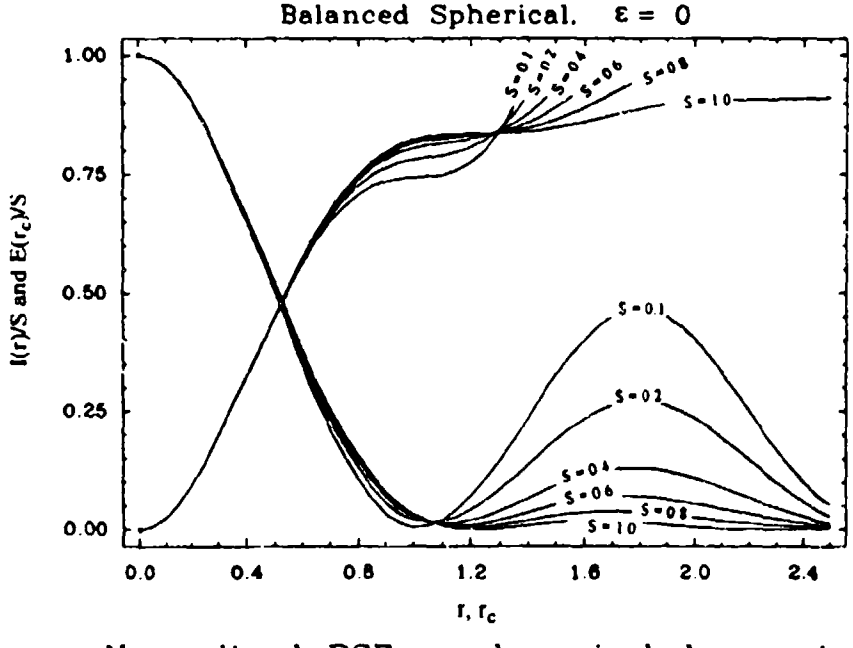

Normalized PSFs and encircled energies
Figure 12b.

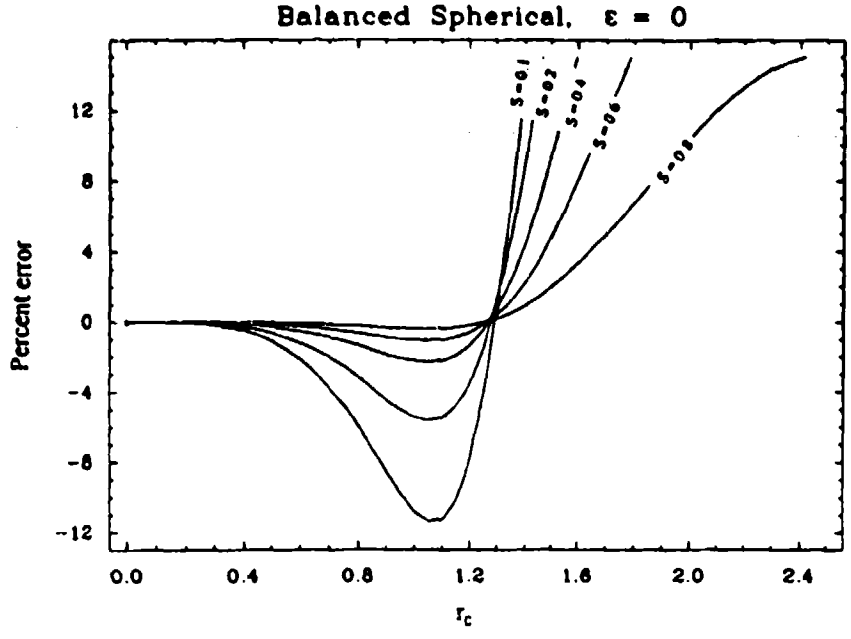

$\%Error_{NENC}$

Figure 12c.

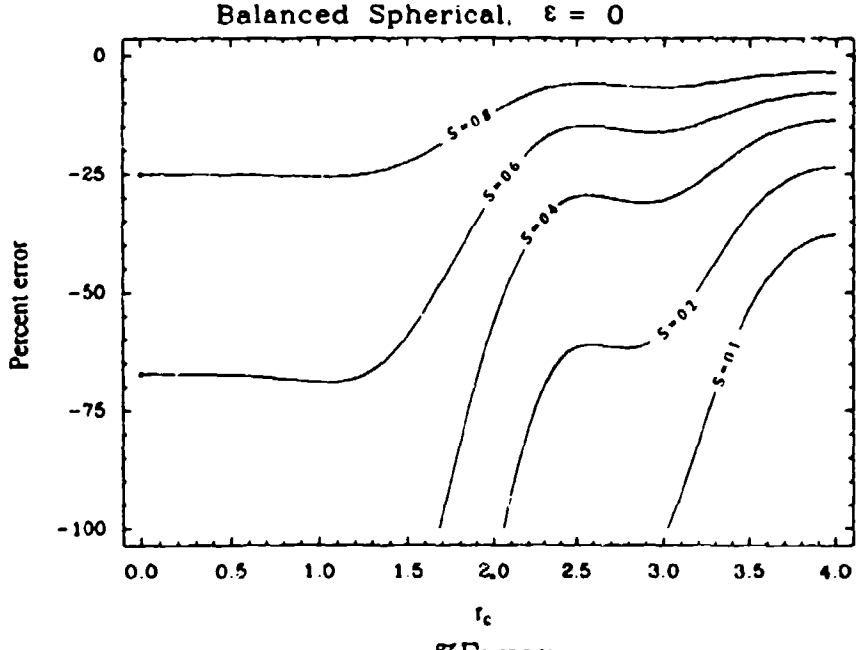

$\%Error_{ENC}$

Figure 12d.

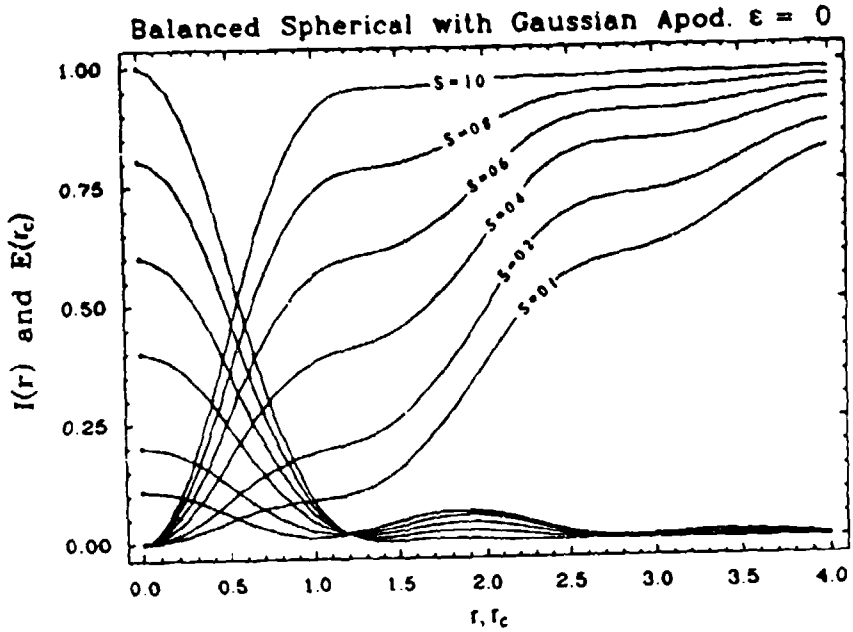

PSFs and encircled energies
Figure 12e.

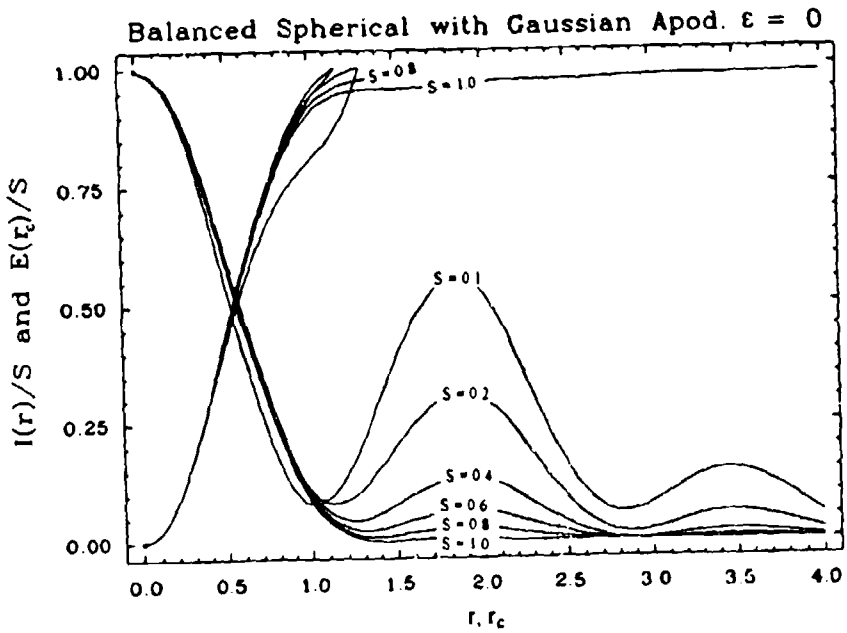

Normalized PSFs and encircled energies
Figure 12f.

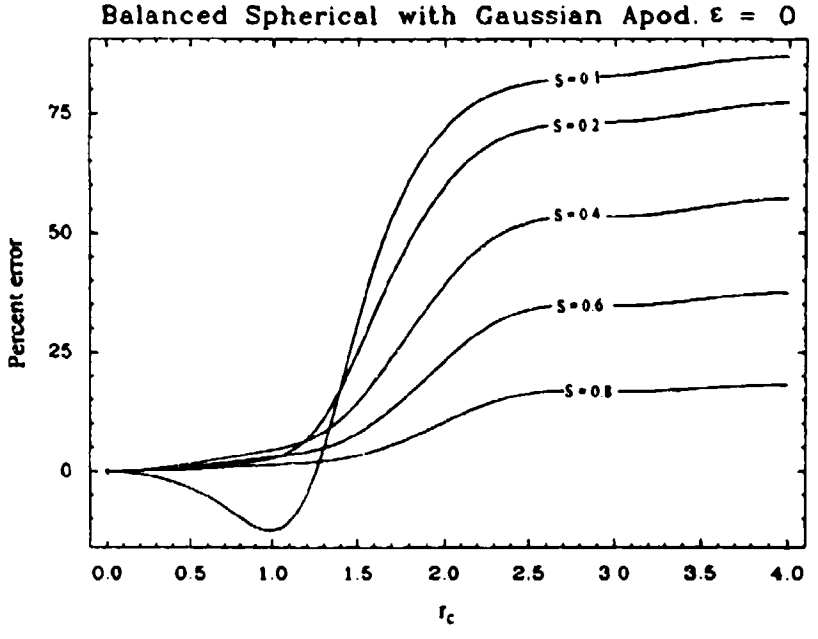

$\%Error_{NENC}$

Figure 12g.

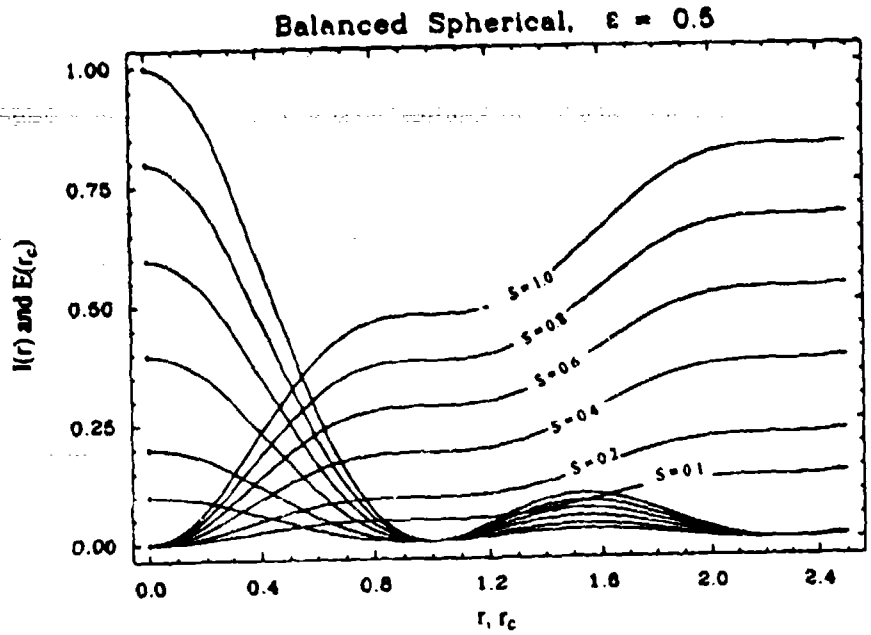

PSFs and encircled energies
Figure 13a.

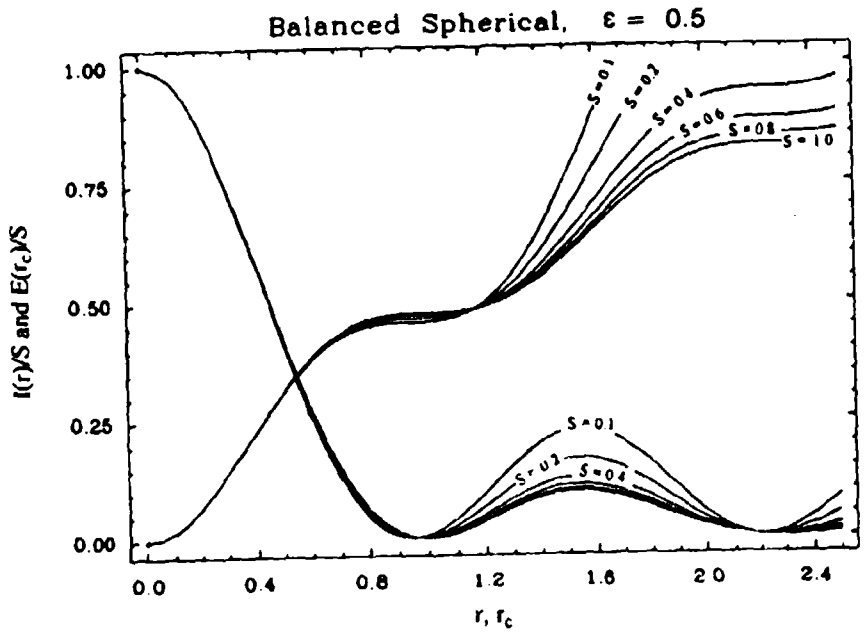

Normalized PSFs and encircled energies
Figure 13b.

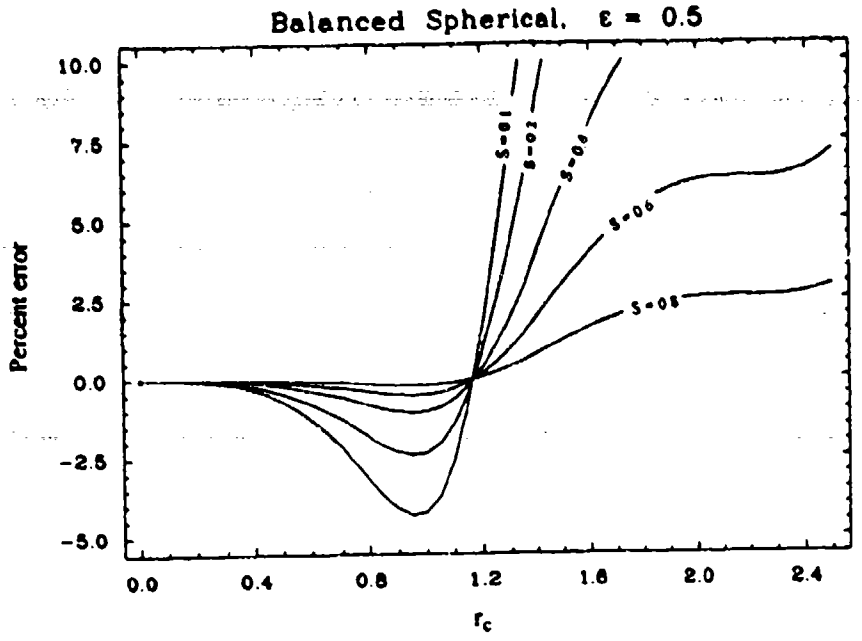

%Error$_{NENC}$

Figure 13c.

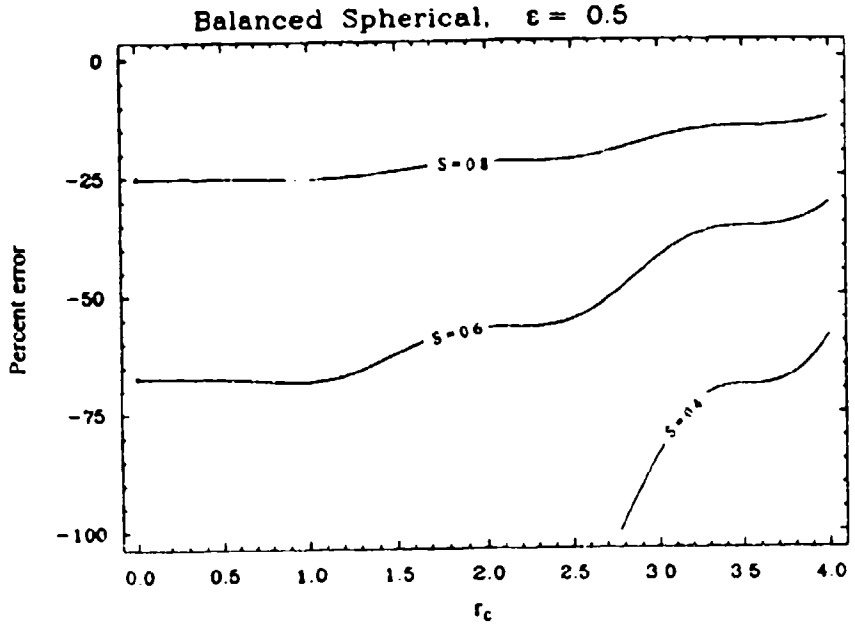

%Error$_{ENC}$

Figure 13d.

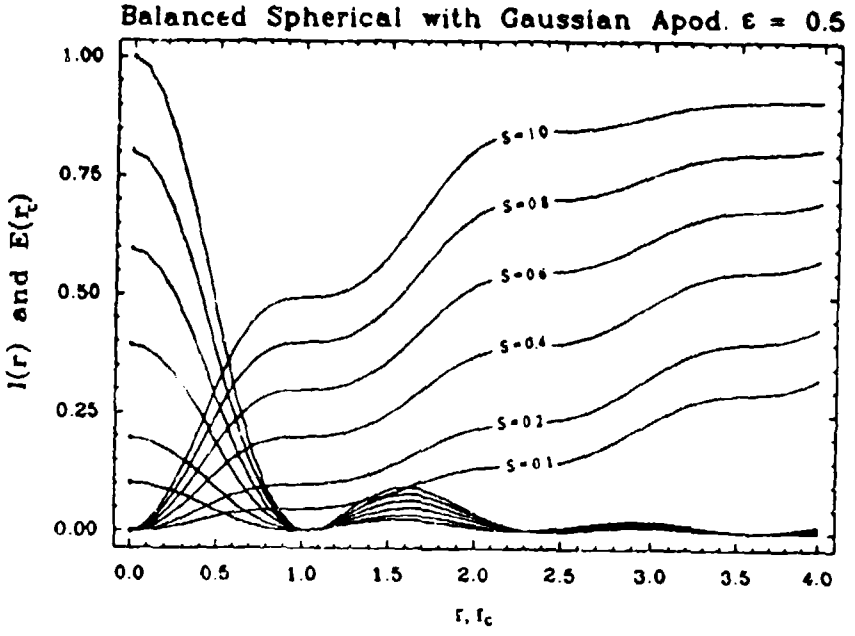

PSFs and encircled energies
Figure 13e.

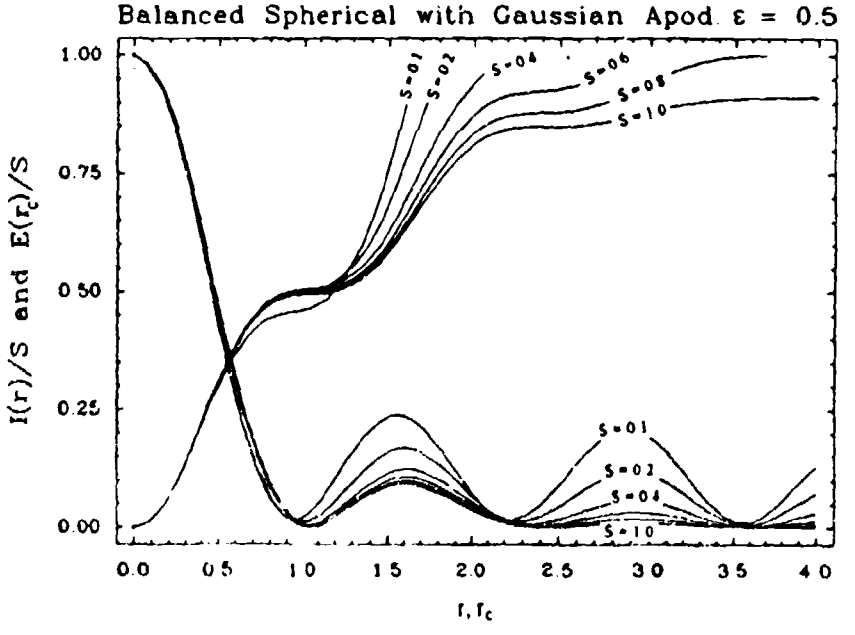

Normalized PSFs and encircled energies
Figure 13f.

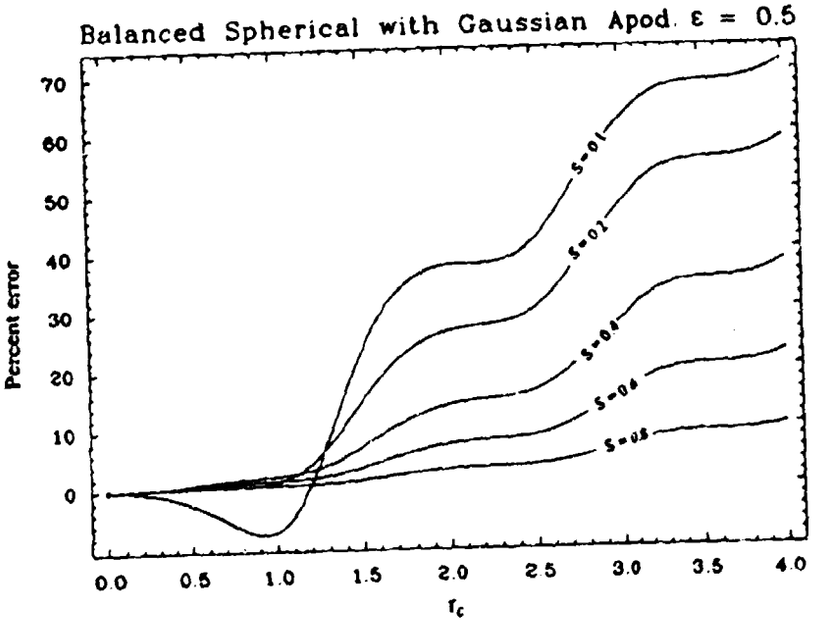

$\%Error_{NENC}$

Figure 13g.

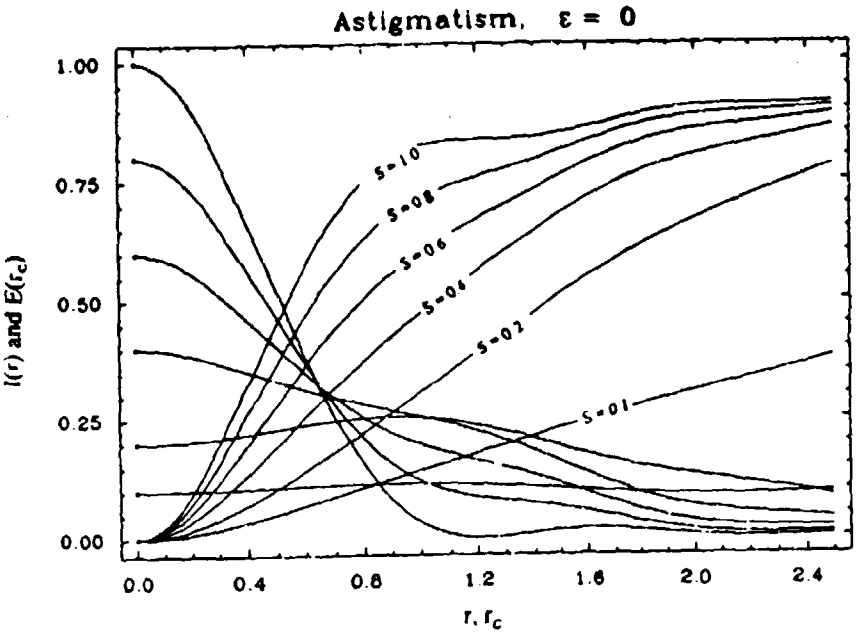

PSFs and encircled energies
Figure 14a.

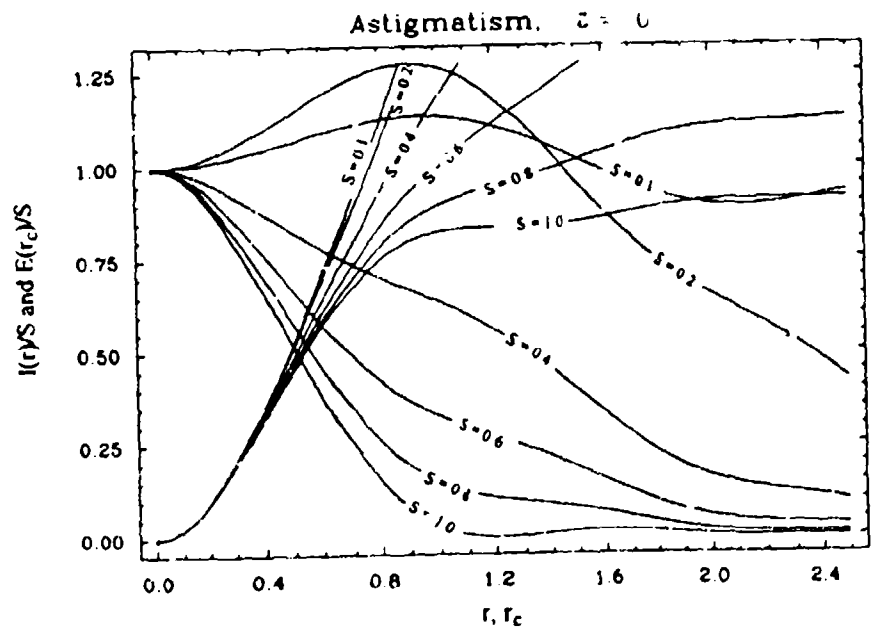

Normalized PSFs and encircled energies
Figure 14b.

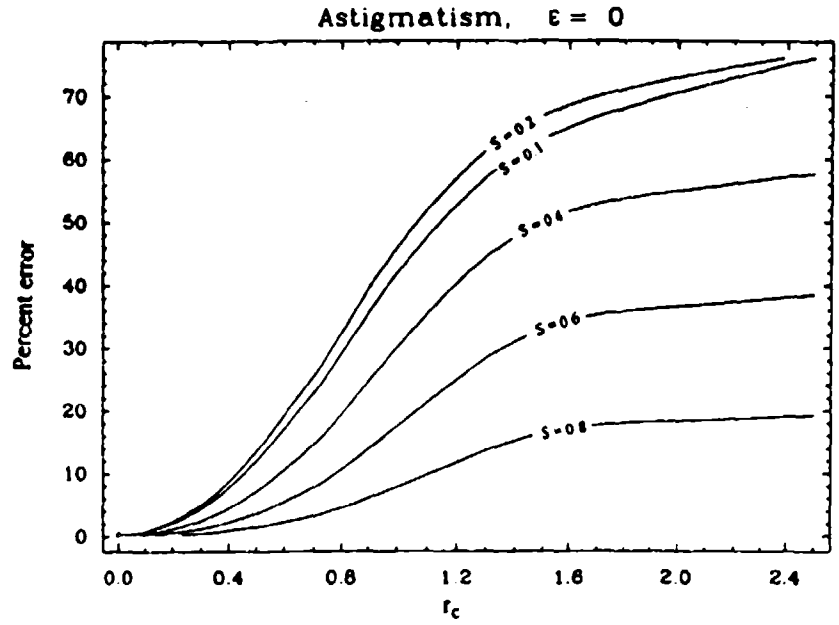

$\%Error_{NENC}$

Figure 14c.

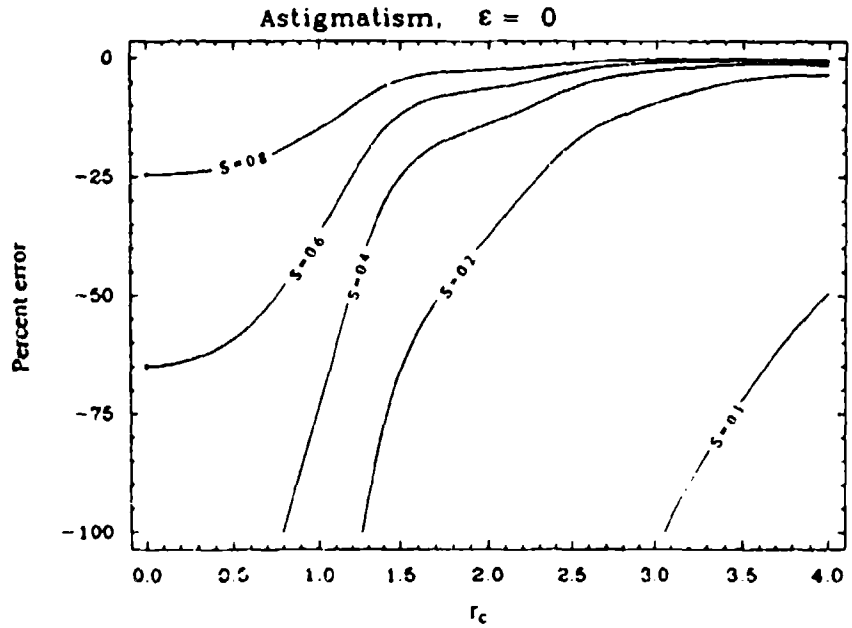

$\%Error_{SNC}$

Figure 14d.

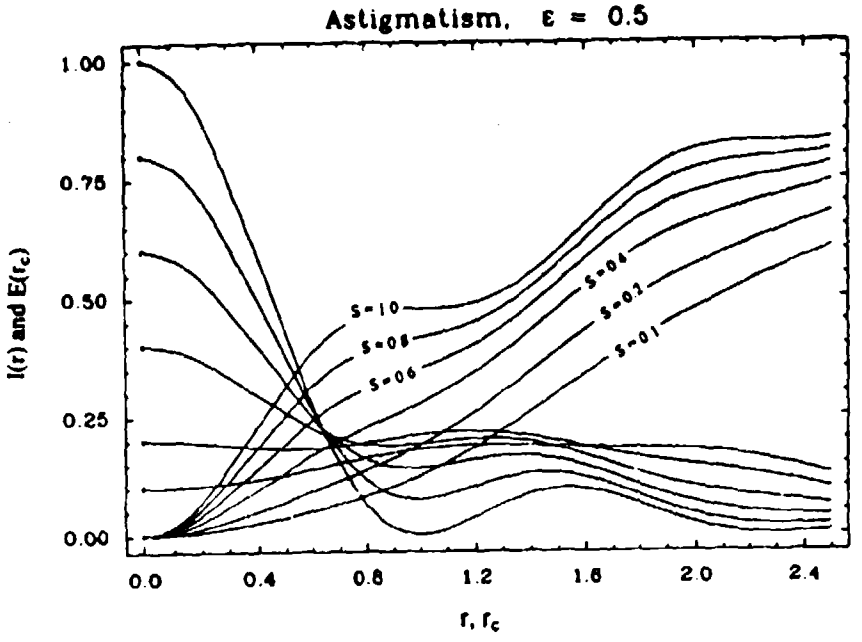

PSFs and encircled energies
Figure 15a.

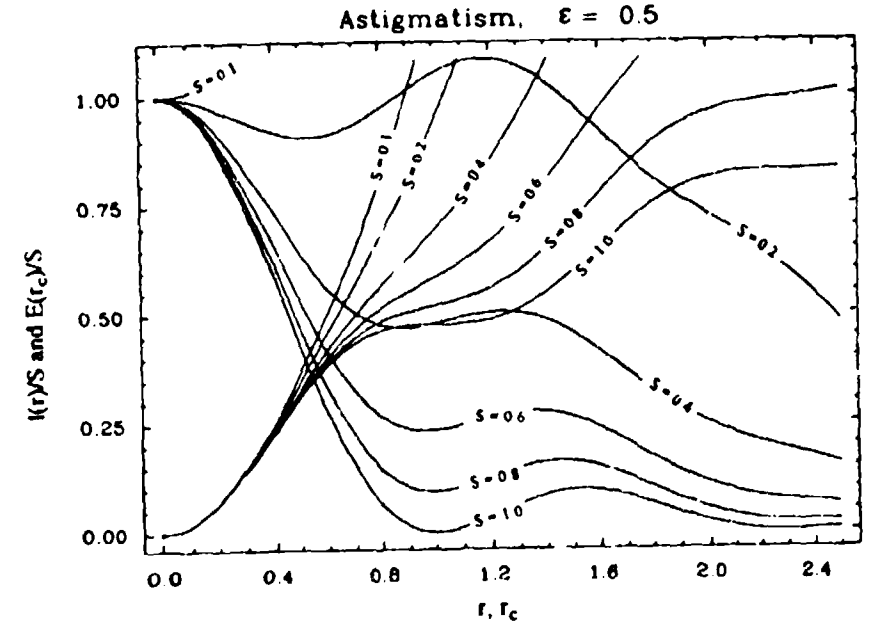

Normalized PSFs and encircled energies
Figure 15b.

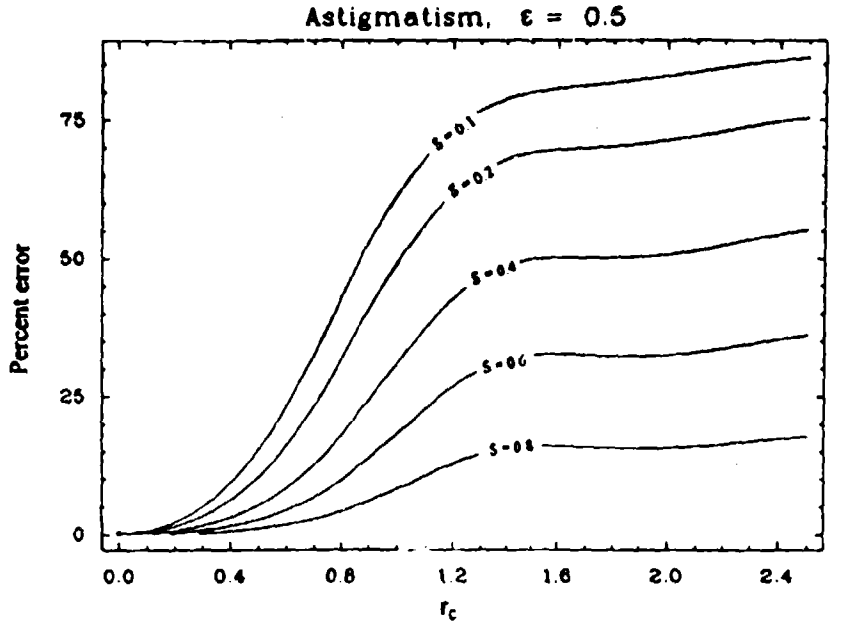

$\%Error_{NE\text{-}NC}$

Figure 15c.

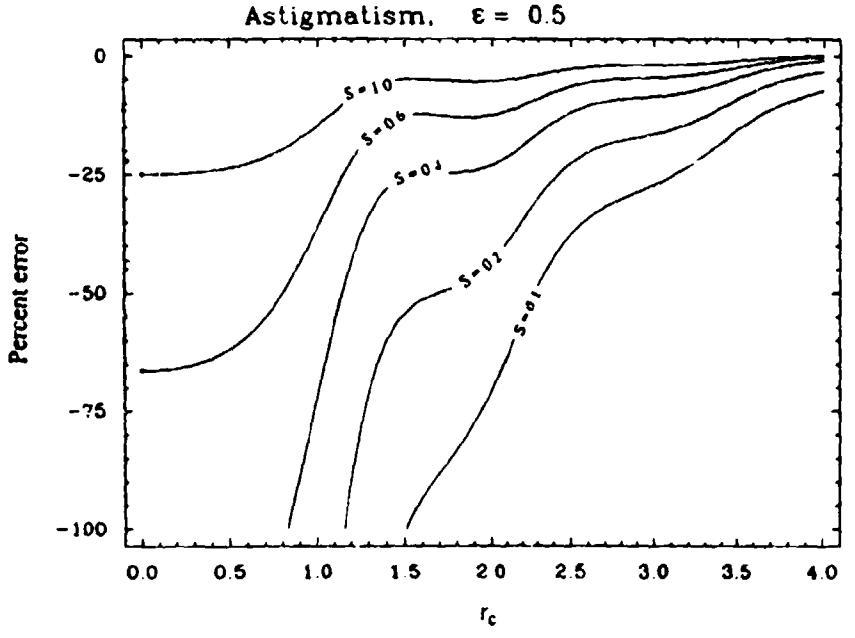

$\%Error_{ENC}$

Figure 15d.

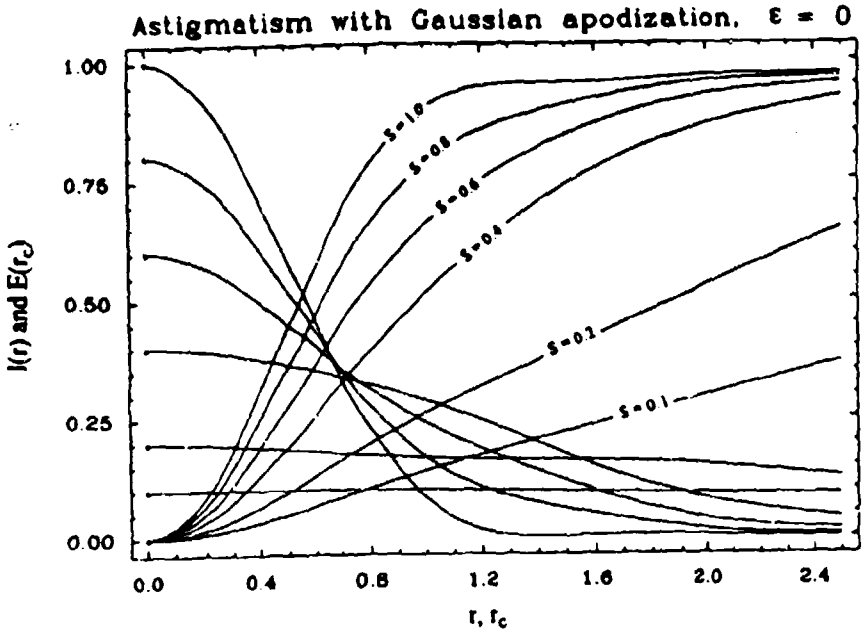

PSFs and encircled energies
Figure 16a.

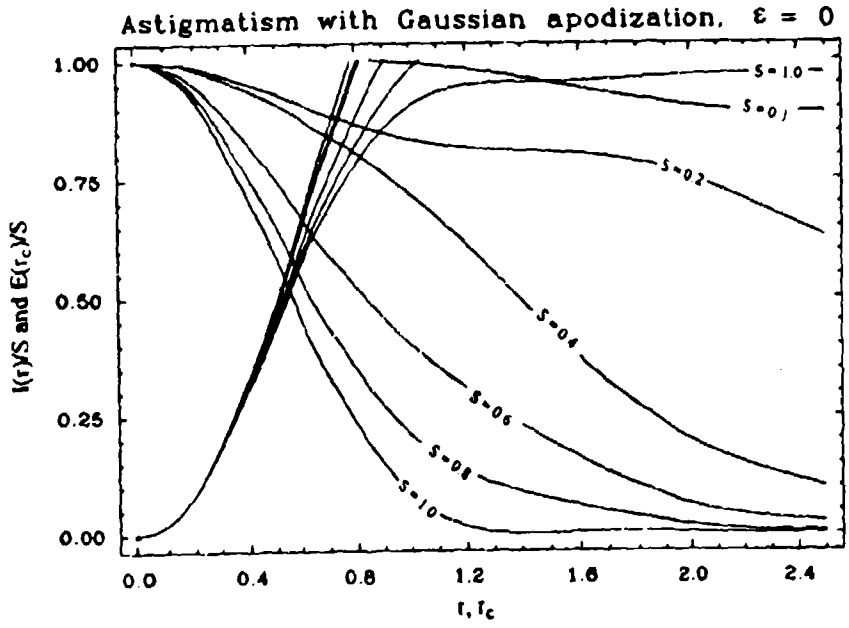

Normalized PSFs and encircled energies
Figure 16b.

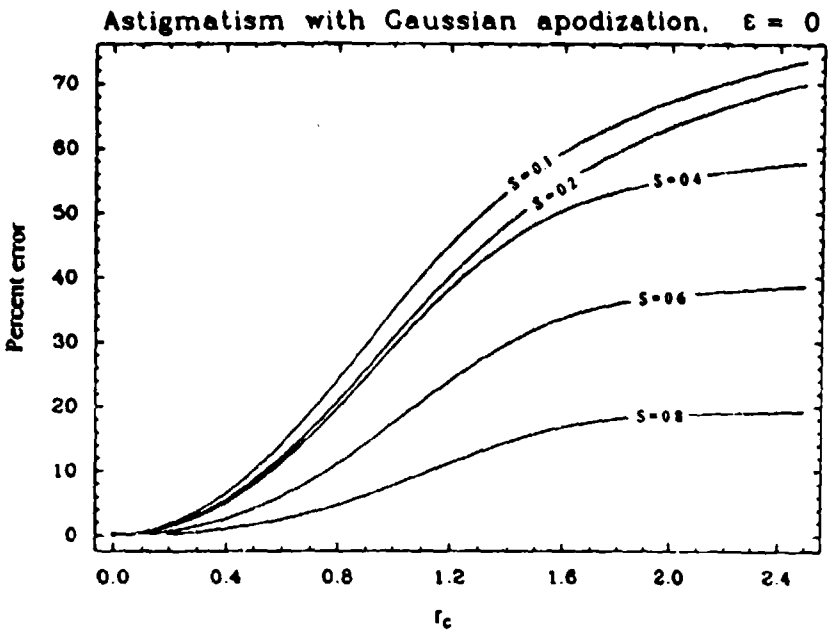

$\%Error_{NENC}$

Figure 16c.

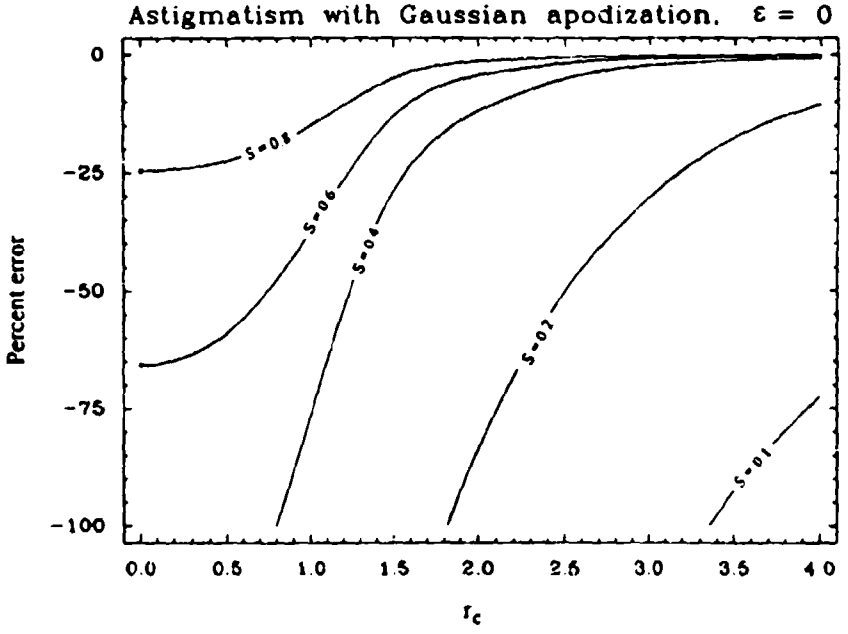

$\%Error_{ENC}$

Figure 16d.

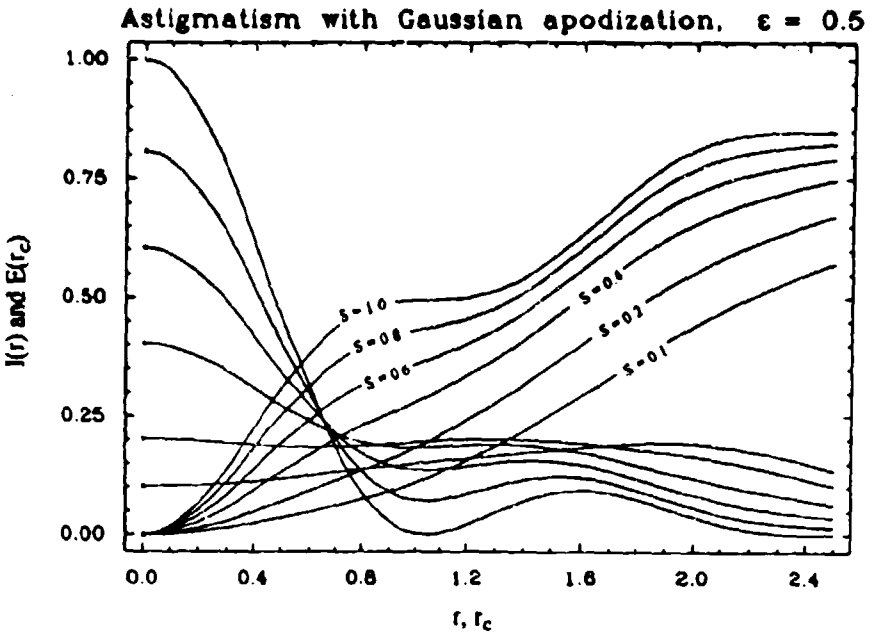

PSFs and encircled energies
Figure 17a.

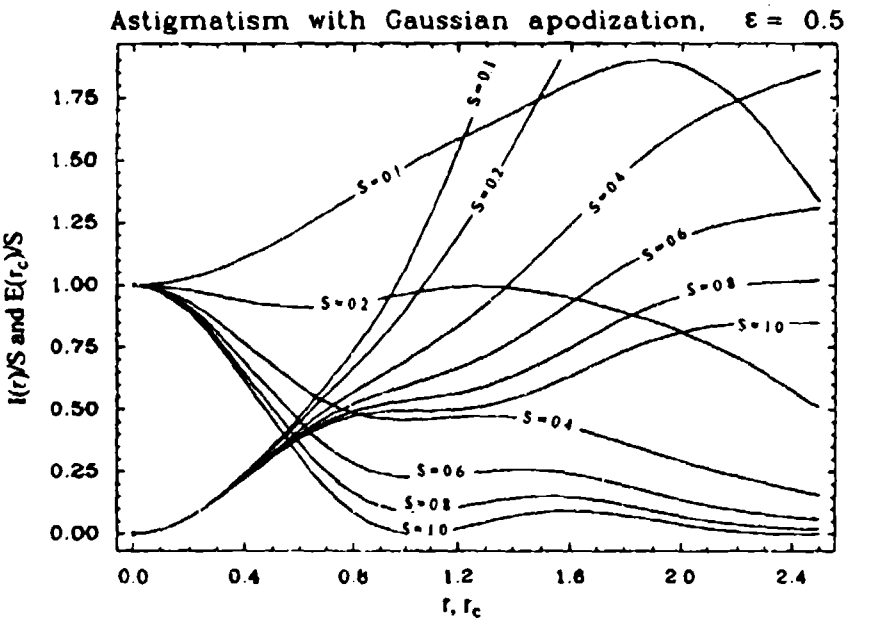

Normalized PSFs and encircled energies
Figure 17b.

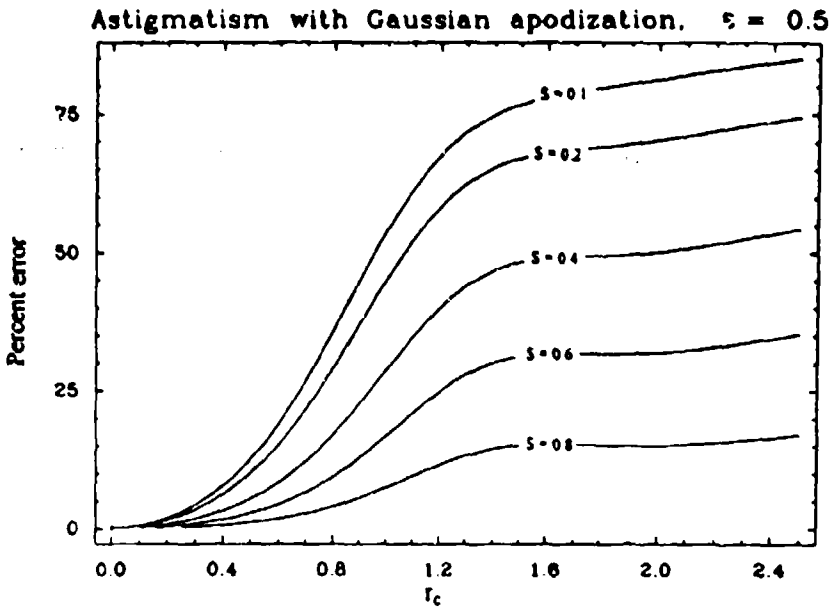

$\%Error_{NENC}$

Figure 17c.

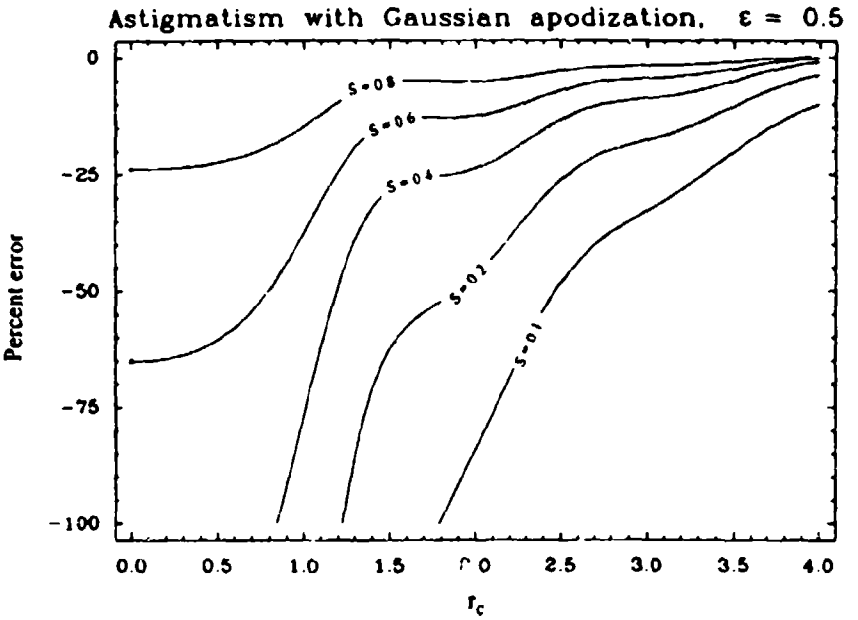

$\%Error_{ENC}$

Figure 17d.

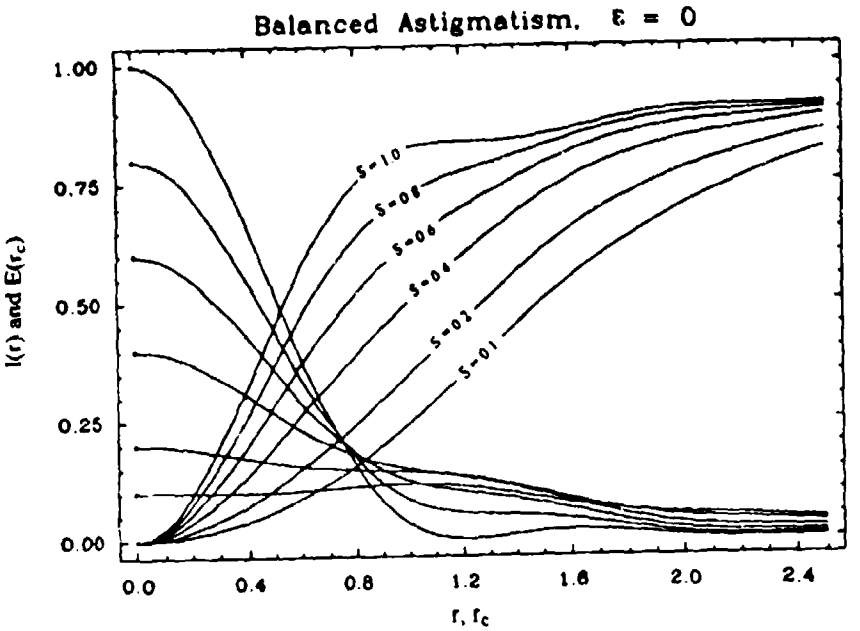

PSFs and encircled energies
Figure 18a.

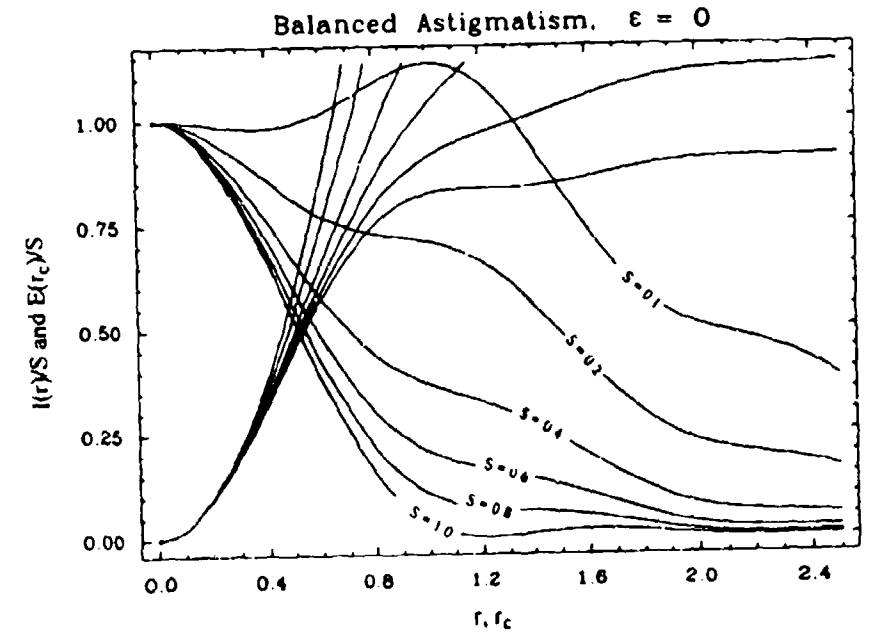

Normalized PSFs and encircled energies
Figure 18b.

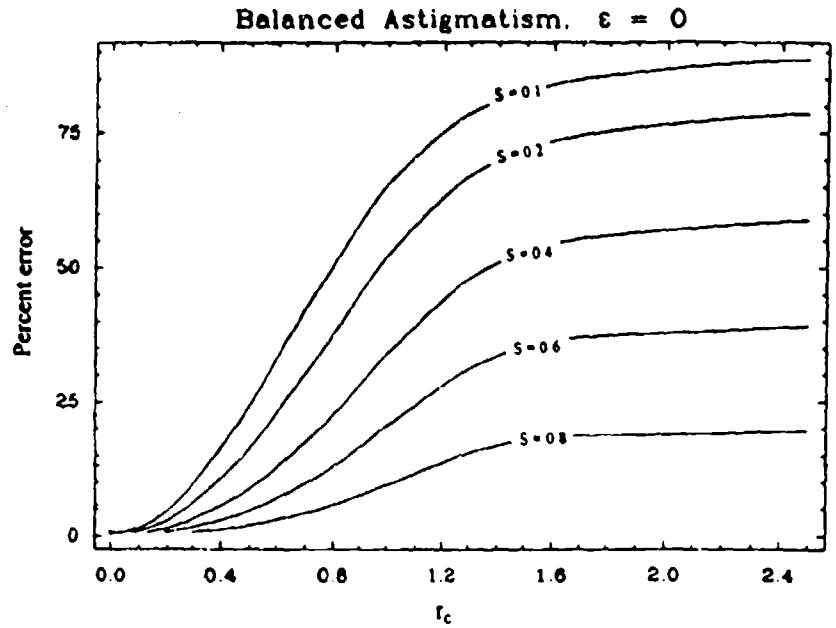

$\%Error_{NENC}$

Figure 18c.

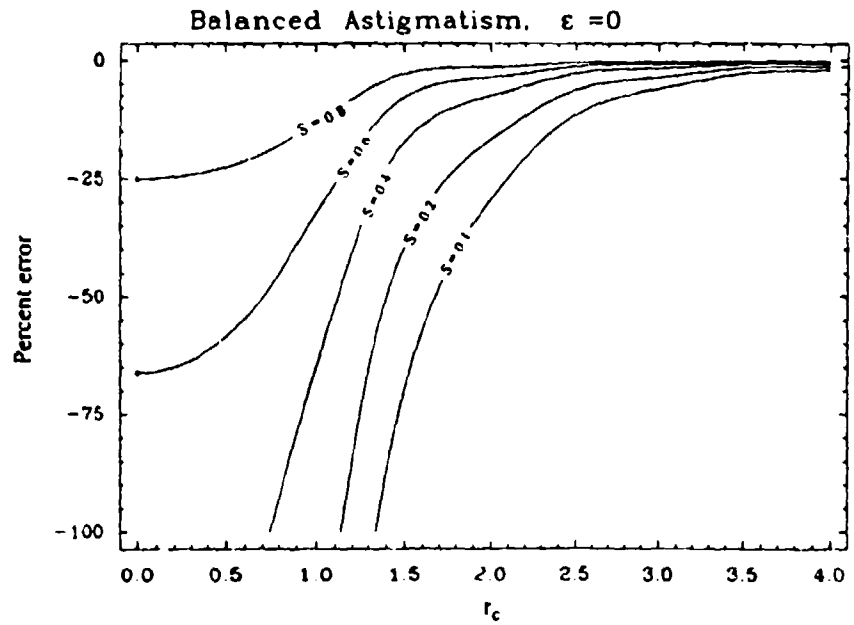

$\%Error_{ENC}$

Figure 18d.

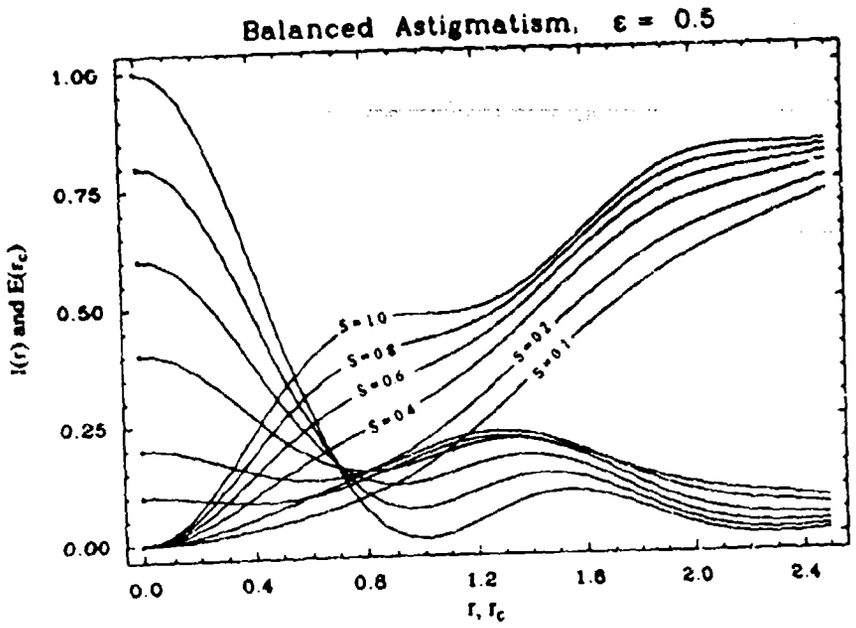

PSFs and encircled energies
Figure 19a.

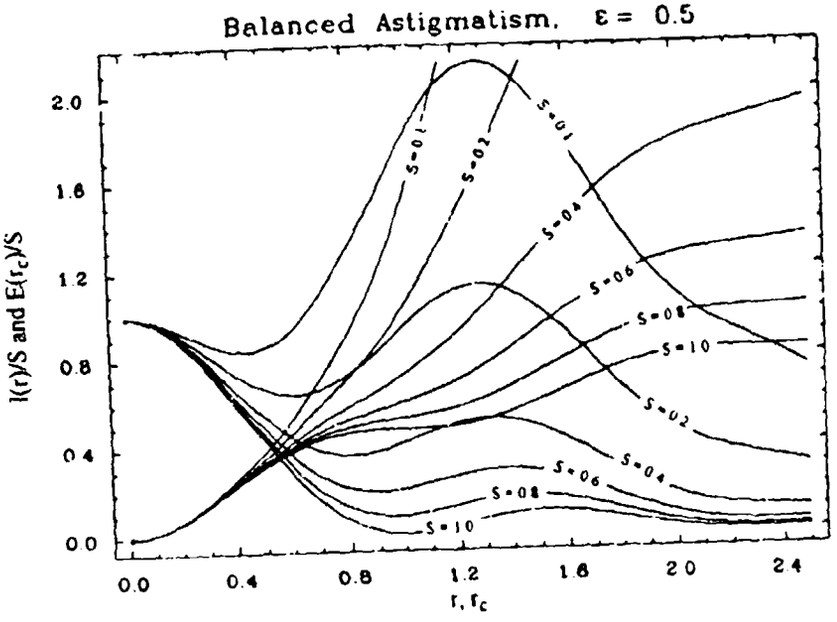

Normalized PSFs and encircled energies
Figure 19b.

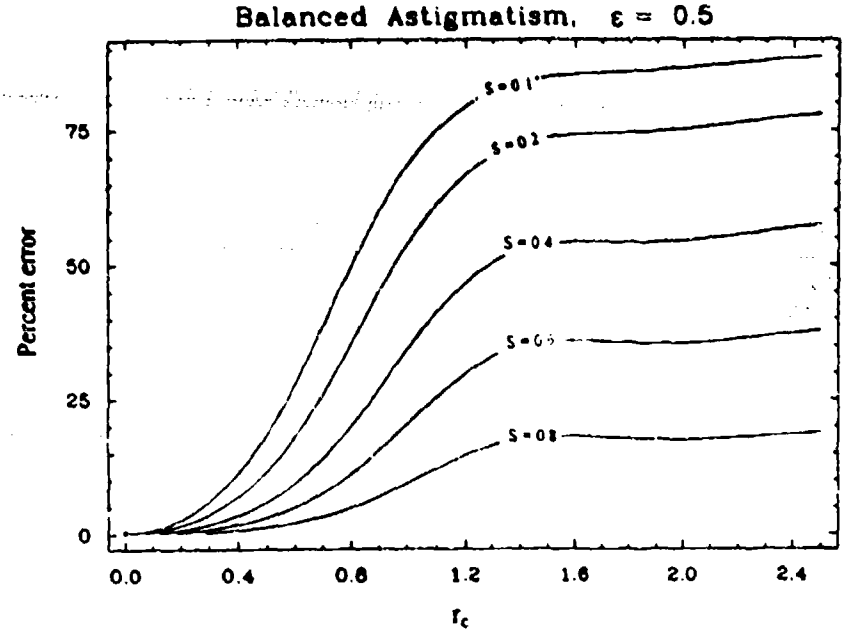

$\%Error_{MENC}$

Figure 19c.

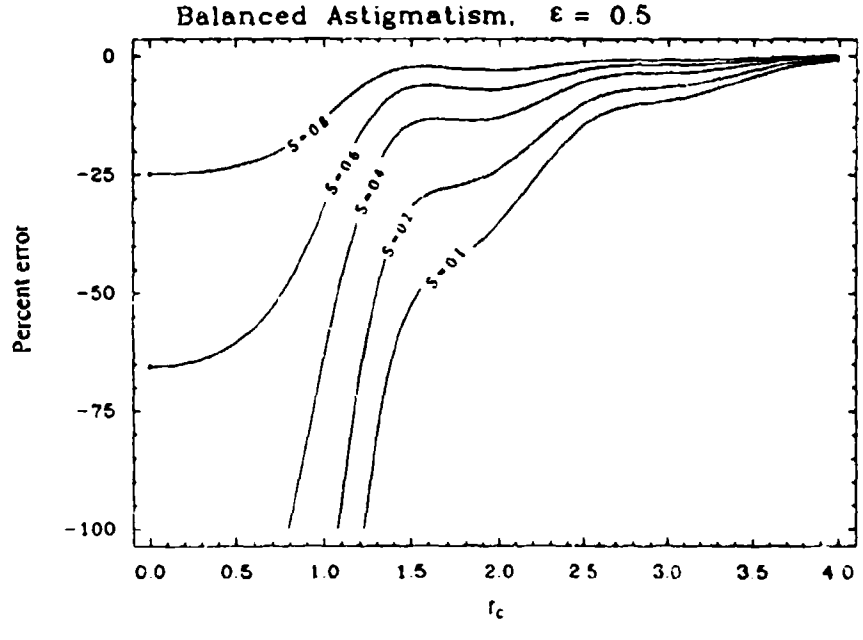

$\%Error_{EMC}$

Figure 19d.

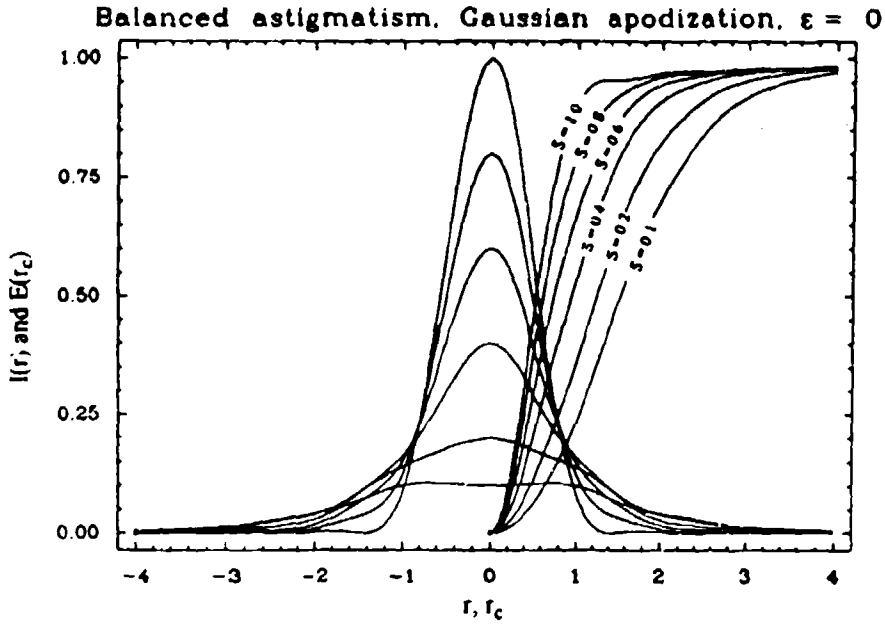

PSFs and encircled energies
Figure 20a.

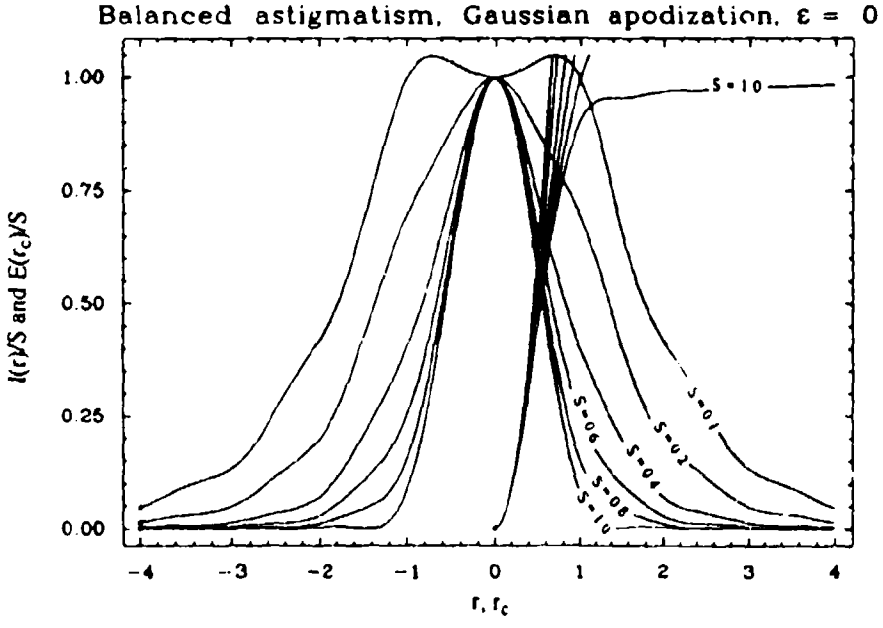

Normalized PSFs and encircled energies
Figure 20b.

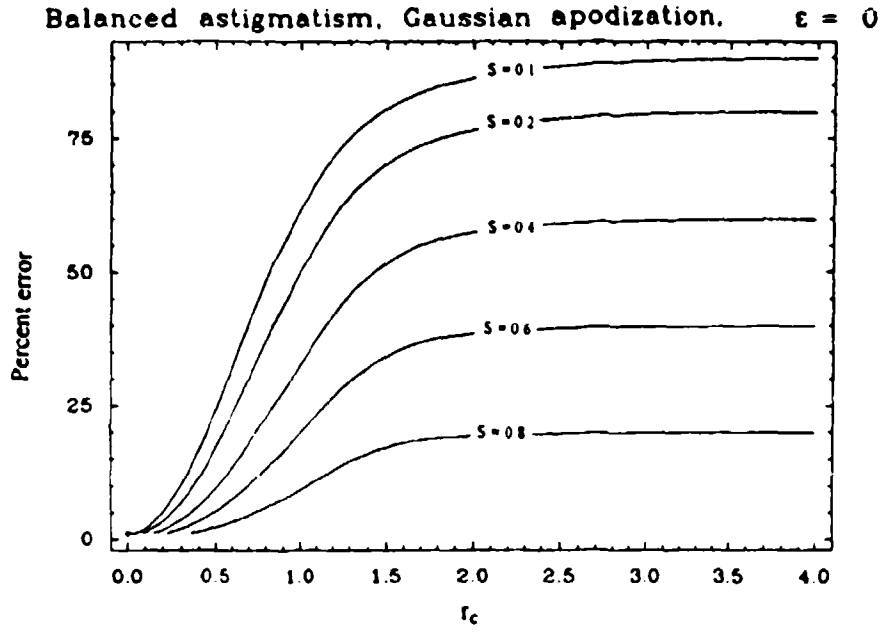

$\%Error_{NENC}$

Figure 20c.

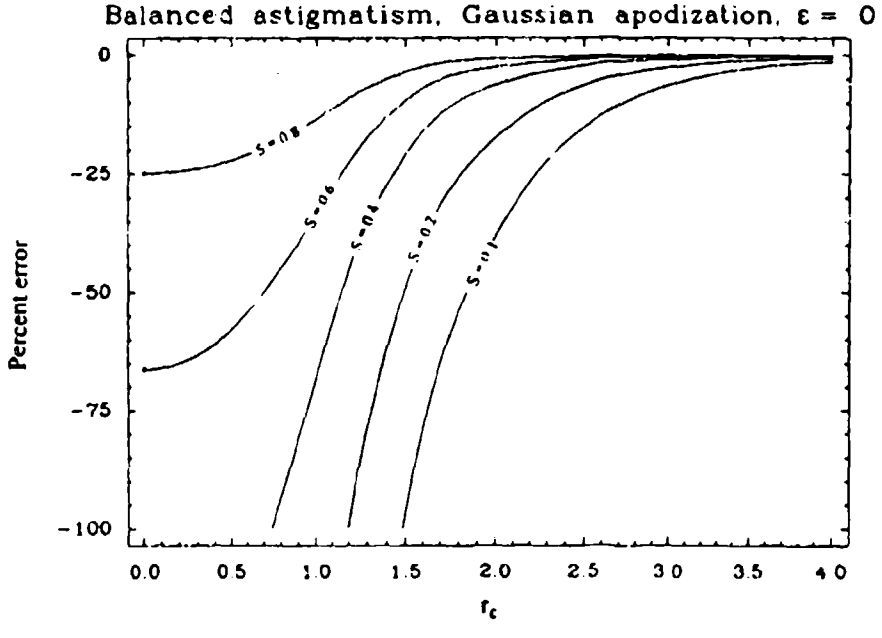

$\%Error_{ENC}$

Figure 20d.

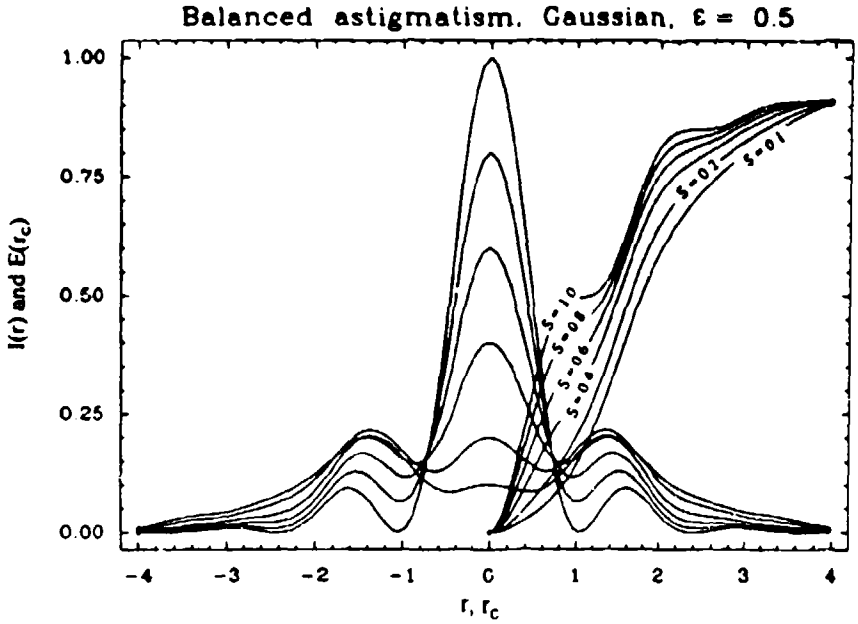

PSFs and encircled energies
Figure 21a.

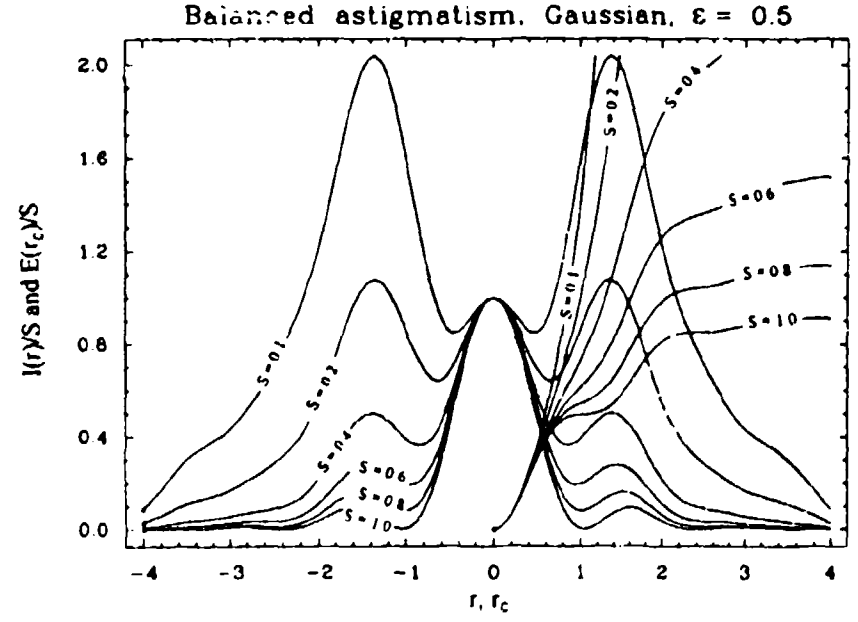

Normalized PSFs and encircled energies
Figure 21b.

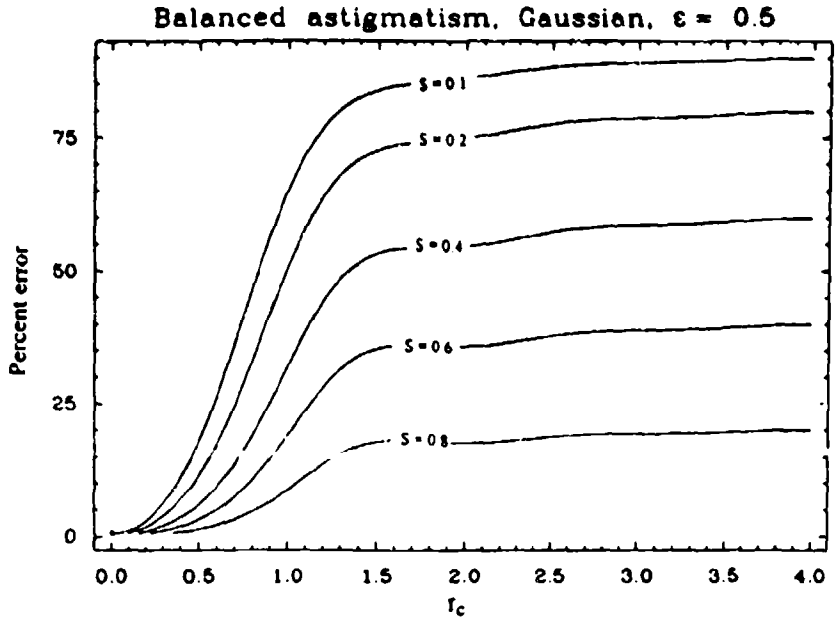

$\%Error_{NENC}$

Figure 21c.

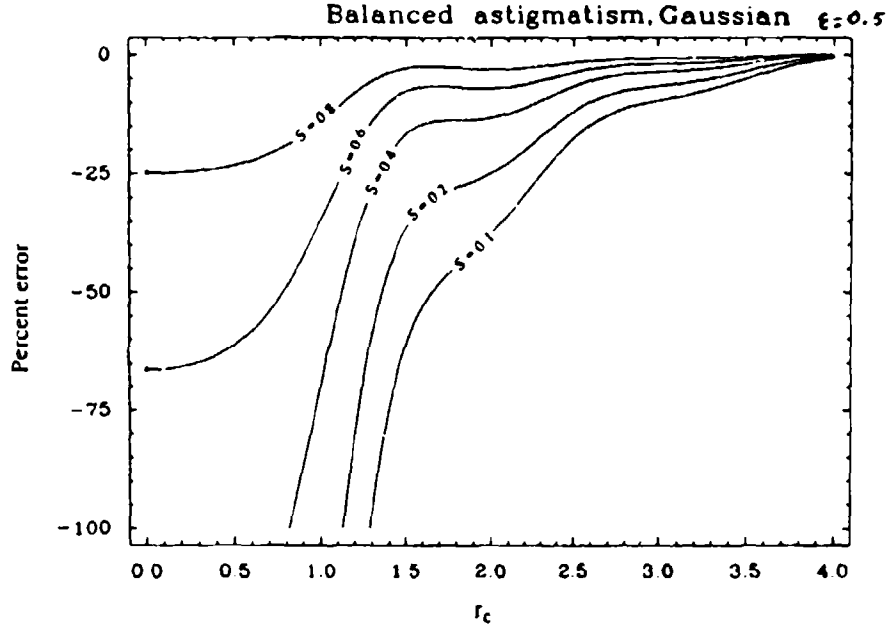

$\%Error_{ENC}$

Figure 21d.

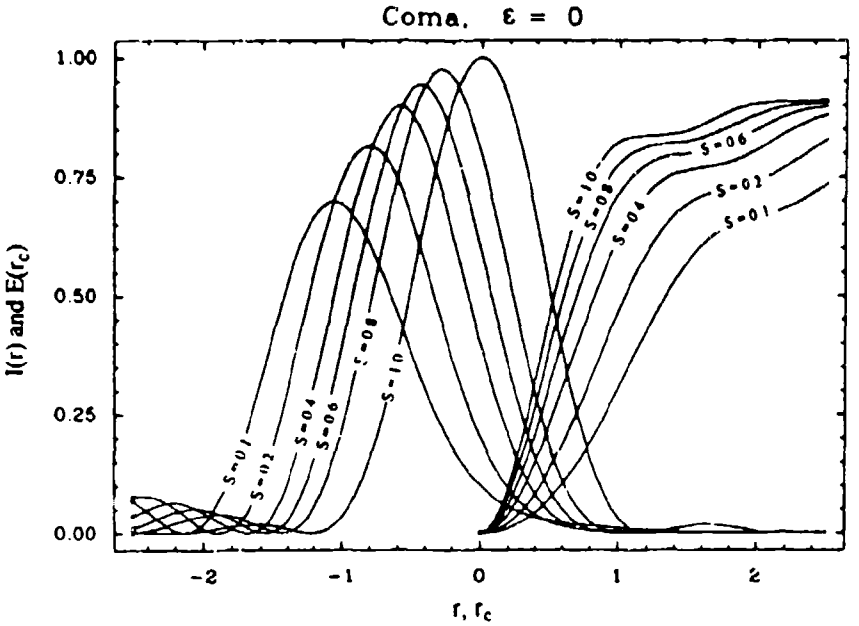

PSFs and encircled energies
Figure 22a.

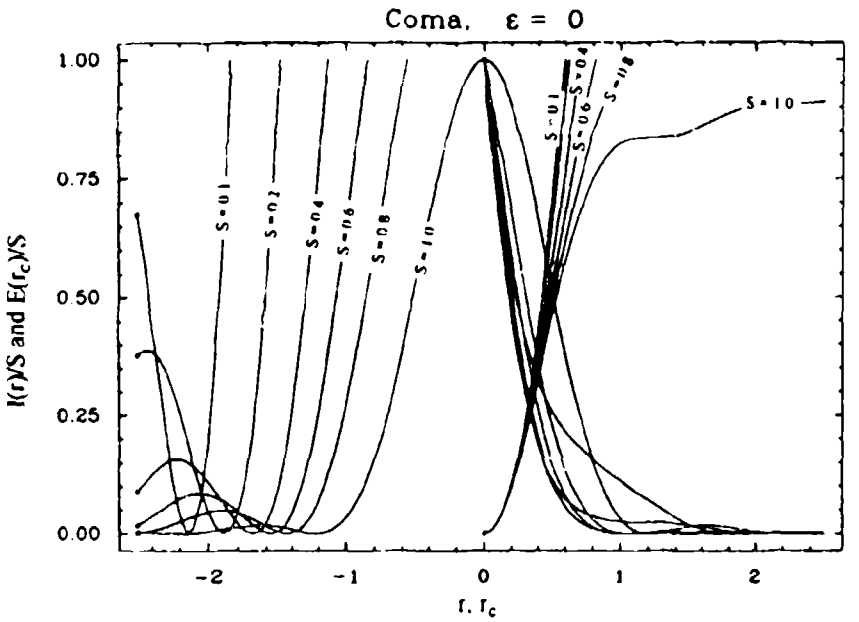

Normalized PSFs and encircled energies
Figure 22b.

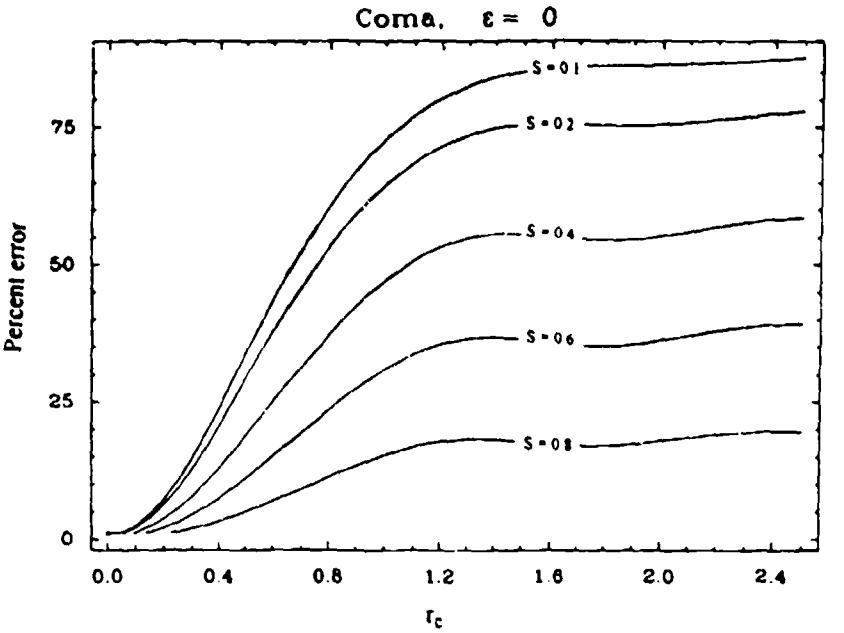

$\%Error_{NENC}$

Figure 22c.

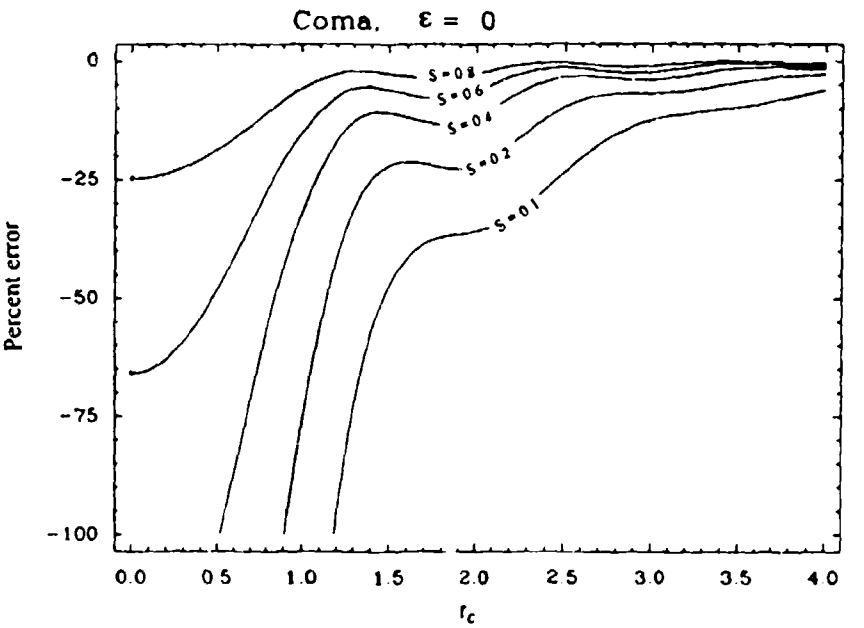

$\%Error_{ENC}$

Figure 22d.

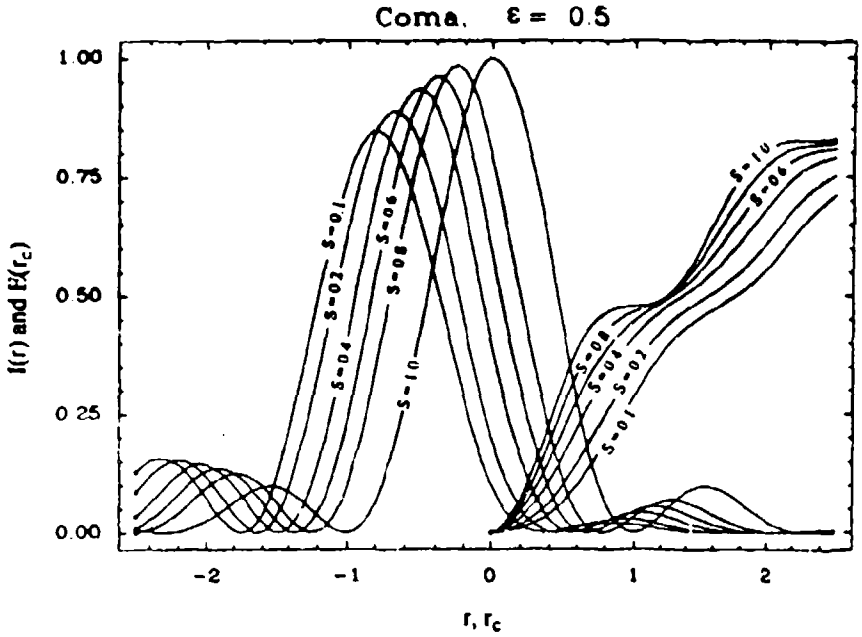

PSFs and encircled energies
Figure 23a.

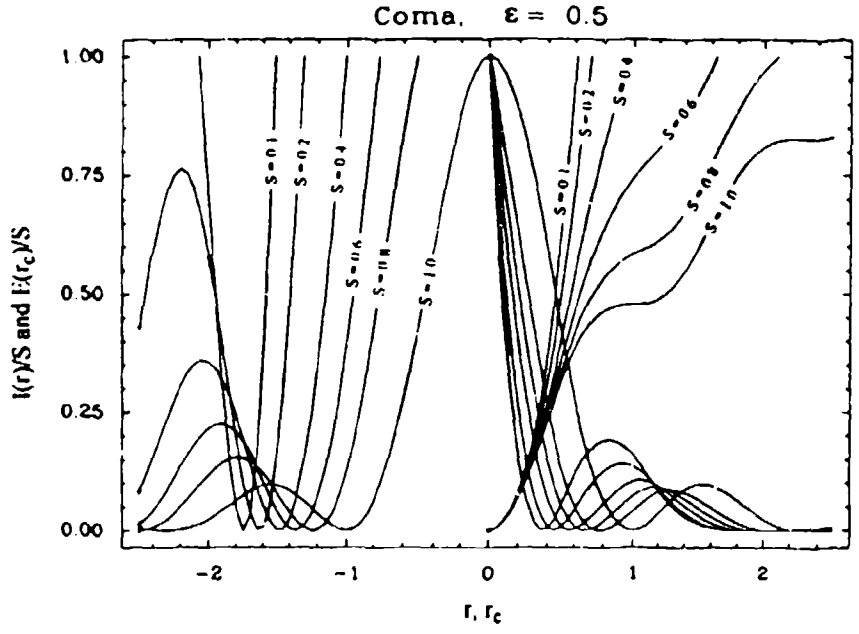

Normalized PSFs and encircled energies
Figure 23b.

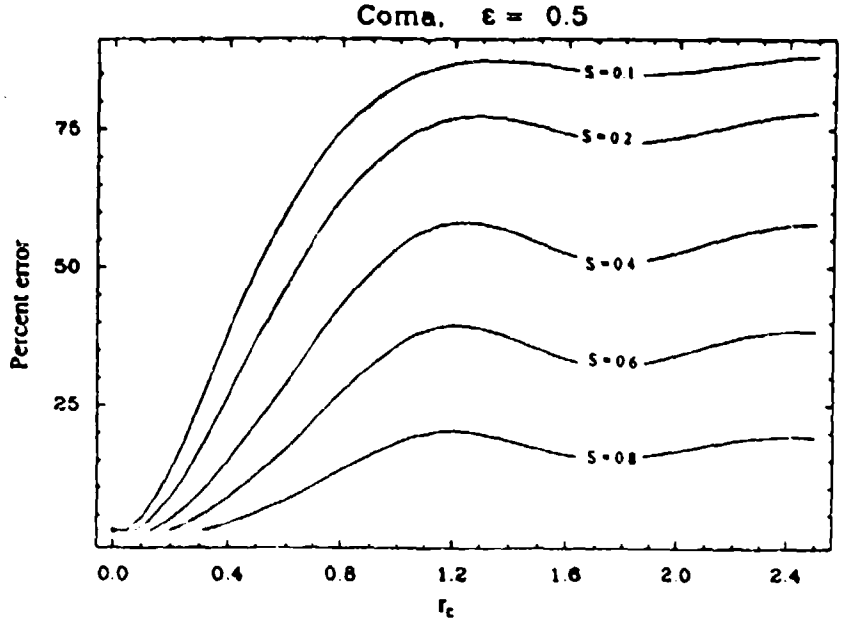

$\%Error_{NENC}$

Figure 23c.

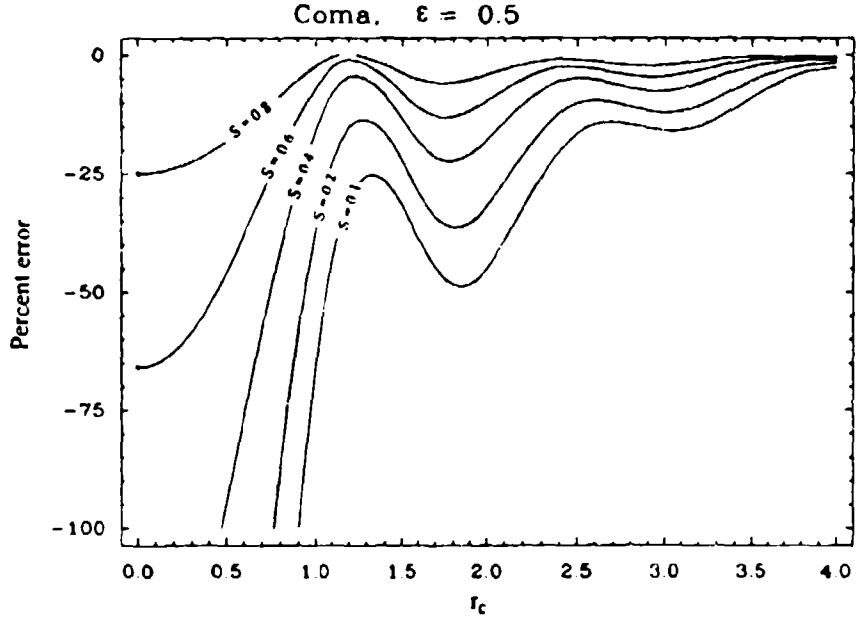

$\%Error_{ENC}$

Figure 23d.

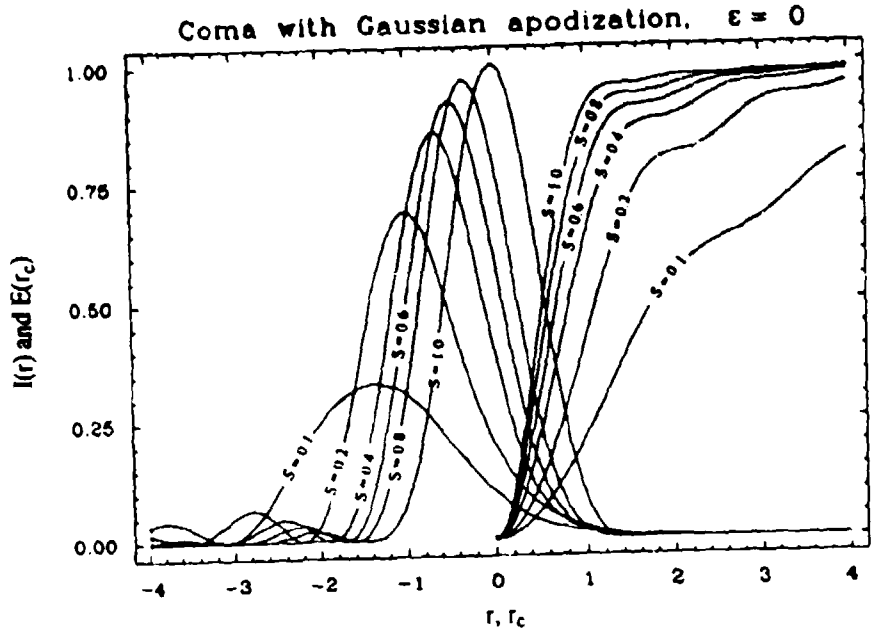

PSFs and encircled energies
Figure 24a.

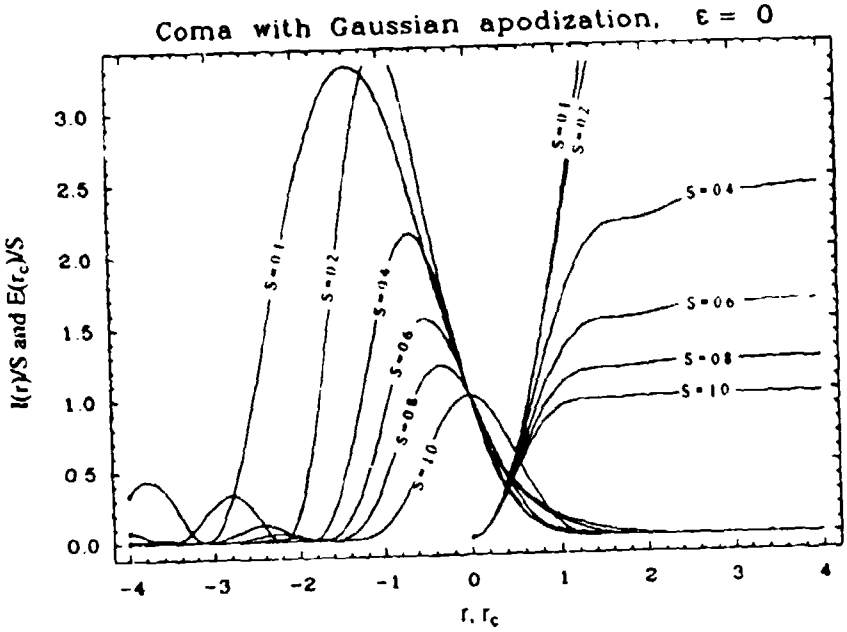

Normalized PSFs and encircled energies
Figure 24b.

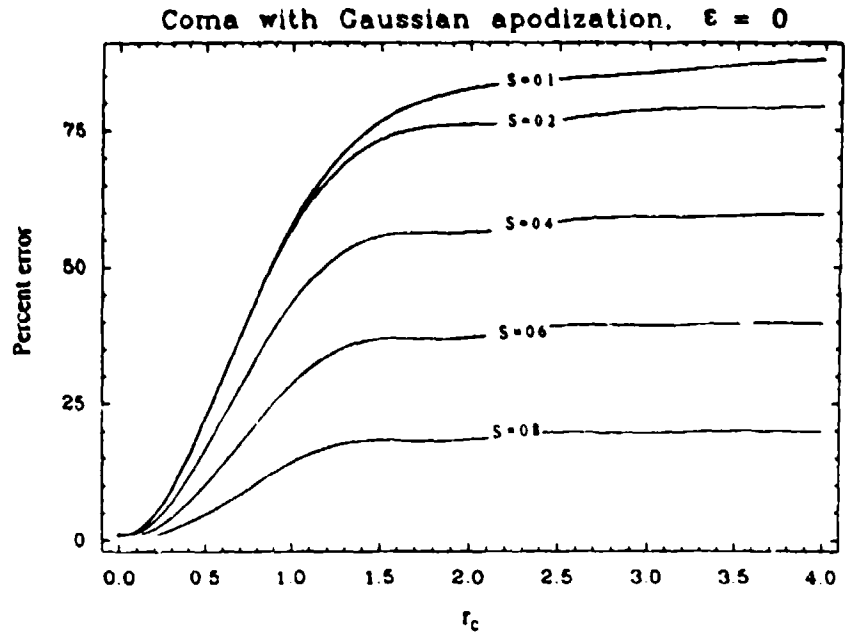

$\%Error_{NENC}$

Figure 24c.

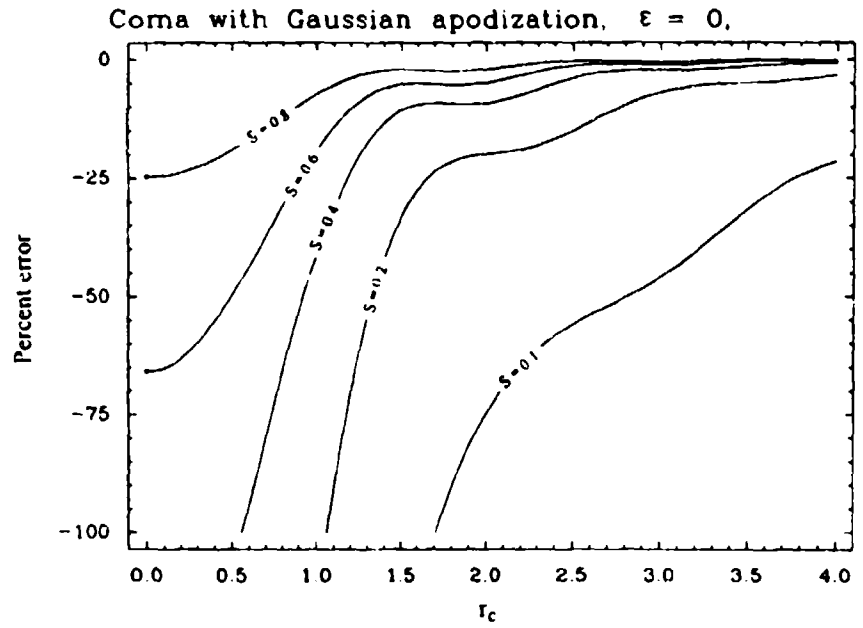

$\%Error_{ENC}$

Figure 24d.

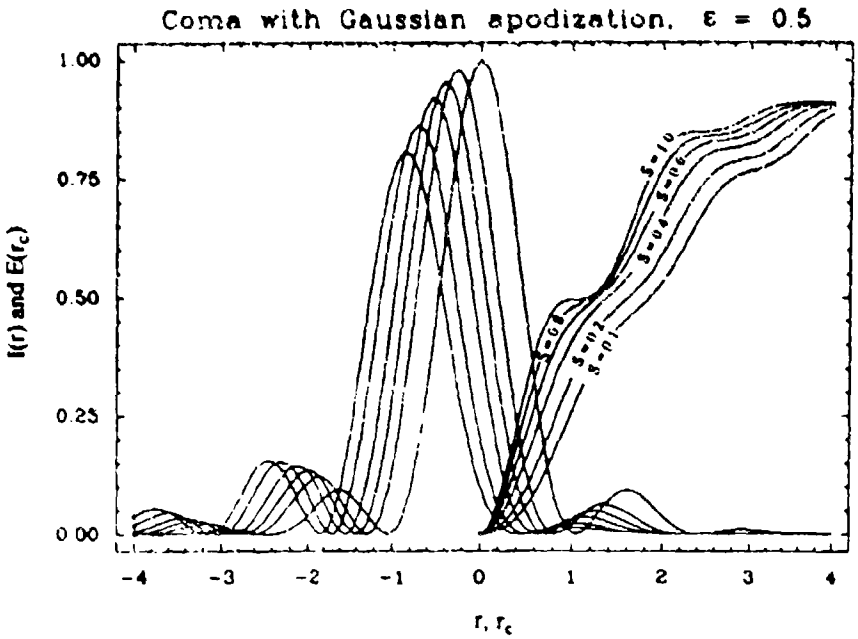

PSFs and encircled energies
Figure 25a.

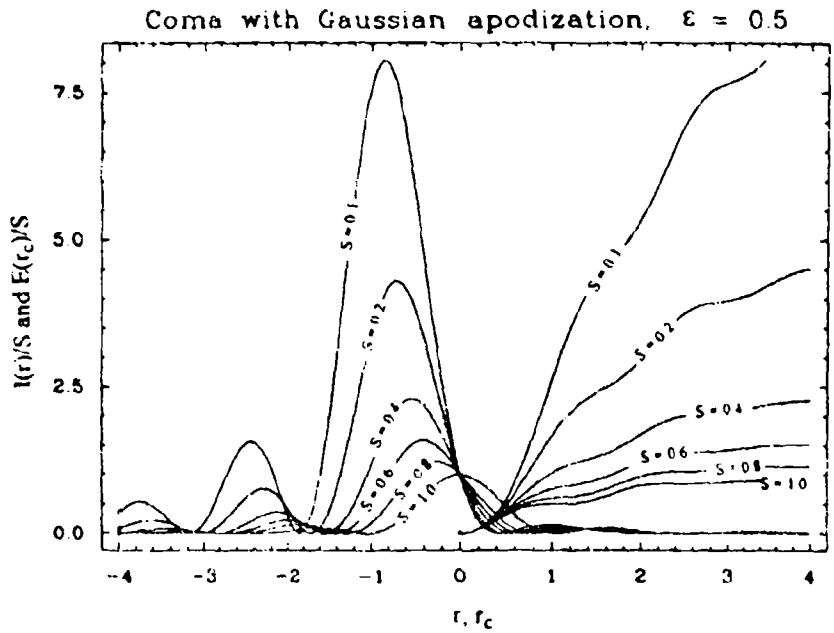

Normalized PSFs and encircled energies
Figure 25b.

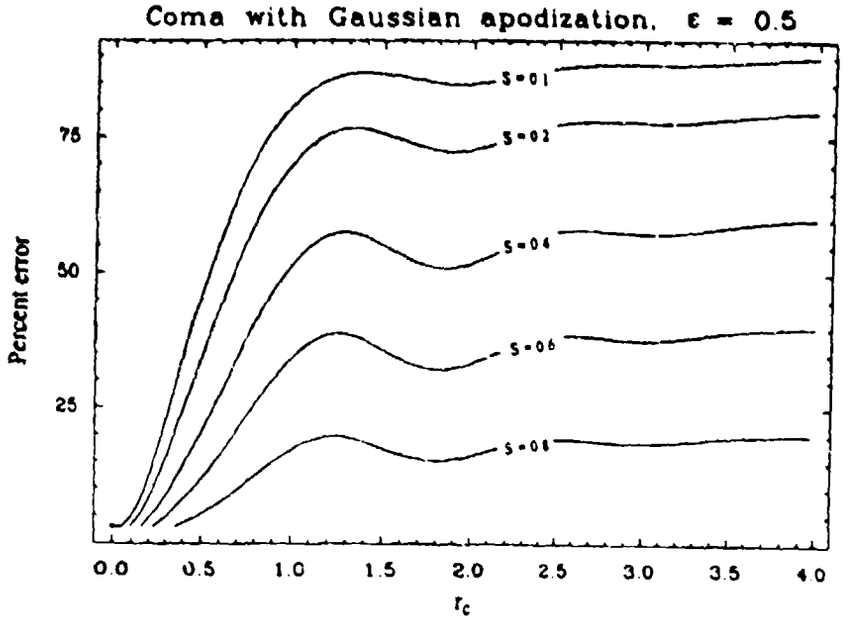

$\%Error_{NENC}$

Figure 25c.

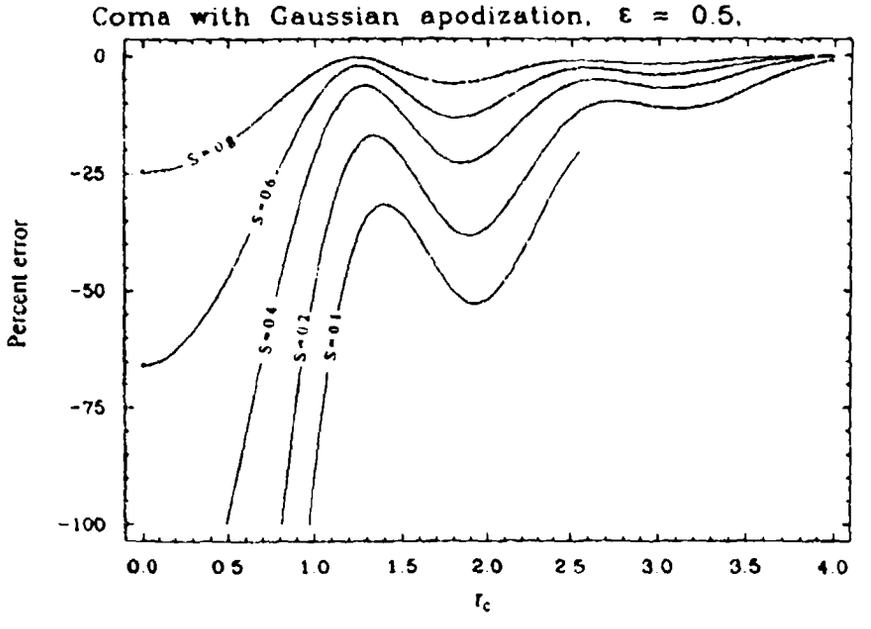

$\%Error_{ENC}$

Figure 25d.

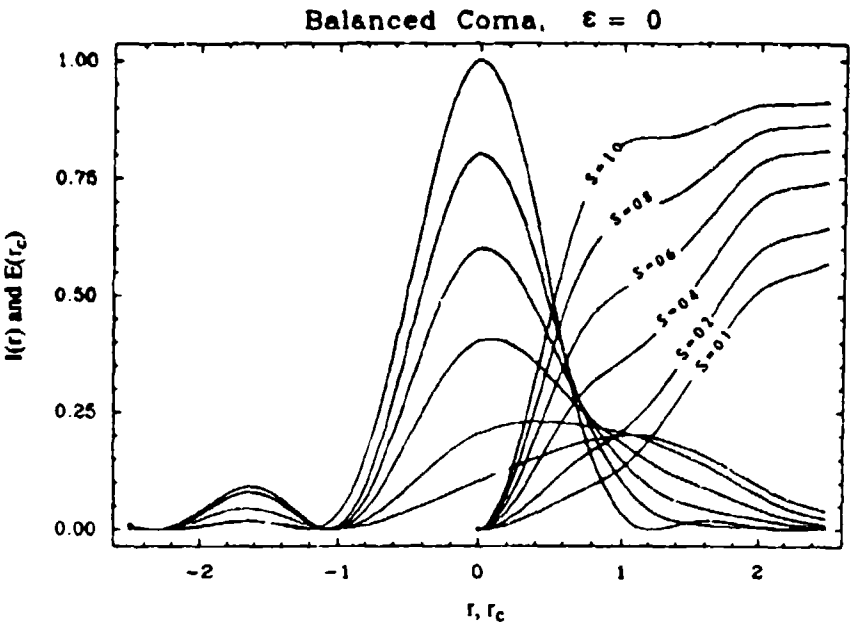

PSFs and encircled energies
Figure 26a.

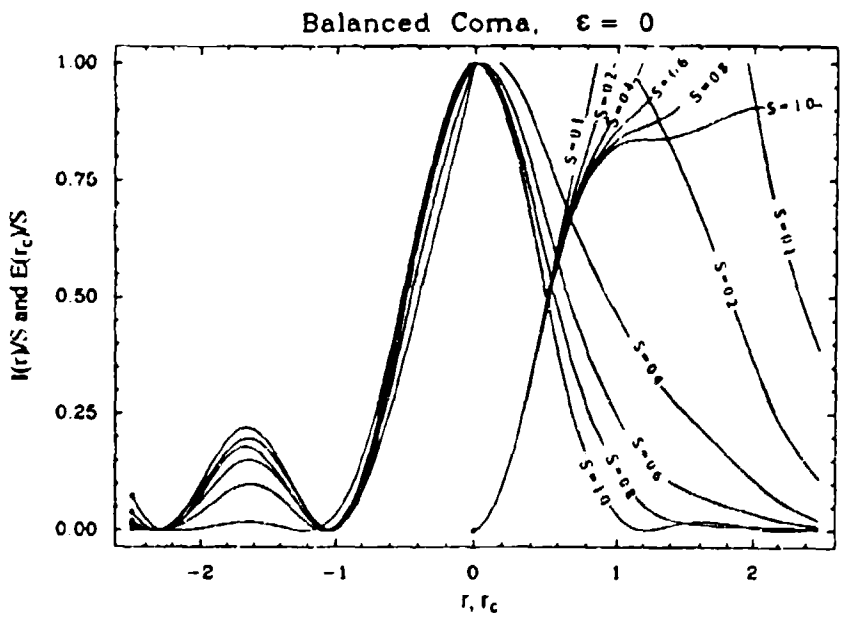

Normalized PSFs and encircled energies
Figure 26b.

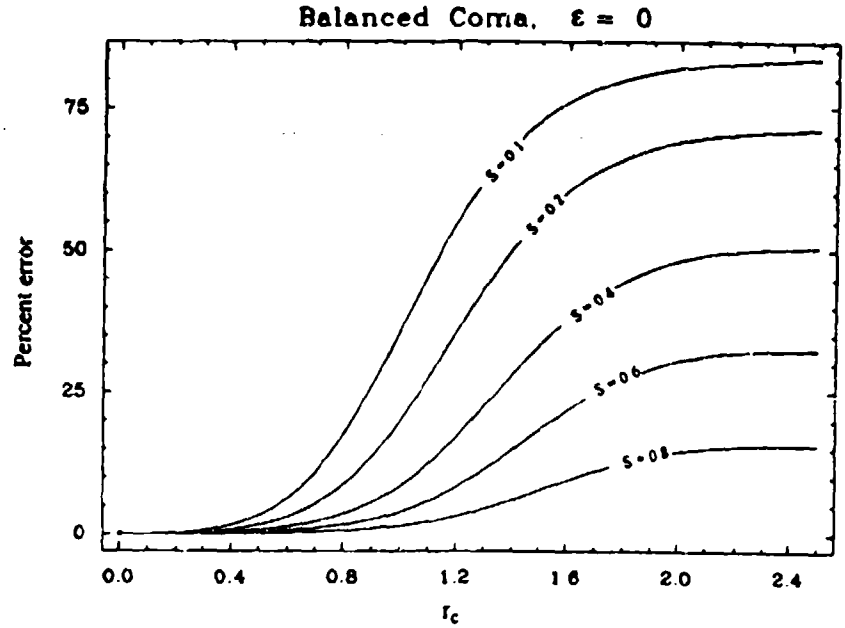

$\%Error_{NEMC}$

Figure 26c.

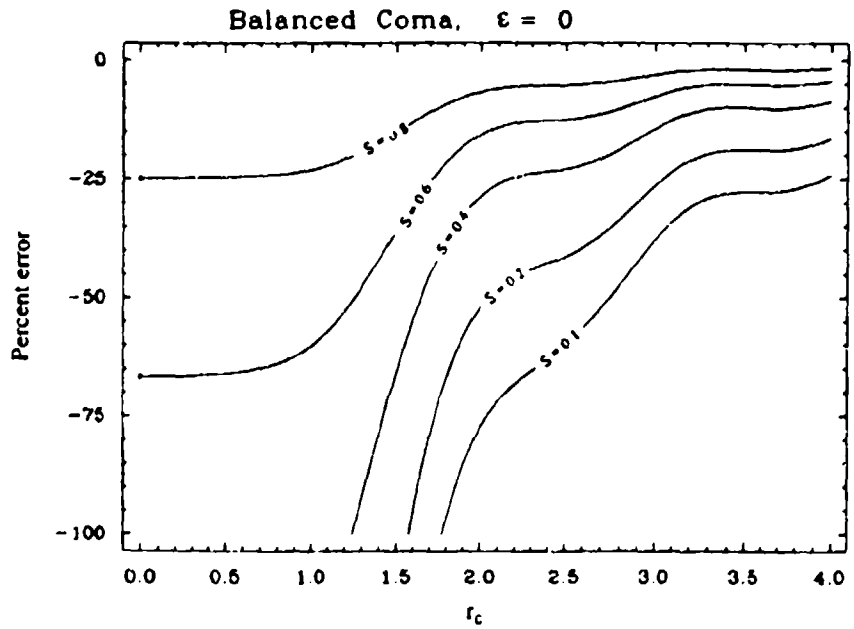

$\%Error_{FMC}$

Figure 26d.

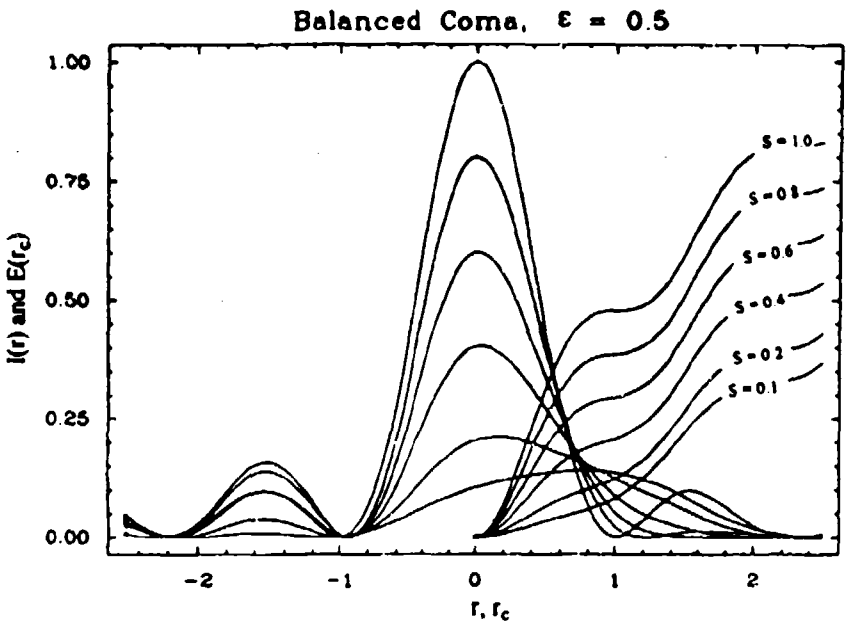

PSFs and encircled energies
Figure 27a.

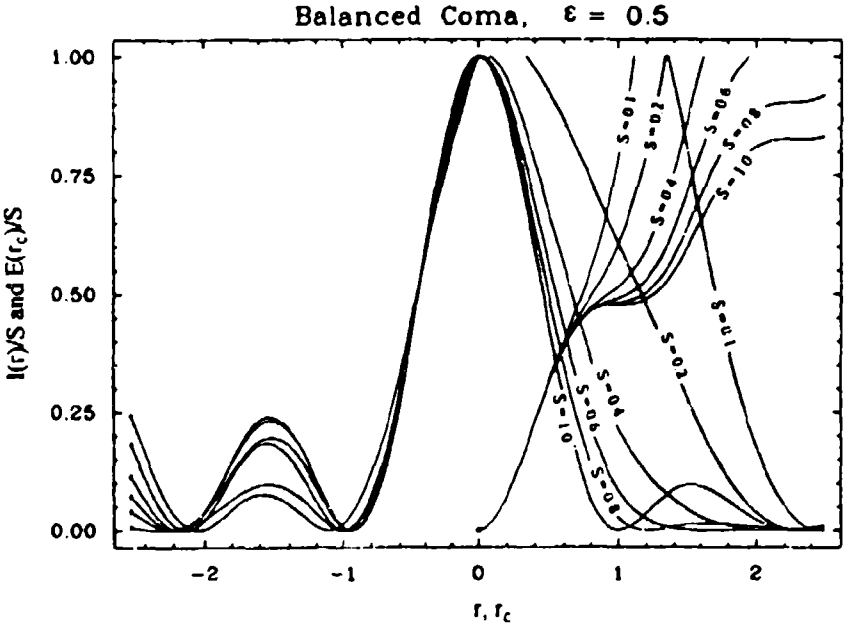

Normalized PSFs and encircled energies
Figure 27b.

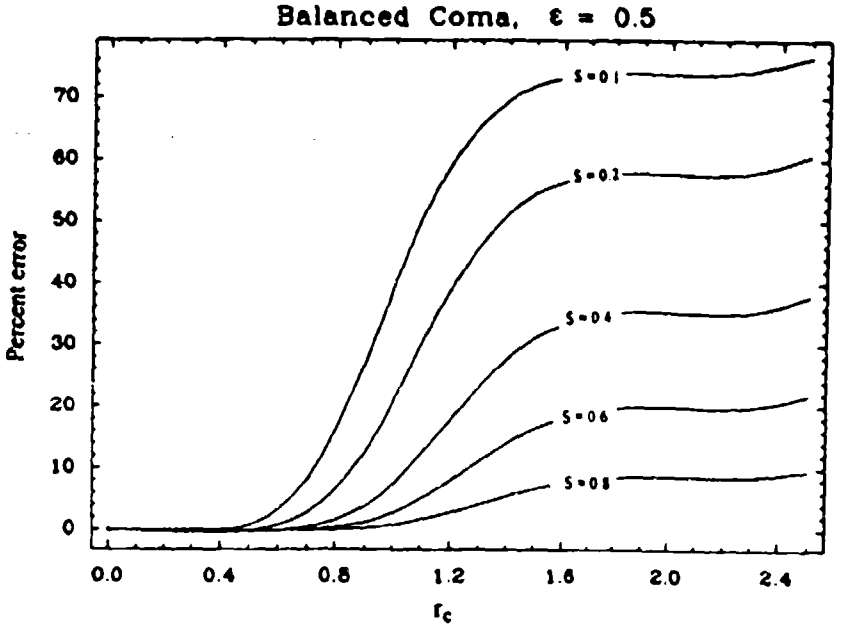

$\%Error_{NENC}$

Figure 27c.

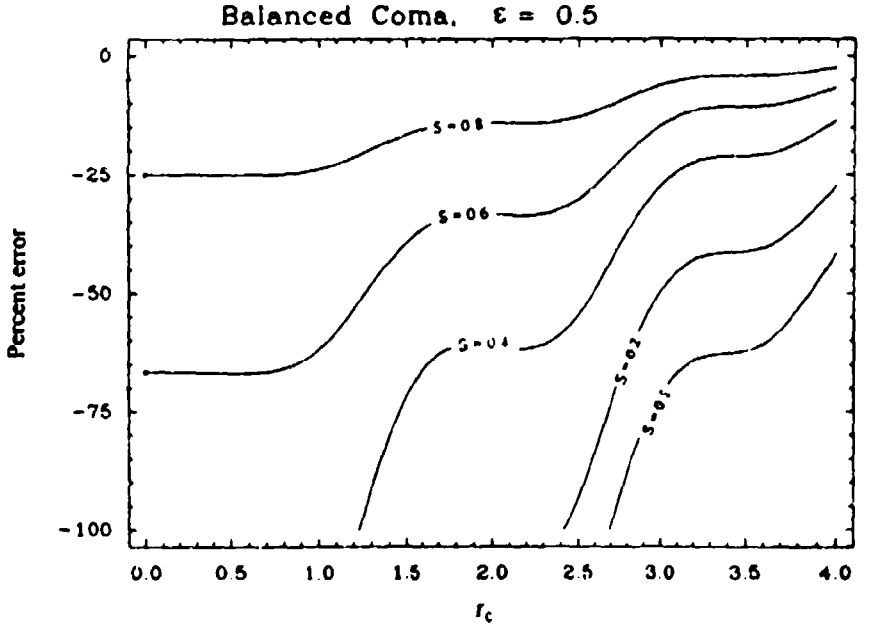

$\%Error_{ENC}$

Figure 27d.

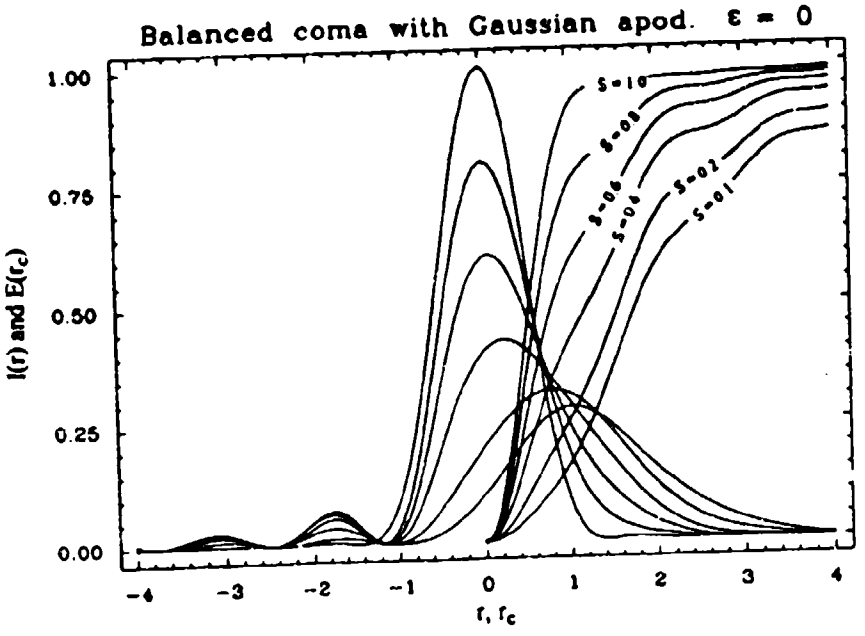

PSFs and encircled energies
Figure 28a.

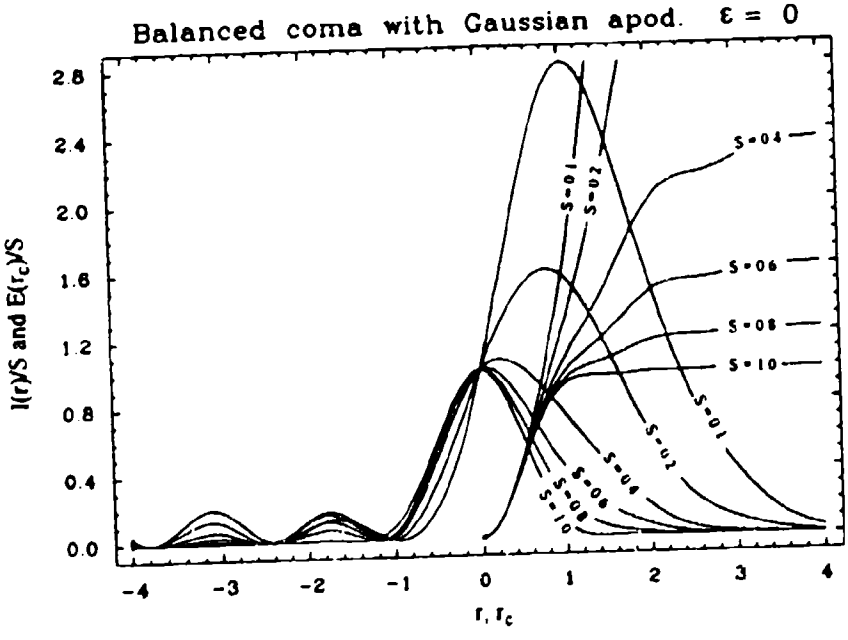

Normalized PSFs and encircled energies
Figure 28b.

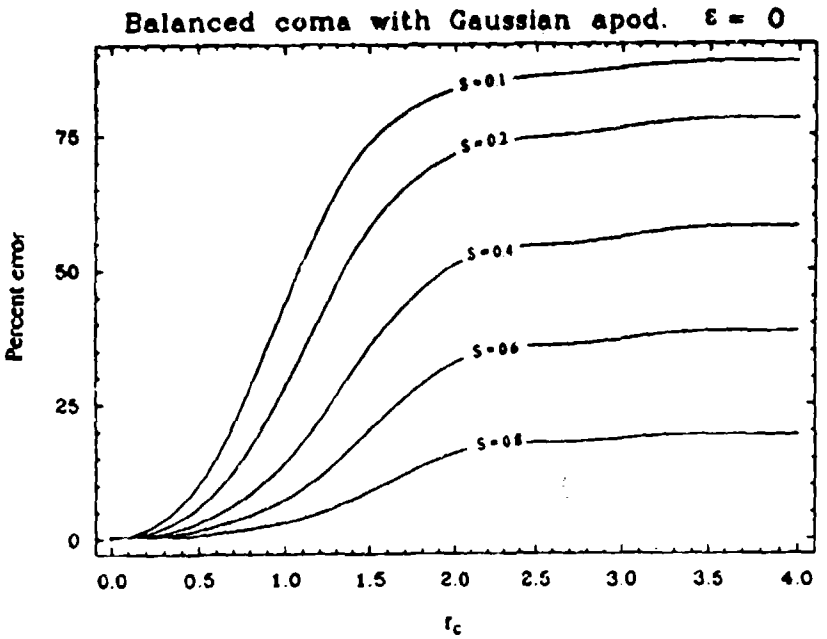

$\%Error_{NENC}$

Figure 28c.

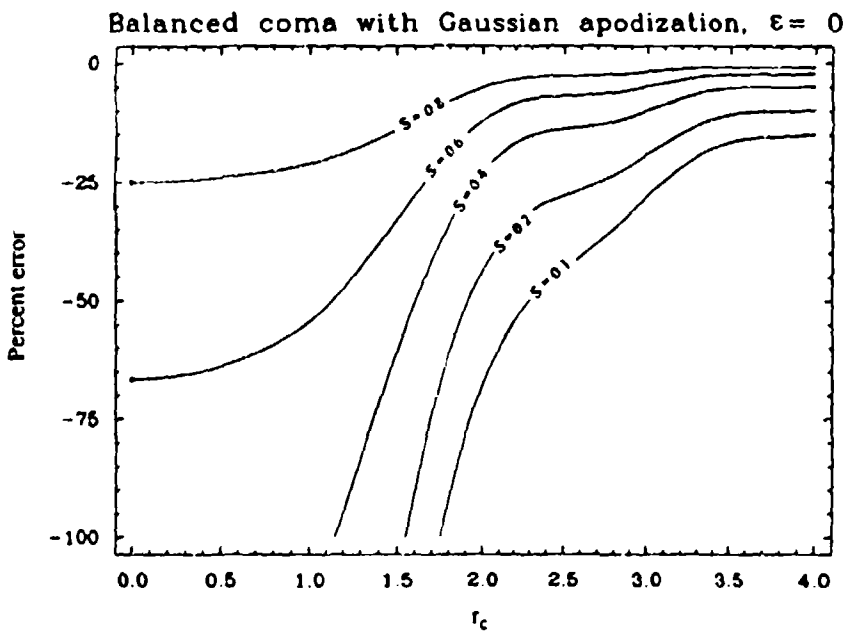

$\%Error_{ENC}$

Figure 28d.

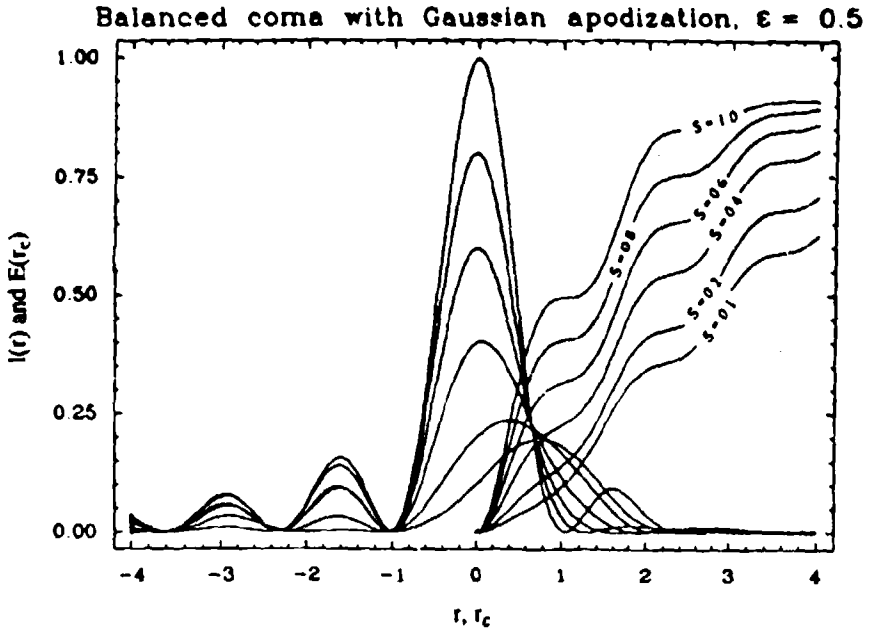

PSFs and encircled energies
Figure 29a.

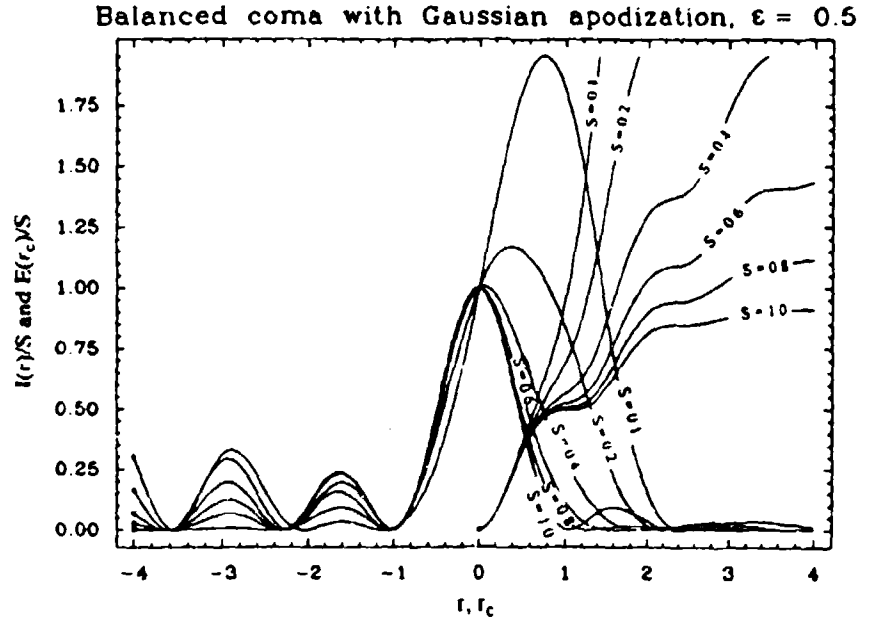

Normalized PSFs and encircled energies .
Figure 29b.

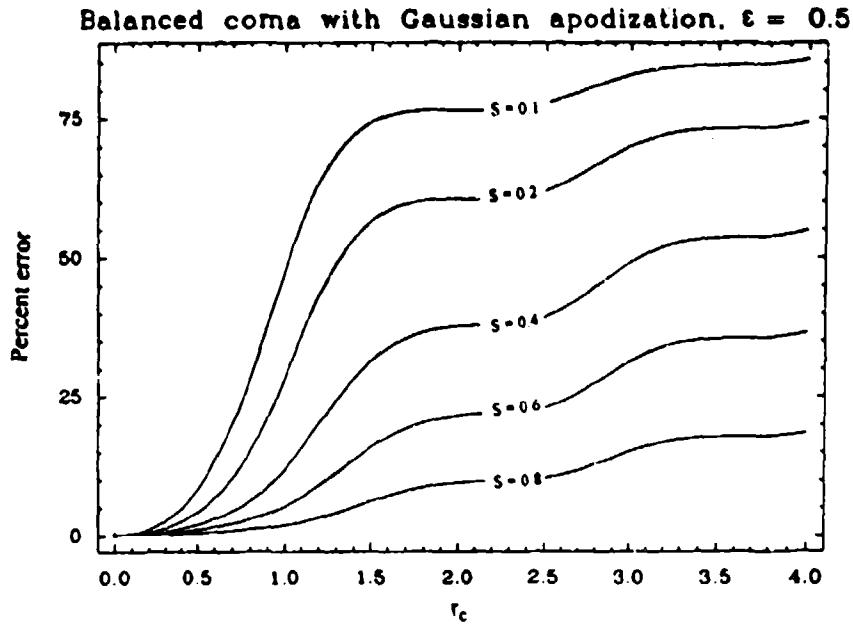

$\%Error_{NENC}$

Figure 29c.

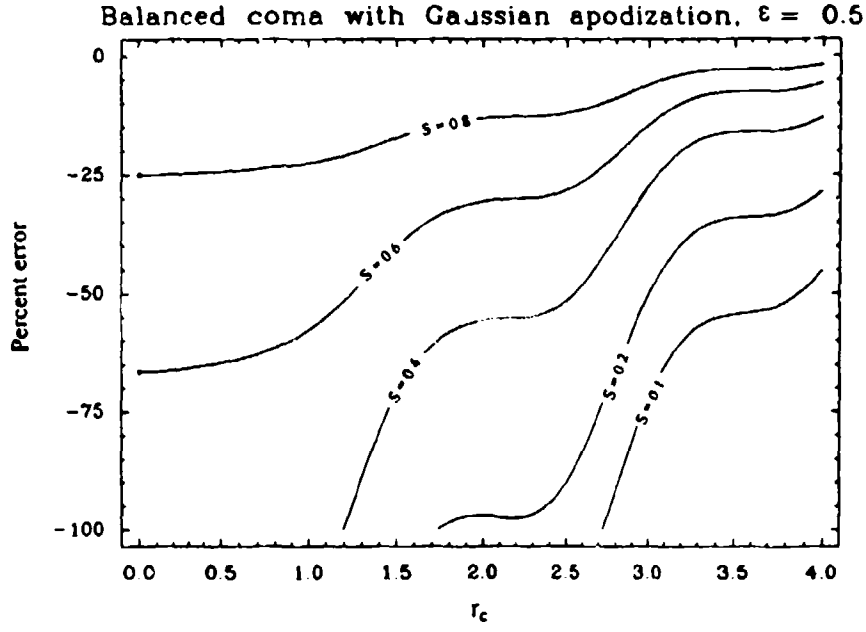

$\%Error_{ENC}$

Figure 29d.

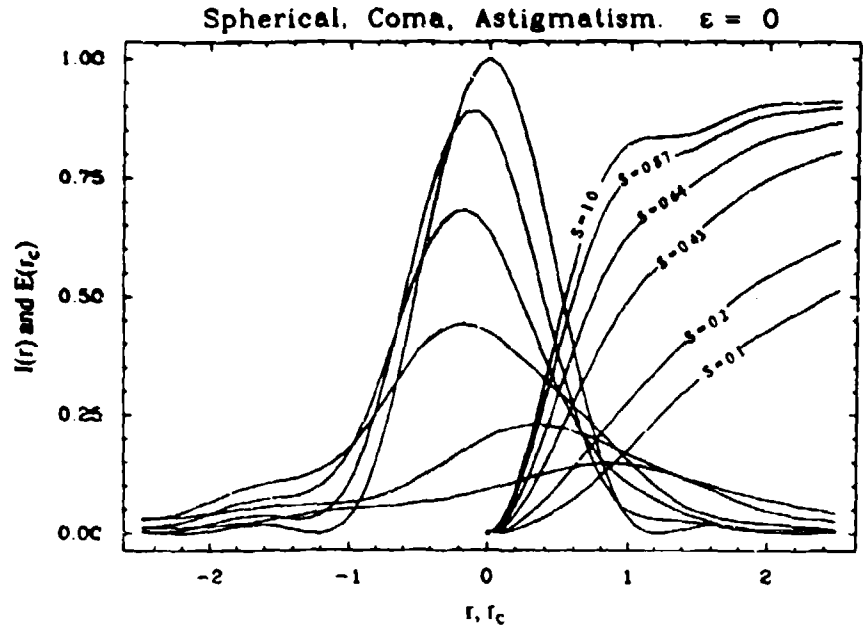

PSFs and encircled energies
Figure 30a.

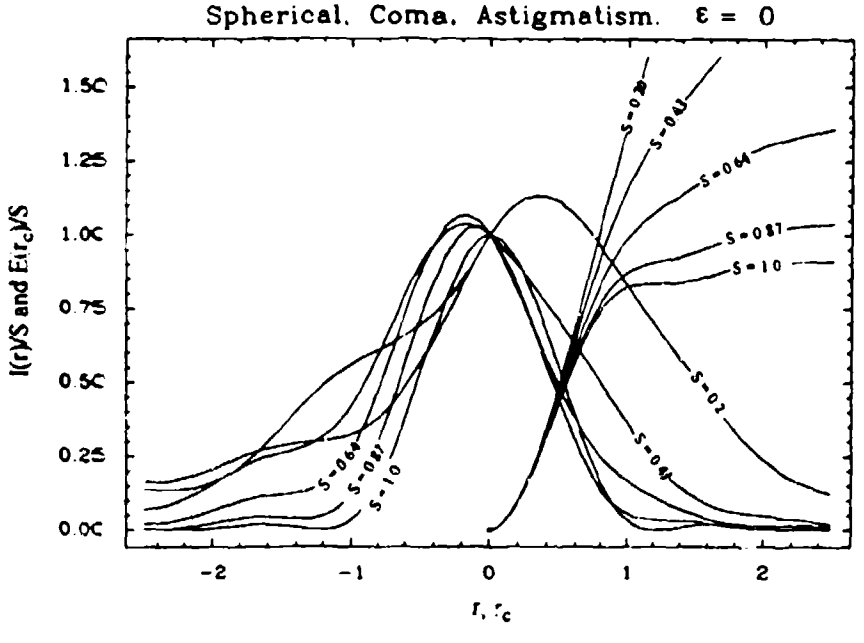

Normalized PSFs and encircled enrgies
Figure 30b.

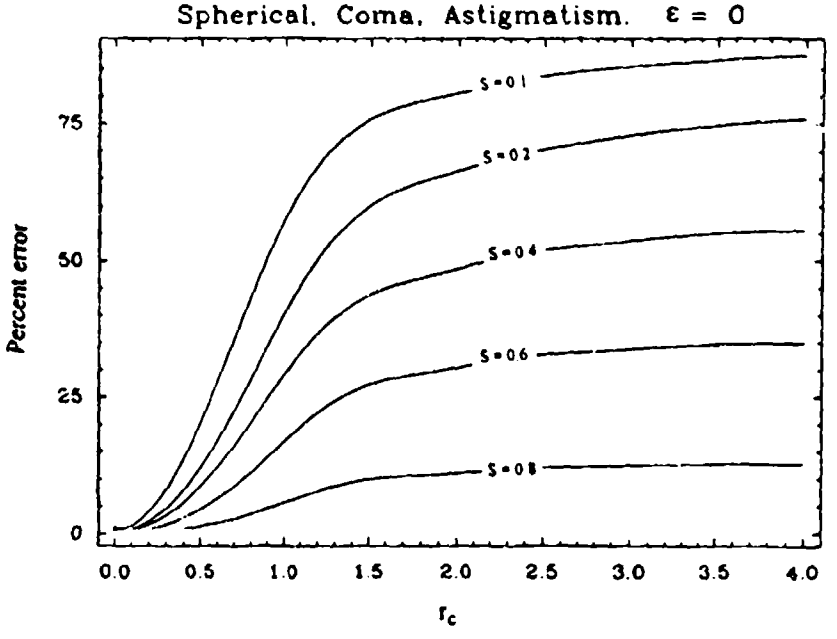

$\%Error_{NENC}$

Figure 30c.

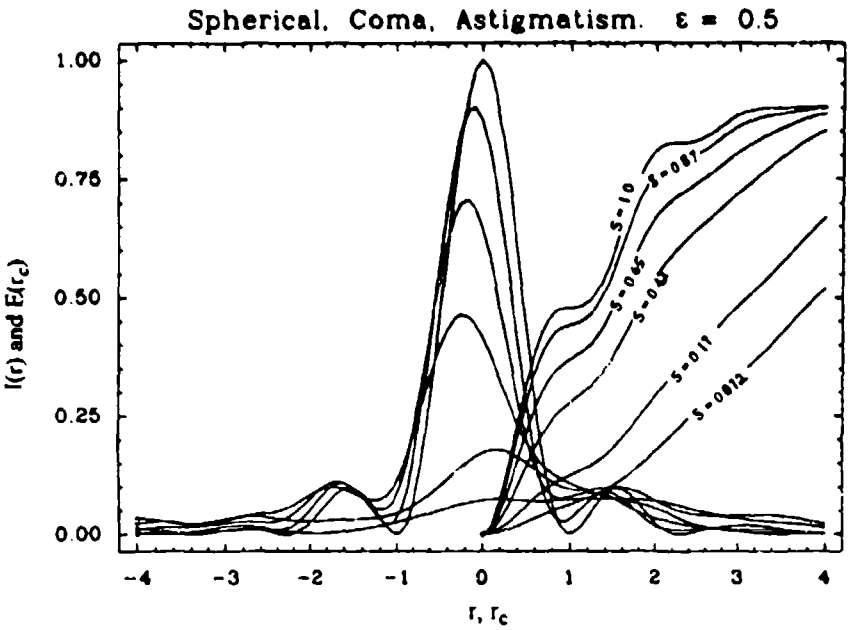

PSFs and encircled energies
Figure 31a.

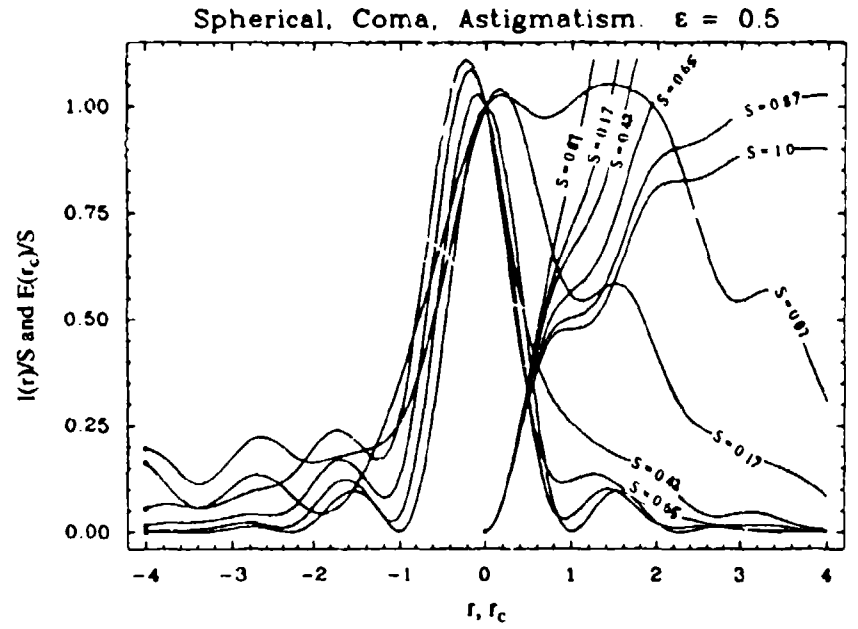

Normalized PSFs and encircled energies
Figure 31b.

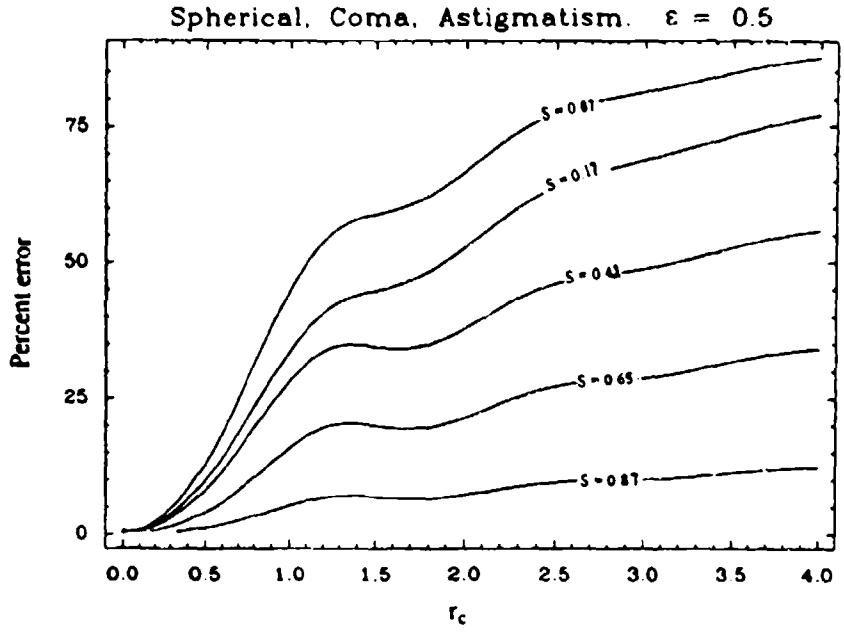

$\%Error_{NENC}$

Figure 31c.

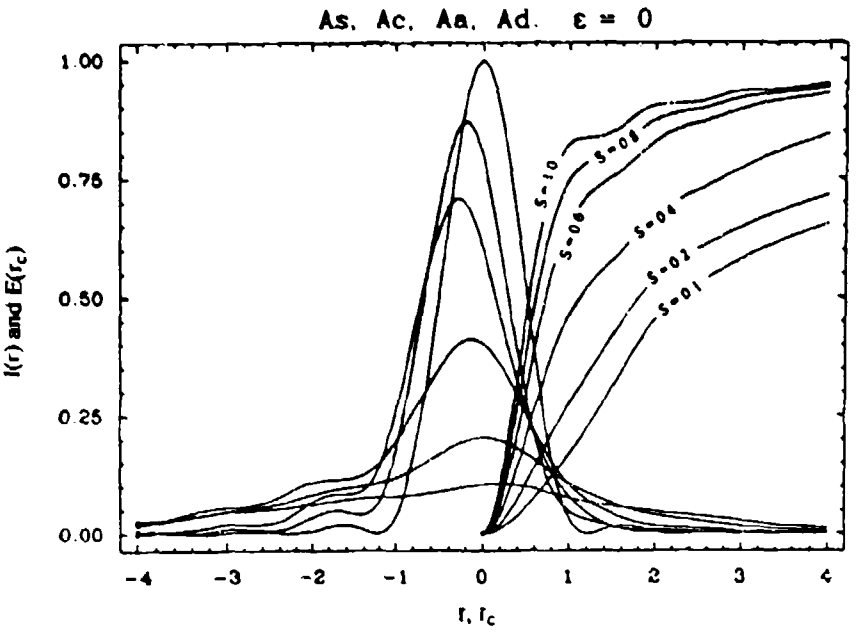

PSFs and encircled energies
Figure 32a.

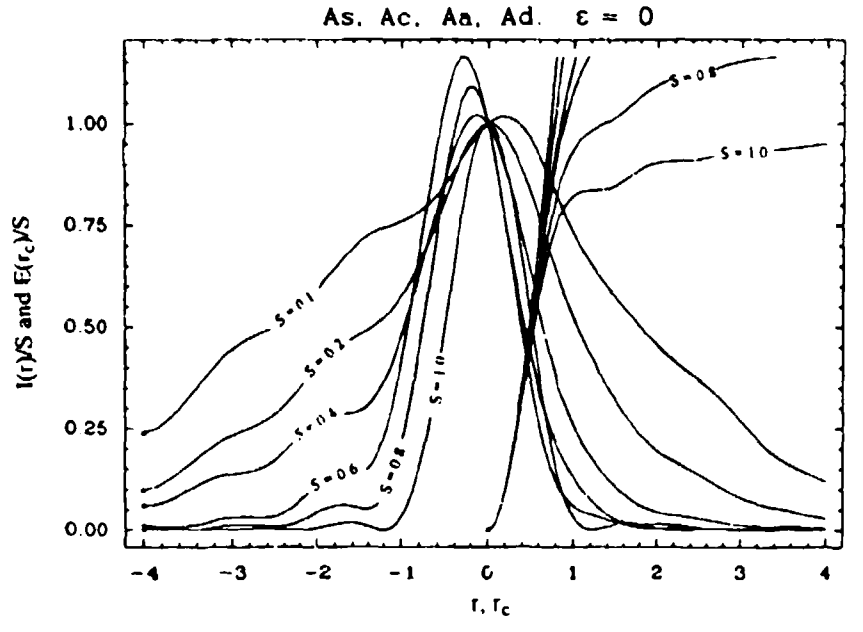

Normalized PSFs and encircled energies
Figure 32b.

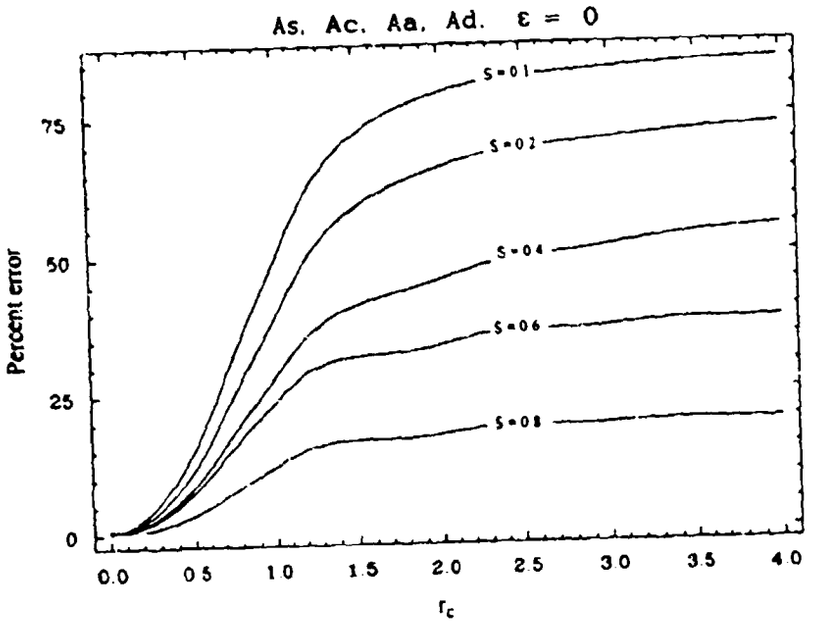

$\%Error_{NENC}$

Figure 3.c.

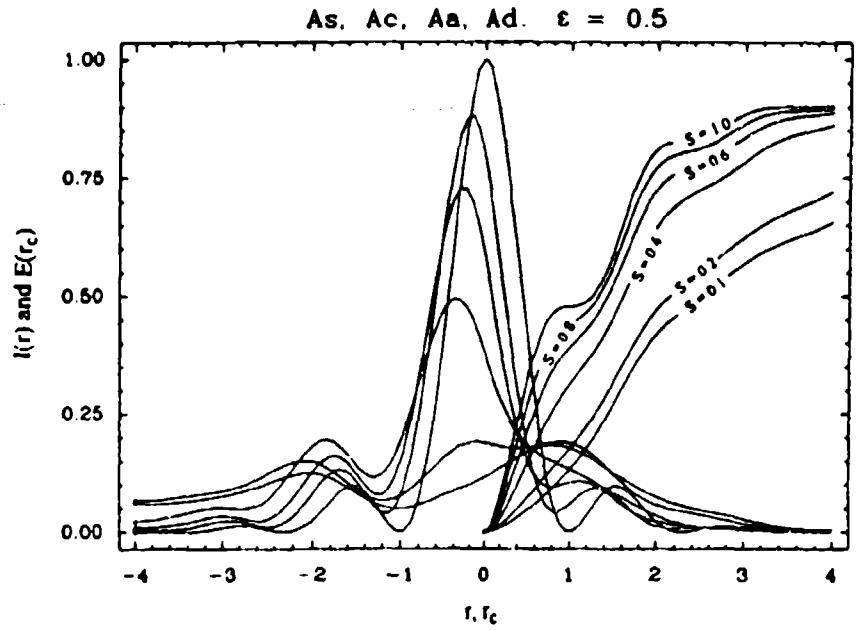

PSFs and encircled energies
Figure 33a.

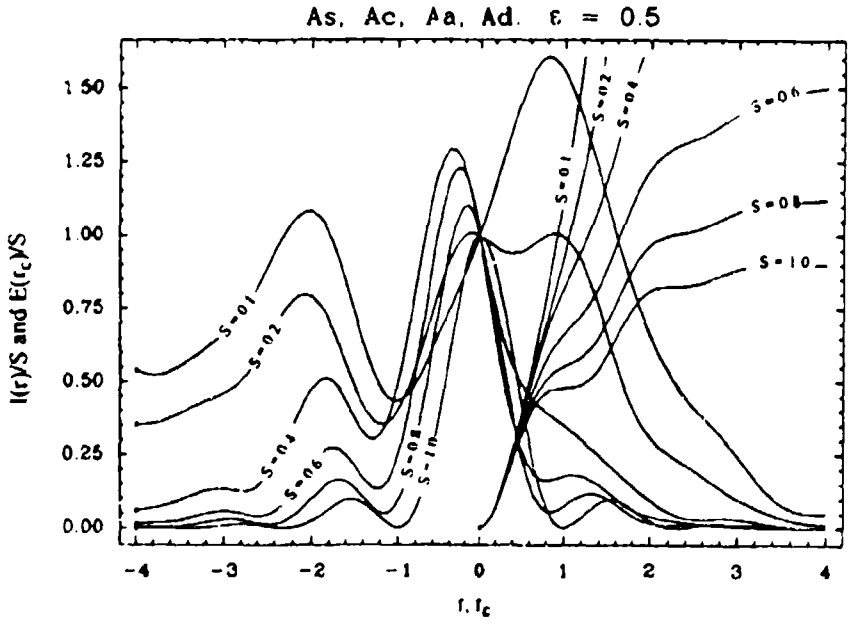

Normalized PSFs and encircled energies
Figure 33b.

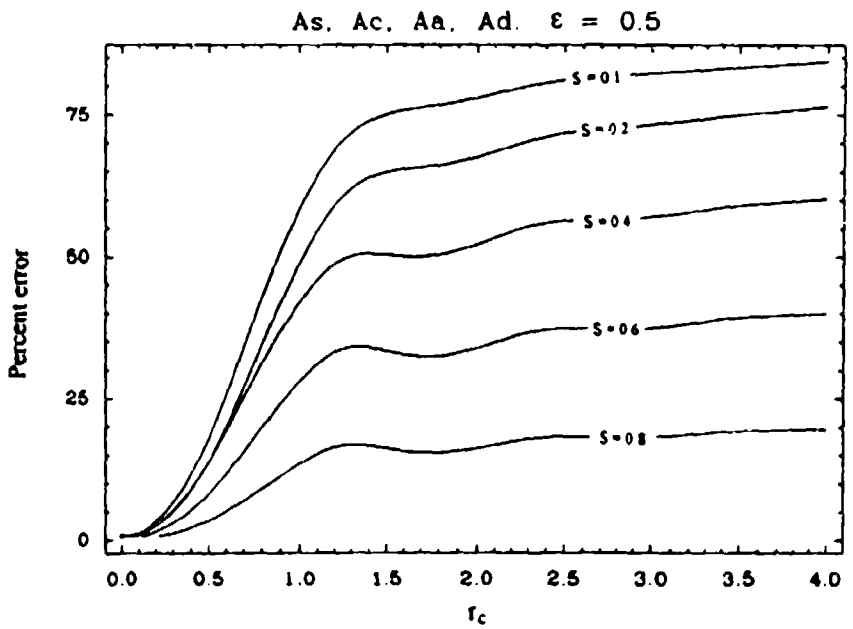

$\%Error_{NENC}$

Figure 33c.